



TALLINN UNIVERSITY OF TECHNOLOGY

SCHOOL OF ENGINEERING

Department of Electrical Power Engineering and Mechatronics

**RESEARCH AND DEVELOPMENT OF POWER HARDWARE
IN THE LOOP TEST SETUP FOR SIMULATION OF
FLYWHEEL CONTROL SCENARIOS**

**REAALAJASIMULAATORI RAKENDUSE
VÄLJATÖÖTAMINE HOORATAS-ENERGIASALVESTI
JUHTIMISSTSENAARIUMITE UURIMISEKS**

MASTER THESIS

Student: Luca Link

Student code: 215500AAAM

Supervisor: Tobias Häring, Junior Researcher

Tallinn, 2021

(On the reverse side of title page)

AUTHOR'S DECLARATION

Hereby I declare, that I have written this thesis independently.

No academic degree has been applied for based on this material. All works, major viewpoints and data of the other authors used in this thesis have been referenced.

"....." 202.....

Author:

/signature /

Thesis is in accordance with terms and requirements

"....." 202....

Supervisor:

/signature/

Accepted for defence

".....".....202... .

Chairman of theses defence commission:

/name and signature/

Non-exclusive Licence for Publication and Reproduction of Graduation Thesis¹

I, Luca Link hereby

1. grant Tallinn University of Technology (TalTech) a non-exclusive license for my thesis Research and development of power hardware in the loop test setup for simulation of flywheel control scenarios,

supervised by Tobias Häring,

1.1 reproduced for the purposes of preservation and electronic publication, incl. to be entered in the digital collection of TalTech library until expiry of the term of copyright;

1.2 published via the web of TalTech, incl. to be entered in the digital collection of TalTech library until expiry of the term of copyright.

1.3 I am aware that the author also retains the rights specified in clause 1 of this license.

2. I confirm that granting the non-exclusive license does not infringe third persons' intellectual property rights, the rights arising from the Personal Data Protection Act or rights arising from other legislation.

_____ (date)

¹ The non-exclusive licence is not valid during the validity of access restriction indicated in the student's application for restriction on access to the graduation thesis that has been signed by the school's dean, except in case of the university's right to reproduce the thesis for preservation purposes only. If a graduation thesis is based on the joint creative activity of two or more persons and the co-author(s) has/have not granted, by the set deadline, the student defending his/her graduation thesis consent to reproduce and publish the graduation thesis in compliance with clauses 1.1 and 1.2 of the non-exclusive licence, the non-exclusive licence shall not be valid for the period.

ABSTRACT

Author: Luca Link

Type of the work: Master Thesis

Title: Research and development of power hardware in the loop test setup for simulation of flywheel control scenarios

Date: January 2022

130 pages (the number of thesis pages including appendices)

University: Tallinn University of Technology

School: School of Engineering

Department: Department of Electrical Power Engineering and Mechatronics

Supervisor(s) of the thesis: Tobias Häring

Consultant(s): Prof. Dr.-Ing. Dr.H.c. Helmuth Biechl

Abstract:

Volatile energy production from renewable sources increases the demand of energy storages. Due to the high cycle capability without degradation, flywheel energy storage systems are beneficial over other storage systems in scenarios with a lot of charging cycles. To investigate control algorithms for flywheel energy storages, a power hardware in the loop test setup is developed. Therefore, an existing flywheel is modernized with state-of-the-art components. To control the charging and discharging power, a power controller is implemented. The controller enables the system to reach the desired power in around 200 ms. A performance study of the modernized flywheel energy storage system shows, that the self-discharge rate is a strong disadvantage of flywheel energy storages. The present flywheel discharges itself completely in around 10 min. The round-trip efficiency during a test with 15 kW power shows decent results, with 71.8 %. By performing research on different scenarios like power levelling or power buffering, the applicability of the power hardware in the loop test setup for development and optimization of control algorithms is shown. By using flywheel energy storages, the grid reliability can be increased, and the stress introduced by peak power decreased.

Keywords: power hardware in the loop (P-HIL), flywheel energy storage system (FESS), hybrid energy storage, microgrid, power control

LÕPUTÖÖ LÜHIKOKKUVÕTE

Autor: Luca Link

Lõputöö liik: Magistritöö

Töö pealkiri: Reaalajasimulaatori rakenduse väljatöötamine hooratas-energiasalvesti juhtimisstsenaariumite uurimiseks

Kuupäev:

130 lk

Jaauuar 2022

Ülikool: Tallinna Tehnikaülikool

Teaduskond: Inseneriteaduskond

Instituut: Elektroenergeetika ja mehhatroonika instituut

Töö juhendaja(d): Tobias Häring

Töö konsultant (konsultandid): Prof.Dr.-Ing.Dr.h.c. Helmuth Biechl

Sisu kirjeldus:

Taastuenergiatallikate muutlik tootmine suurendab vajadust energiasalvestite järele. Antud töö käsitleb hooratas-energiasalvestit, mis on suure tsüklite arvuga rakendustes eelistatud võrreldes teiste energiasalvestitega tänu kõrgele tsüklilisele elueale ja muutumatule tühjendamissügavusele eluea jooksul. Hooratas-energiasalvestites kasutatavate juhtimisalgoritmide uurimiseks töötati käesoleva töö raames välja reaalajasimulaatori rakendus. Selleks rekonstrueeriti olemasolevat salvestit, lisades salvesti laadimise ja tühjendamise reaalajas juhtimiseks tööstusarvuti-võimsuskontroller (*power controller*). Tänu täiustatud juhtimisele on võimalik süsteemil saavutada soovitud võimsus 200 ms jooksul. Töö käigus leiti, et kasutatavatel suure massiga hooratas-energiasalvestite oluliseks puuduseks on kõrged tühijooksukaod. Töös kasutatud hooratta puhul saadi 15 kW võimsusega testi puhul ringtsükli kasuteguriks 71,8 % ning täielik isetühjenemine toimus 10 minutiga.

Töö käigus uuritakse ja demonstreeritakse tööstusarvutil põhineva reaalajasimulaatori rakendatavust erinevate juhtimisstsenaariumite arendamiseks ja optimeerimiseks. Hooratas-energiasalvesti abil saab parandada elektrivõrgu töökindlust ning vähendada võimsustippusid.

Märksõnad: power hardware in the loop (P-HIL), flywheel energy storage system (FESS), hybrid energy storage, microgrid, power control

THESIS TASK

Thesis title: **RESEARCH AND DEVELOPMENT OF POWER HARDWARE IN THE LOOP TEST SETUP FOR SIMULATION OF FLYWHEEL CONTROL SCENARIOS**

Student: **Luca Link, 215500AAAM**

Programme: **AAAM**

Type of the work: **Master Thesis**

Supervisor of the thesis: **Tobias Häring**

Co-supervisor of the thesis: **Helmuth Biechl**
(company, position and contact) **(University of Applied Sciences Kempten, Professor, biechl@hs-kempten.de)**

Validity period of the thesis task: 2021/2022 2021/2022 Sügis
(Validity period is given by supervisor)

Submission deadline of the thesis: **21.12.2021**

Student (signature)

Supervisor (signature)

Head of programme
(signature)

Co-supervisor (signature)

1. Reasons for choosing the topic

The European Union introduced its European Green Deal with the target climate neutrality by 2050. This deal includes clean and secure energy for everyone. Clean energy sources like wind power plants and solar are very volatile. This leads to a mismatch between energy production and demand. This thesis contributes to the investigations on flywheel energy storage systems in microgrids for an increase of their reliability.

2. Thesis objective

The aim of this thesis is to modernize a flywheel energy storage system (FESS) as a power hardware in the loop test setup, to analyze different control scenarios.

3. List of sub-questions:

Which components are necessary for the FESS modernization?

How can the FESS power be controlled?

Do the existing FESS models fit the modernized FESS?

Except of load levelling, which other beneficial use cases exist for FESS?

4. Basic data:

Measurement data from the PLC.

Datasheets from manufacturer.

Data from previous master theses.

Data from Simulations in MATLAB Simulink.

Data from literature.

5. Research methods

The research in this thesis is based on literature analysis, functional tests on the developed power hardware in the loop test setup and MATLAB Simulink simulations. For the development of the test setup and the MATLAB Simulink simulations different sources like books, datasheets and user guides are used. For the analysis and interpretation of the collected data excel and MATLAB is used.

6. Graphical material

Explanatory drawings, diagrams, small schematics or tables are part of the main work. In the appendix will be a detailed documentation of the new setup with schematics.

7. Thesis structure

Introduction

1. State of the art
 - 1.1. Electricity grid
 - 1.2. Energy storage systems
2. Development of power hardware in the loop test setup

- 2.1. Previous hardware setup
- 2.2. Modernized hardware setup
- 2.3. Implementation of utilities
- 3. Development of FESS power control strategy
 - 3.1. System identification
 - 3.2. Linearization of system
 - 3.3. Verification of linearization
 - 3.4. Development of PI power controller
 - 3.5. Implementation of FESS power controller
 - 3.6. Optimizing of FESS power controller
- 4. Modernized FESS performance study
 - 4.1. FESS self-discharge behavior
 - 4.2. Charge retention
 - 4.3. Repeatability of FESS power control
 - 4.4. Round trip efficiency
- 5. Validation of test setup for control scenarios
 - 5.1. Moving average controller for load levelling
 - 5.2. Implementation of moving average controller
 - 5.3. Test setup for load levelling
 - 5.4. Results of load levelling
 - 5.5. Optimizing of load levelling algorithm
- 6. Research on FESS control scenarios
 - 6.1. FESS for power compensation
 - 6.2. FESS as buffer for fast charging

Summary and Conclusion

8. References

F. Plaum, T. Häring, R. Ahmadiyahangar, A. Rosin, "Power Smoothing in Smart Buildings using Flywheel Energy Storage," 2020 IEEE 14th International Conference on Compatibility, Power Electronics and Power Engineering (CPE-POWERENG), Setubal, Portugal, 2020, pp. 473-477, doi: 10.1109/CPE-POWERENG48600.2020.9161458.

C. Nazli, "Research and development of control strategies for energy storages in an islanded microgrid," 2020 Tallinn, Master thesis, Tallinn University of Technology, Department of Electrical Power Engineering and Mechatronics

F. Plaum, "Development of power conditioning control strategies for flywheel storage in microgrid," 2019 Tallinn, Master thesis, Tallinn University of Technology, Department of Electrical Power Engineering and Mechatronics

Siemens AG, "SIMATIC ET 200SP Distributed I/O system," 2019, System Manual, A5E03576849-AJ

Rosseta Technik GmbH, "Flywheel storage system T3-15," Technical documentation

9. Thesis consultants

Argo Rosin

10. Work stages and schedule

- State of the art/ literature study (01.05.2021)
- Modernizing of FESS setup (31.05.2021)
- Documentation of the new setup (15.06.2021)
- Development of controller for FESS power (15.07.2021)
- Implementation of different load profiles and control strategies (15.08.2021)
- Research on new FESS control strategies (15.10.2021)
- Description of study results (31.10.2021)
- Conclusion of thesis (30.11.2021)
- Final version of thesis (15.12.2021)

CONTENTS

ABSTRACT	4
LÕPUTÖÖ LÜHIKOKKUVÕTE	5
PREFACE	13
List of abbreviations and symbols	14
INTRODUCTION.....	15
1.State of the art	17
1.1 Electricity grid	17
1.1.1 Existing grid	18
1.1.2 Microgrids	21
1.2 Energy storage systems	25
1.2.1 Overview of different energy storage systems.....	25
1.2.2 Flywheel energy storage system (FESS)	33
1.2.3 Comparison between energy storage systems.....	36
1.3 FESS control scenarios	37
1.3.1 Load levelling of building with moving average controller	37
1.3.2 PV output levelling	40
1.3.3 FESS as power buffer in microgrid applications	40
1.3.4 FESS as buffer for fast charging of electric vehicles	41
1.4 Power hardware in the loop test setup.....	41
2.Development of P-HIL test setup	43
2.1 Previous hardware setup	43
2.2 Modernized hardware setup	44
2.3 Implementation of utility programs	47
2.3.1 Datalogging of signal	47
2.3.2 Implementation of MATLAB Simulink code	48
2.3.3 Transformation from physical to signal values.....	48
2.4 Analyzes of measured signal quality	49

3. Development of FESS power control strategy	53
3.1 FESS system identification	53
3.2 Approximation of FESS system behavior	54
3.3 Verification of approximation.....	56
3.4 Development of FESS power controller	56
3.5 Implementation of FESS power controller	59
3.6 Validation and optimization of FESS power controller.....	60
4. Modernized setup performance study	63
4.1 FESS self-discharge behavior	63
4.2 Charge retention.....	65
4.3 Repeatability of FESS power control	66
4.4 Round trip efficiency	67
5. Research on control scenarios with P-HIL	69
5.1 Load levelling of buildings	69
5.1.1 Implementation of moving average controller	69
5.1.2 Test setup for moving average load levelling	70
5.1.3 Results of moving average load levelling	70
5.1.4 Optimizing of load levelling algorithm	72
5.2 PV power levelling with P-HIL	75
5.3 FESS as buffer in hybrid storage.....	77
5.3.1 Hybrid storage simulation	77
5.3.2 Hybrid storage simulation with P-HIL.....	79
5.4 FESS as buffer for EV fast charging	81
5.4.1 Simulation of FESS as buffer for EV charging	81
5.4.2 P-HIL simulation of FESS as buffer for EV charging.....	82
SUMMARY.....	83
KOKKUVÕTE (SUMMARY IN ESTONIAN)	85
LIST OF REFERENCES	87

APPLICATION IN ENGLISH

15.09.2021

From: Luca Link (215500AAAM)

To: Ivo Palu

Application

I, Luca Link would like to request the permission to write this master in English due to the following reasons:

This thesis is prepared to obtain the double master's degree from Kempten University of Applied Sciences and Tallinn University of Technology based on the international cooperation agreement between those two universities.

I, as an Erasmus student from Germany, am not sufficiently educated in Estonian to write a Master thesis in Estonian language.

Thank you for your understanding.

Luca Link

PREFACE

This thesis was developed at the Department of Electrical Power Engineering and Mechatronics at Tallinn University of Technology for the double master's degree cooperation with University of Applied Sciences Kempten.

The thesis topic was initiated by the supervisor, early stage researcher Mr. Tobias Häring and Prof. Argo Rosin to contribute to the research and education in the Microgrids and Metrology research group. I would like to thank Mr. Tobias Häring for to support during the development of the thesis. Also, I would like to thank Prof. Argo Rosin for his support during my time in Tallinn.

Further I would like to thank Prof. Helmuth Biechl from my home university for establishing the double master's degree between the University of Applied Sciences Kempten and Tallinn University of Technology and for introducing me to the agreement.

In addition, I would like to thank research scientist Tarmo Korõtko and the other members of the research group for valuable consultations.

Luca Link

List of abbreviations and symbols

FESS – Flywheel energy storage system

P-HIL – Power hardware in the loop

PLC – Programmable logic controller

AC – Alternating current

DC – Direct current

SOC – State of charge

VRB – Vanadium redox battery

AEL – Alkaline electrolysis

PEM – Proton exchange membrane

HTES – High temperature electrolysis of steam

SOEL – Solid oxides electrolysis

PHES – Pumped hydropower energy storage

CAES – Compressed air energy storage

SESS – Supercapacitors energy storage system

MAC – Moving average controller

SIL – Software in the loop

HIL – Hardware in the loop

DUT – Device under test

BESS – Battery storage system

RTDS – Real time digital simulator

IPC – Industrial PC

TIA – Totally Integrated Automation

OB – Organization block

FC – Function

FB – Function blocks

rpm – Rotations per minute

RMS – Root mean square

INTRODUCTION

Stopping climate change is one of the biggest challenges of the current generation. Due to all the greenhouse gases emitted by humans since the beginning of the industrial revolution, the temperature of the planet started to rise. If humanity does not act, the temperature will continue to rise to a level with bad consequences. The sea level will rise, droughts will occur more often in more areas, and floods will destroy more frequently harvests. A shortage of food will put many people in danger of starvation and could force them to migrate somewhere else [1, 2]. It is assumed that climate change will be responsible for a lot of deaths due to malnutrition, heat shocks during heat waves and bad air quality [1].

To prevent this, less greenhouse gases must be released to the atmosphere. But without energy, the modern life is not possible. It is necessary in all situations, no matter if it is for heating, lighting, information, or cooking. Electricity is a very flexible energy form. It can be converted easily to other energy forms like heat or motion. Further, it can be used to produce gases like hydrogen or methane. It is assumed that due to an increase of electrification of mobility, chemical processes, and heating, the global energy demand will continue to increase in future [1].

Most of the electricity is produced by fossil fuels. Fossil fuels use natural resources like coal, gas, or petrol to produce energy. Their energy production is adjustable to the demand of energy. During the process of energy production, fossil fueled power plants emit greenhouse gases. These gases like carbon dioxide (CO₂) have a bad influence on the environment. Currently, the electrical energy production is responsible for around 27 % of global greenhouse gases emissions [1]. States plan to cut their emissions to stop climate change [2]. Therefore, alternative sources of energy are necessary.

One widely used energy source which does not produce any greenhouse gases are nuclear power plants. However, there are discussions about not using this energy source in future due to risk of nuclear disasters like Fukushima or Chernobyl and the radioactive waste which is produced as by product and must be stored over many generations. Countries like France, Finland or Great Britain are currently building new nuclear power plants [3], while other countries like Germany or Spain plan to turn off all their nuclear power plants [4, 5]. The so called fourth generation of nuclear power plant should be much saver compared to previous power plants [1]. This new generation should also be able to reuse old nuclear waste [1]. However, so far all the fourth generation reactors are still in development and testing phase [6].

Renewable energy sources do not produce any greenhouse gases during energy production. They convert natural sources like wind, sunlight, or water streams into electricity. One big drawback of renewables is the volatile behavior of nature. If it is cloudy and no wind is blowing, the energy production is low, if it is sunny and windy, the energy production is high. To compensate the energy shortage, energy storages are necessary. Another possibility to include more renewable energy sources to the energy mix without running into energy shortages is to adjust the demand of energy to the available energy. This process is called demand side management [7].

A change from fossil fuels to renewables also changes the location of energy production. With fossil fuels, a few big power plants produced a lot of energy. From this power plants, transmission lines spread the produced energy. Renewable energy sources have specific environments where they work best. For wind power plants it is for example coasts or hills, due to their stronger and more steady wind conditions. In general, the energy production is more distributed, since many smaller power plants are connected, compared to one big fossil fuel powered plant. Therefore, a change in grid architecture is necessary to share the energy more efficient. Microgrids are one solution, how to increase the overall efficiency of the grid. Here the grid is separated into several smaller cells. In a microgrid, energy production, energy storage and demand side management are controlled together [8].

This thesis will focus on flywheel energy storage systems (FESS) as one storage system component in the network of storage systems. Simulations show that FESS can be used as short term storage for power smoothing [9] or to increase the lifetime of battery storages [10]. So far, all these scenarios were only verified with simulations. In this thesis, a power hardware in the loop (P-HIL) test setup is developed. This setup enables the use of a real FESS for the analysis of control scenarios. While using a powerful programmable logic controller (PLC), different models like a battery storage can be added to the system. Due to the interface between MATLAB Simulink and the PLC programming environment, it is easy to implement different control strategies and different components. Further, the chosen PLC enables the expansion of the P-HIL with other real hardware, like a battery storage. In the end of the thesis, several use cases of FESS are analyzed with the P-HIL setup.

Keywords:

Flywheel Energy Storage System (FESS), Microgrid, power hardware in the loop (P-HIL)

1. State of the art

Due to an increase of volatile renewable energy sources, energy storages will secure the availability of energy if the demand is higher than the supply from renewable energy. Since the energy will be produced by many small and distributed sources, the grid design needs to be changed [8]. The idea is to build many small microgrids or cells, which connects the sources, storages systems and the controllable demand in a region.

In this chapter, the existing grid and the possibility of microgrids is explained. Furthermore, available energy storages systems are introduced, and their benefits and drawbacks mentioned. In detail, the principal function of a flywheel energy storage system (FESS) is demonstrated. As last, several control scenarios of FESS in a microgrid are described.

1.1 Electricity grid

The electricity grid is a network of transmission lines, which connects the producer of electrical energy with the consumers. A grid can exist of alternating current (AC) or direct current (DC), different frequencies and different voltage levels. For example, the standard voltage level in Germany can vary between 380 kV as highest level, and 230 V as lowest level [11]. The first electrical grid was installed in San Francisco in 1879. It was a system consisting of two generators powered by a coal steam engine as source, and lamps as consumer [12]. From back then to the grid we have today, it was a long journey. Most of the installed power plants in 1907 were owned by private person or companies which used the electricity on their side [12]. For their closed local systems, DC grids worked fine, since the electricity did not have to be transported. However, the DC grids of that time broke down after some kilometers. A new DC source was necessary in close distance to keep the voltage high. Different companies started their business with different approaches to bring electricity to potential customers. Some used DC, some used AC, at different voltage levels or frequencies. All wanted to sell their small power plants and small grids to as many households as possible. The result is visible in Figure 1.1. It shows a street in New York City with many individual electricity grids in 1888. Above the streets is a web of wires. Some grid works with DC voltage at 100,110,500, or higher while other companies worked with AC and a frequency of 25,30 up to 125 Hz. To bring them in order, authorities stepped in and started to regulate the electricity market. At that time, AC had two advantages over DC. It could be transported with transmission lines over longer distances, and the voltage level could be changed easily with a transformer. With the large scale power generation plant at the Niagara Falls, together with the proof of long distance electricity transmission over 170 km in Germany, the AC grid we know today got its shape [12]. The Niagara Falls power plant

was the first of many big power plants. It started the shift from local production to big plants and long transmission lines.

Due to the development of technology, today the breakdown of DC voltage over long distances is not a problem anymore. The technology of today makes it possible to step up or step down the DC voltage as required. It is even possible to convert between AC and DC voltage with a small amount of losses. Since power plants often use an electric drive to generate electricity, by default they already produce AC voltage. But with an increase of photovoltaic or fuel cells as source or batteries as energy storage system, DC voltage is getting more attention again. Even for the connection of wind farms in the North Sea, DC cables are used to connect them to the mainland [13]. High voltage DC cables are cheaper than AC wires and do not have an issue with the capacitance of the transmission line, but for the conversion from AC to DC an inverter is necessary. If the wind farm is far away from the mainland, it is economically reasonable to connect it with DC.



Figure 1.1 Electricity grid of New York City in 1888 [12]

1.1.1 Existing grid

In Western and Central Europe, the transmission system operator combined their grids to the European Network of Transmission System Operators for Electricity (ENTSO-E). It is separated into five synchronous transmission systems, see Figure 1.2. The region grid continental European (RG CE) is by power the biggest electricity grid in the world. The United Kingdom has its own transmission system (RG UK), as well as the Scandinavian countries (RG Nordic) and Ireland. The Baltic regional grid (RG Baltic) is

still synchronized with the Russian Integrated Power System / Unified Power System (IPS/UPS). For 2025 it is planned to separate the Baltic grid from IPS/UPS and synchronous it with the central European grid [14]. This will remove the energy dependency from Russia, which dates back to the Soviet Union. To connect RG Baltic to RG CE new transmission lines are necessary. The regional grids are connected via DC transmission lines for power exchange over longer distances. Currently, more DC transmission lines are under construction to generate a more optimal balance between supply and demand and use the possibility of storing energy produced by wind farms in the North Sea in pumped hydropower plants [15]. While Iceland is part of RG Nordic, it does not have any transmission line to any European country [16]. Due to its geological location, Iceland produced in 2016 65 % of its energy with geothermal power plants, and 20 % of energy with hydropower plants. The share of energy generation with fossil fuels was 15 % in 2016, mostly used in the transport sector [17]. The European and the African continent are connected via Spain and Morocco at the Straits of Gibraltar and through Turkey [16].

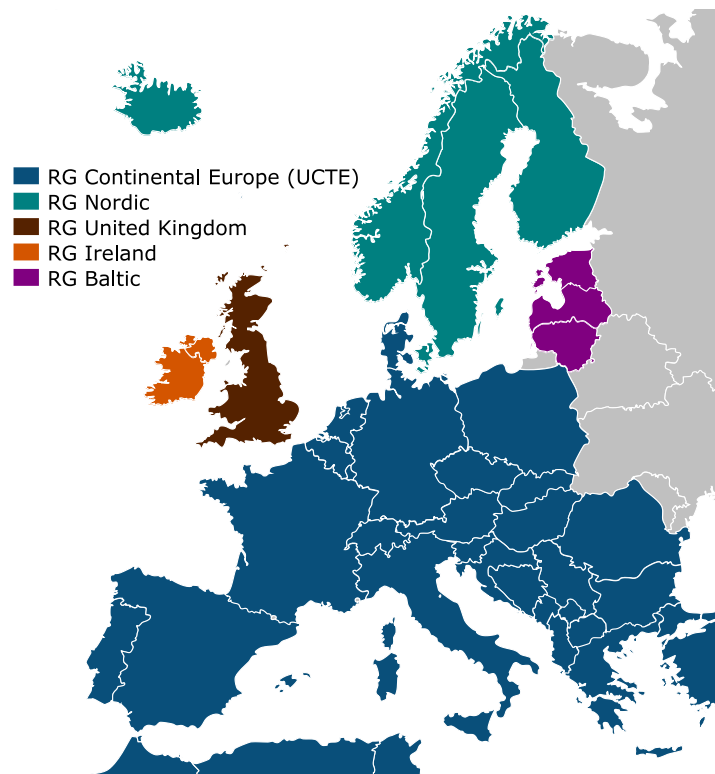


Figure 1.2 Overview of ENTSO-E regional grids [18]

The existing electricity grid is based on several bulk power plants which distributed their electricity over long transmission lines. There is only a one directional power flow from the power generation, through ultra-high voltage transmission lines and high voltage sub-transmission lines to the consumers which use medium and low voltage [19]. In

the following, the existing grid in Germany is explained in detail. The whole system is based on AC, since most power plants produce AC with their turbines that are connected to generators. Figure 1.3 indicates the locations of Germany's 20 biggest power plants in 2020. The power plants, which use lignite as fuel, are located close to the lignite mines, since lignite carries only a low amount of energy. Transporting it over longer distances makes it unprofitable. Since the south and north of Germany do not have coal as natural resource, nuclear power plants were installed to satisfy the energy demanding regions. The nuclear power plants are positioned close to rivers since they need floating water for cooling. If the water temperature is too high, the nuclear power plants have to go offline or throttle their power since they could disturb the ecosystem [20] and also since their efficiency is decreasing due to lower cooling performance [21]. The hard coal power plants are distributed more all over Germany, since the stored energy in hard coal is higher than lignite. Germany is planning to shut down their nuclear power plants in 2022 and do not use either hard coal nor lignite power plants after 2030. This means, that Germany will turn off 171 power plants of its 232 power plants with a power output bigger 100 MW. The 171 power plants produce 31,2 % of the total electrical power [22]. Germany does not have a big potential in increasing its hydropower plants. The only option to produce big amounts at one location are offshore wind farms in the northern and Baltic sea. But so far, the long transmission lines were centered around the coal and around nuclear power plants in central and southern Germany. New transmission lines are necessary to carry the electricity produced in the north to the consumers in the south [19].



Figure 1.3 Germany's 20 biggest power plants by 2020, blue pumped hydro power, yellow nuclear, brown lignite, black hard coal, ochre natural gas, data based on [22]

1.1.2 Microgrids

Since most of the bulk power plants will be turned off in future, a change in the grid design necessary. Apart from the already installed big pumped hydropower plants and offshore wind farms, most of the energy will be generated in smaller distributed power plants [8].

The main task of the electricity grid is to always serve the customer's demand in electricity. Recent events showed that the existing grid is quite fragile [19, 23, 24] and with an increase of renewable energy sources, this fragility due to imbalance between supply and demand will increase. Smart microgrids can help to solve the problems of fragility and energy supply shortages. In a smart microgrid, different small power plants, energy storages and controllable demand are connected and controlled as a unit. The microgrids are interlinked to each other and share power if necessary, but if a disturbance occurs, they can separate themselves and work in island mode. This reduces the damage and buys the transmission service operator time to fix the root of the disturbance. A schematic of a smart microgrid is shown in Figure 1.4. In the following, different aspects of a smart microgrid are introduced.

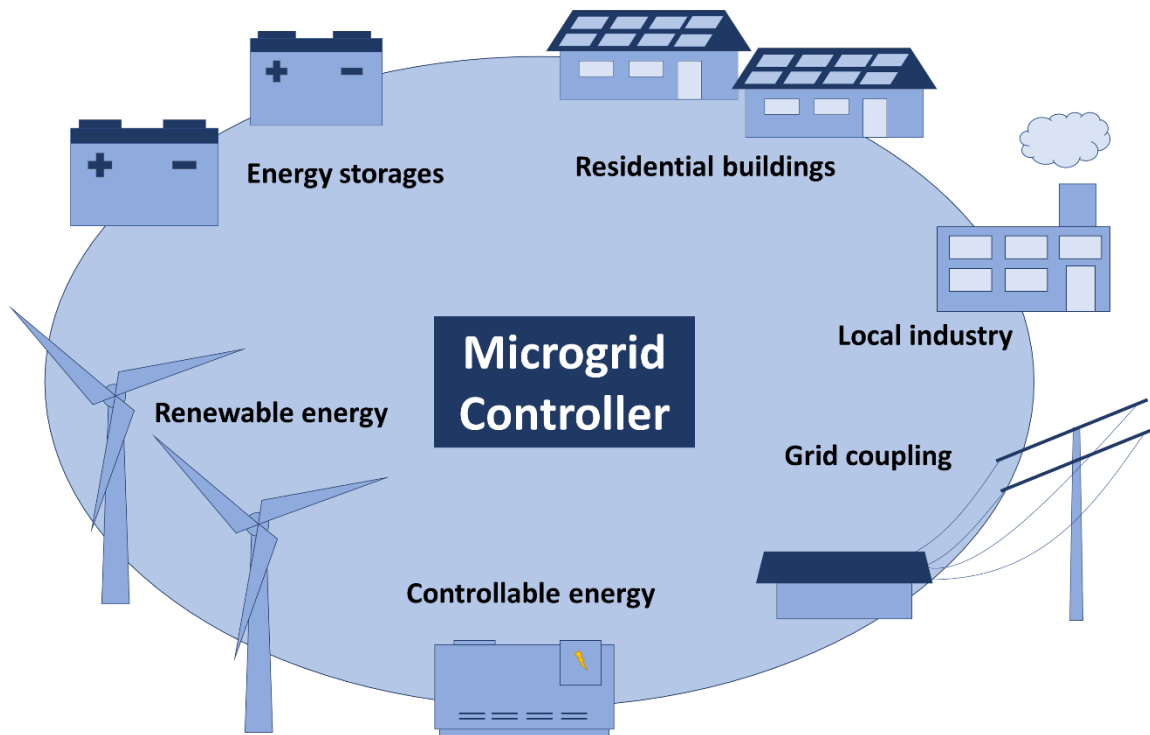


Figure 1.4 Schematic of smart microgrid and its components

1.1.2.1 Smart microgrid components

A microgrid consists of several components with different purposes. The electricity is produced in small power plants [25]. Depending on the geological circumstances, wind power, photovoltaic or hydropower can be used. Wind and PV are very volatile power sources, while hydropower is more constant. Wind power plants and hydropower plants are only one directional controllable. They can reduce the output power by throttle the torque on the generator. To do so, wind power plants change the pitch angle of the rotor blade [19] or hydropower plants reduce the amount of water which runs through the turbine [26]. Fully controllable power plants are diesel generators, fuel cells or small natural gas power plants. Diesel and natural gas plants emit greenhouse gases while producing energy. To fulfil the goal of the Paris Agreement [2] the used fuel must be produced with renewable energy sources. The same is true for the gas used in fuel cells. Producing the fuels is an energy intensive process. The controllable power plants can be used to serve high demands or as backup. An overview of the power plants is shown in Figure 1.5.

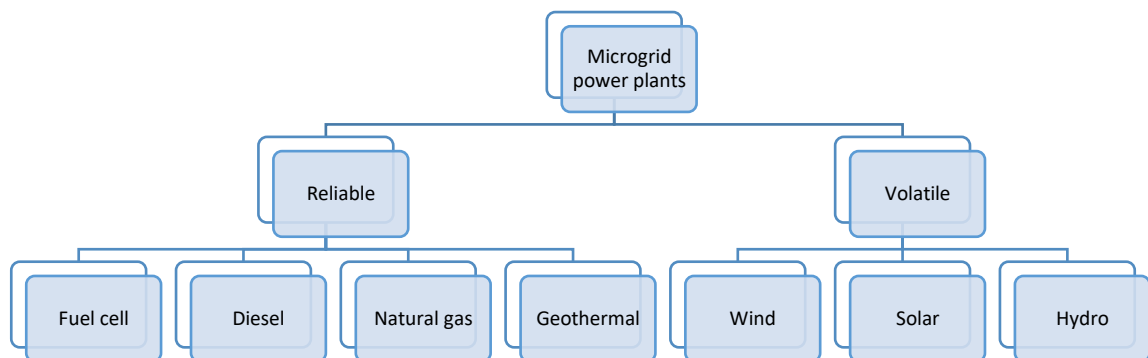


Figure 1.5 Overview of possible power plants in a microgrid

The benefits of the controllable power plants over other energy storage systems are that their fuels could also be transported from regions with a high share of renewable energy.

Energy storage systems are also part of microgrids [25]. They are, compared to the backup power plants with fuels from renewable sources, more efficient. If the demand for energy is smaller than the produced energy, the storage systems are charged. If the demand is higher than the supply, the storages are discharged. The possible storage systems are presented in chapter 1.2.

The share of prosumers, members of the energy market which produce energy but are also customers, increased in the last years, and it is expected to continue to rise with around 4 % per year till 2030 [27]. Prosumers produce energy with their power plants, mostly with PV. Some of them have their own energy storage system, which helps them to increase their energy independence from the grid further.

Microgrids have a connection to the overlaying grid. This makes it possible to exchange electrical energy over long distances. Further, the bulk power plants from renewables like offshore wind farms or pumped hydropower plants deliver energy to many customers. The voltage level of microgrids is much lower than the long, ultra-high voltage transmission lines. New transmission lines are necessary to connect the components in the microgrid and the bulk power plants.

The last component in a microgrid are the loads. A lot of research is performed on demand side management. While a lot of energy is available, the demand side management increases the demand. If less energy is available, the demand is reduced. Controllable demands are for example fridges, heating devices, or water heater. They have a variable range they can work. A freezer could reduce its temperature from the standard temperature of -18 °C to -21 °C while a high amount of energy is available, so it does not have to cool again when the energy production is reduced.

1.1.2.2 Smart microgrid design

Microgrids can work with either AC or DC [28]. Since all the current connections to households and industry are done via AC and most of the loads are designed to work with AC, it is estimated that the main grid design stays AC [28]. Using AC would make it possible to adopt a lot of the existing infrastructure. But for charging of batteries and for connecting photovoltaic to the microgrid, extra inverters are necessary. A DC grid would make it easier to integrate photovoltaic and batteries. It would work more efficient and simplifies the microgrids control [28]. In a DC grid, the current connections of wind power and hydropower plants would need a changed design for their connections. Further, household and industry must adopt their devices to the changed supply. A hybrid solution of AC and DC grid would reduce the amount of necessary inverter, but it increases the necessary infrastructure. Since currently sometimes two inverters are used for connecting a wind power plant, it is also possible to connect the DC grid to the DC-link between the inverters. However, commonly installed wind power plants use a doubly fed induction generator. They would need an extra inverter. So far, no clear advantage of one grid type is visible, and in the near future both technologies will be used.

A microgrid system consist of a distribution layer, a central control layer and individual control layer [28], see Figure 1.6. The distribution layer is the highest level. It is responsible for the distribution of energy between several underlying microgrids. It builds the market where microgrids can buy or sell energy [28]. Below the distribution layer is the central control layer, which controls the components in a microgrid. Its task is to operate the microgrid reliable and efficient [28]. The individual control layer consists of many controllers which control all the participants. This thesis is focusing on a controller on the individual control layer for flywheel energy storage systems. Depending on the used grid type and the included infrastructure, very complex control algorithms are necessary to manage the microgrid efficiently.

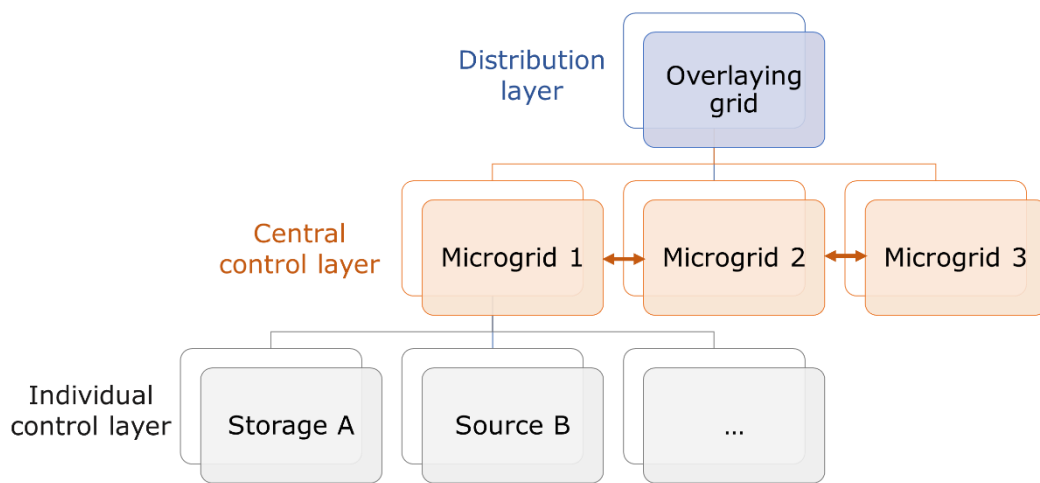


Figure 1.6 Overview of microgrid layer architecture

1.2 Energy storage systems

Energy storages systems are systems, which collect energy, store the energy, and release the energy again. The three processes are called charging, storing, and discharging [29]. During all of these processes, losses can be observed, see Figure 1.7.

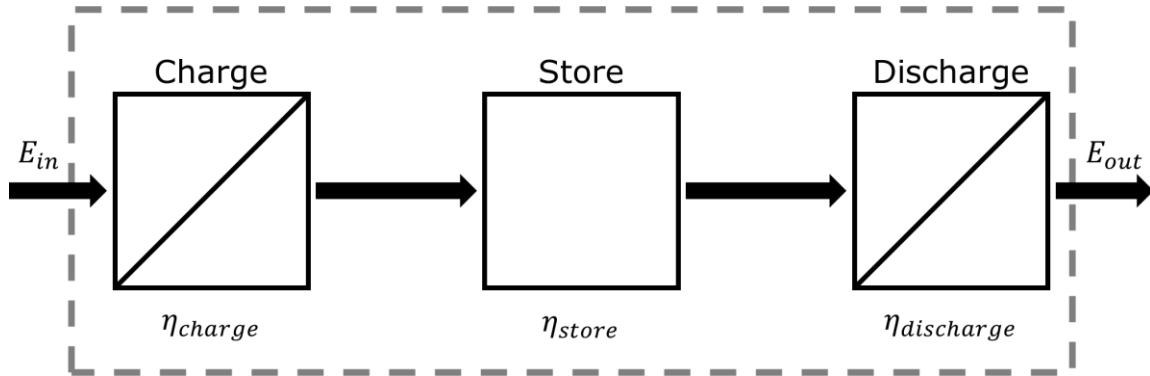


Figure 1.7 Schematic of an energy storage system, based on [29]

The output energy E_{out} is always smaller than or equal to the input energy E_{in} and can be calculated with equation (1.1) while $\eta \leq 1$:

$$E_{out} = E_{in} \cdot \eta_{charge} \cdot \eta_{store} \cdot \eta_{discharge} \quad (1.1)$$

The losses occur for example due to heating of electrical components or self-discharge due to friction. Depending on the storage system, the energy is converted from one type of energy to another. In this thesis, the focused energy type is electrical energy. The benefit of electrical energy is that it is easily converted to different energy sources like heat or motion. The problem with electrical energy is that it most likely must be used at the moment of its production. The following subchapters focus on storage systems which use electrical energy for charging, while during discharging electrical energy is released again.

1.2.1 Overview of different energy storage systems

The most known energy storage system is the battery. Batteries are electrochemical energy storage systems. Electrical energy is used for charging and released while discharging. In the storing stage, the energy is stored as chemical energy. Some of the most common batteries are lead acid, nickel, or lithium. Not all batteries are rechargeable. This is depending on the used material and its design. The most widely used battery in smartphones, electric cars, and energy storage systems for households is the lithium-ion battery [30, 31]. Since the electrical energy produced by renewable energy sources must be balanced, rechargeable batteries are necessary. The batteries

are charged with a DC voltage. While charging, electrons travel from the anode through the electric circuit to the cathode. Inside the battery, positive charged ions travel from the anode to the cathode, see Figure 1.8. For this reaction, an electrolyte material at the barrier between anode and cathode is necessary. Only ions can move inside batteries through the barrier. The travel of electrons and ions cause an oxidation on the anode and a reduction on the cathode while charging. The ions and electrons build with the cathode material a connection. Since cathode and anode material are separated via the barrier, this state does not change when no circuit is connected. While discharging, this whole process is performed in reverse [32].

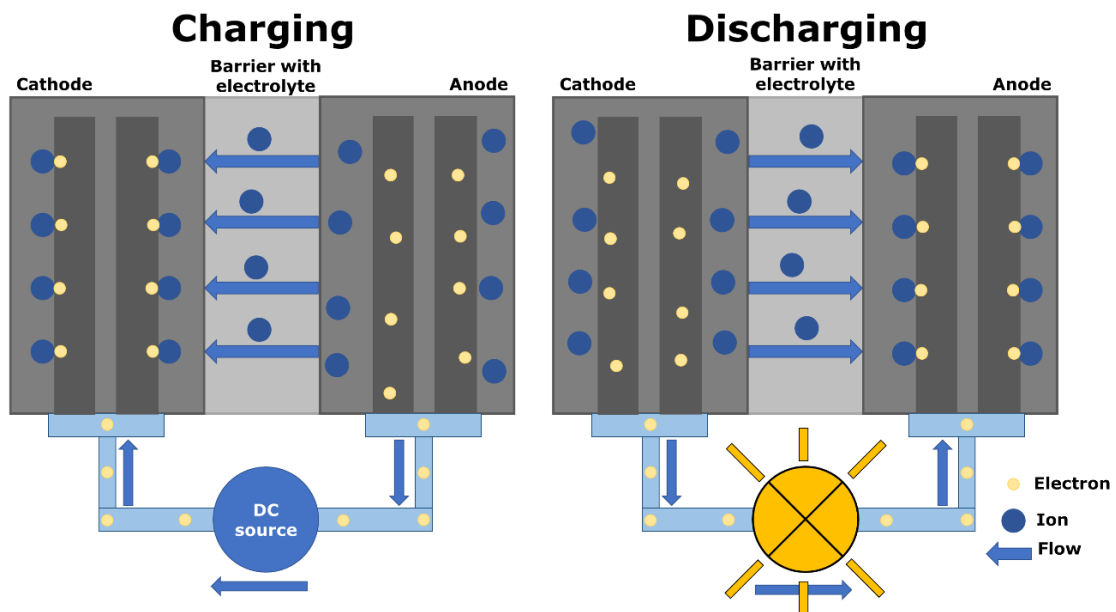


Figure 1.8 Schematic of a battery, based on [29]

In storing state, self-discharge can be observed. The self-discharge rate is depending on several parameters like the electrolyte material, temperature, or the state of charge (SOC). Batteries aging behavior can be defined by aging over time and aging per cycle. The aging over time is influenced by temperature and SOC, while the cycle reliability is influenced by charging and discharging rate, temperature, SOC and discharge depth [29]. Less charging cycles reduce the aging effects on the battery and increase the durability.

One special form of battery is the vanadium redox battery (VRB). Here the charging, storing, and discharging component of the system can be separated. A schematic of the system is visible in Figure 1.9. The system consists of two tanks and two electrodes, which are separated by a membrane. In both tanks, different electrolytes are stored. Pumps are used to circulate the electrolytes. While charging, electrolyte one releases ions. These ions creep through the membrane to electrolyte two and combine there with

the electron from the electrode and electrolyte two. For discharging, the before absorbing electrolyte two releases an electron and an ion. The ion creeps back through the membrane while the electron travels through the load. When both arrive at the electrolyte one, they combine with it. The benefit of this battery storage type is, that the energy storage capacity and power can be scaled individually [29]. Increasing the amount of electrolyte results in an increase of energy storage capacity, while stacking several cells consisting of electrodes and membrane increases the power output. Since there is no chemical reaction with the electrodes, a high durability is achieved. The electrodes only exchange electrons with the electrolytes. Since the electrolytes are stored in separate tanks, very low self-discharge occurs. Further benefits are that the used materials are eco-friendly, and it is possible to exchange the discharged electrolytes with charged electrolytes. This gives the possibility to charge electrolyte local and distributed it to consumers. Disadvantages of vanadium redox batteries are the low power density, the power consuming pump, leakage of electrolytes and the inhomogeneous voltage distribution within the cell stacks. The total system efficiency is around 70 % to 80 %.

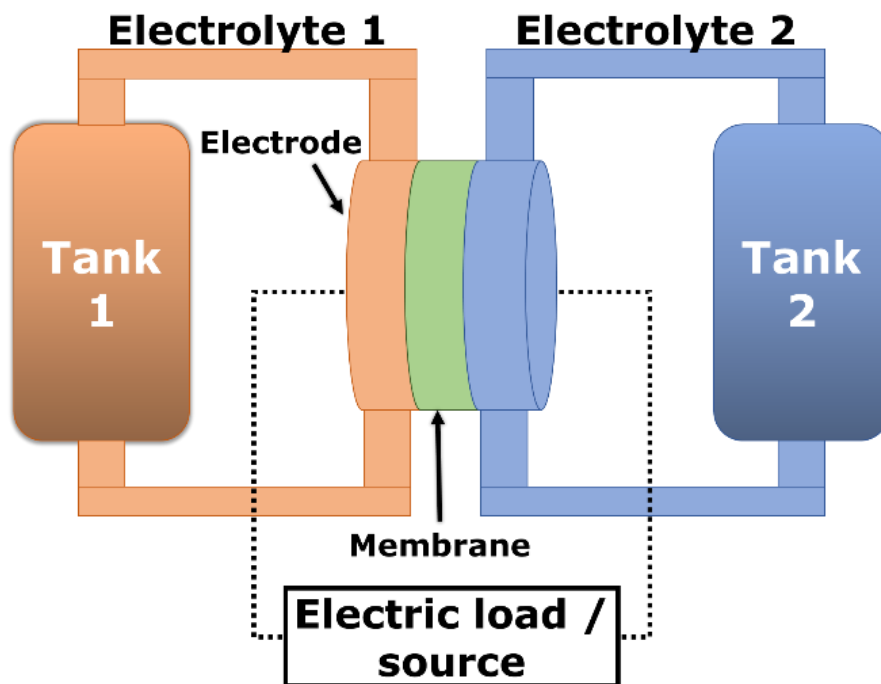


Figure 1.9 Schematic of a redox flow battery, based on[29]

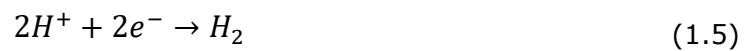
Another energy storage system is the combination of electrolyser and fuel cell [29]. Here the energy is stored in gas state. With electricity from renewable energy, water is separated into hydrogen H and oxygen O . The electrolyse process can be performed with three different methods, alkaline electrolysis (AEL), proton exchange membrane (PEM) electrolysis, and high temperature electrolysis of steam (HTES) also known as solid oxide electrolysis (SOEL). AEL is tested since many years and is available in industrial scale on the market [29]. It uses a mixture of water and potassium hydroxide for increased conductivity. The liquid is circulating in two chambers which are separated by a porous ion-conducting membrane. On both sides of the membrane, porous electrodes are positioned. A DC voltage is conducted to the electrodes. The liquid reacts with the electrons and splits it into hydrogen and hydroxide ions OH^- . The hydroxide ions diffuse to the membrane, emit their electron at the DC minus electrode and combine to water and oxygen. The resulting hydrogen and oxygen are separated from the electrolyser. The chemical equation for the positive electrode is shown in (1.2) while the chemical equation for the negative electrode is shown in (1.3).



The PEM method has its origin in the development of the fuel cell. It combines the functions of an electrolyser and a fuel cell in one component. A schematic of an PEM assembly is shown in Figure 1.10. So far it was only used in small scale applications. The PEM cell consists of two chambers separated by a membrane. On both sides of the membrane, an electrode is positioned. For the use as electrolyser, a DC voltage is applied, and water is supplied at the anode side. At the anode, the water is split into oxygen molecules O_2 and hydrogen protons H^+ and electrons, see equation (1.4).



The oxygen molecules are released while the hydrogen protons conduct through the membrane to the left chamber. In the left chamber, they combine with electrons at the cathode to hydrogen molecules, see equation (1.5). The produced hydrogen has a higher value of purity compared to AEL.



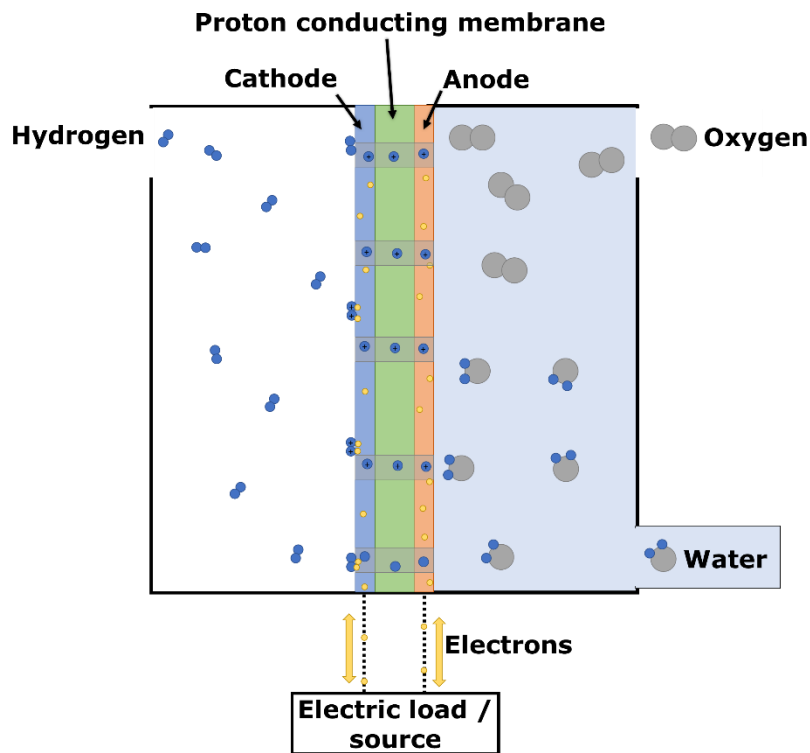


Figure 1.10 Schematic of a PEM electrolyser / fuel cell, based on [29]

The last method for hydrogen production, SOEL uses water steam instead of liquid. This reduces the necessary electrical energy for separating the hydrogen and oxygen by 16 % [29]. The necessary heat energy is supplied externally by industrial processes. As process temperature 850 °C to 1000 °C are required. The SOEL assembly is like the PEM useable as electrolyser and fuel cell. A benefit over PEM is the possibility of also separating carbon dioxide to carbon oxide, which than can be used to produce gases like methane inside the SOEL. SOEL is a young technology. Results for long time investigations are still missing [29].

The three methods of electrolyser vary in efficiency only marginally. The AEL has an efficiency between 62-82 %, the PEM electrolyser between 67-82 % and the SOEL between 65-82 %. The produced hydrogen can be stored and used when necessary. By using fuel cells like PEM fuel cells or solid oxide fuel cells, the process of the electrolyser can be reversed. The total efficiency of the conversion from electricity to hydrogen and back to electricity is between 34-51 % [29]. The before mentioned efficiencies include the use of thermal energy, is possible. Some drawbacks of fuel cell systems are, that hydrogen is a small element which diffuse easily, and the market is not prepared for mass-produced and mass-usage of hydrogen. Converting the hydrogen to methane could reduce the drawbacks, since natural gas consists mostly out of methane [33]. This would enable the use of the existing natural gas infrastructure. However, its efficiency would further decrease.

So far, all introduced energy storage systems were chemical storage systems. One mechanical energy storage system is a pumped hydropower energy storage (PHES) plant. Hydropower plants itself are one of the oldest energy sources. Already at the beginning of the electrification of industry and homes, hydropower plants were positioned at rivers to produce energy [12]. The basic idea of hydropower plants is using the energy stored in water streams to produce electricity with a generator. The stored energy depends on the volume of water, the speed, and the position and can be separated in kinetic and potential energy. The potential energy is responsible for most of the stored energy. In pumped hydropower plants, no initial kinetic energy is available. PHES use at least two reservoirs, see Figure 1.11. There is a height difference between the reservoirs. The higher the difference and the bigger the reservoir, the more energy can be stored. The stored energy can be calculated with equation (1.6). The parameter's volume V , height difference Δh and efficiency η_{total} can be influenced with the design of the power plant, while the parameter's density ρ and gravitation g are natural parameters.

$$E = V \cdot \rho \cdot g \cdot \Delta h \cdot \eta_{total} \quad (1.6)$$

For charging, a pump lifts the water from the lower reservoir to the higher. During charging losses occur due to the components like transformer, motor, pump, or pipes. A charging efficiency of around 85-90 % is reached. The self-discharge rate of pumped hydropower plants is nearly zero. To discharge the pumped hydropower plant, a valve is opened and water streams through a pipe to a generator. The overall efficiency of a pumped hydropower plant is 70-84 % [29]. Today, by far most of the stored energy is stored in pump hydropower plants. One drawback of this technology is the big impact on nature. Building big reservoirs changes the flora and fauna a lot. Also, big height differences are necessary. The alps region and countries like Norway and Sweden have the biggest potential to increase the energy storage capacity with pumped hydropower plants, but the grid is not prepared for massive energy storage in these regions.

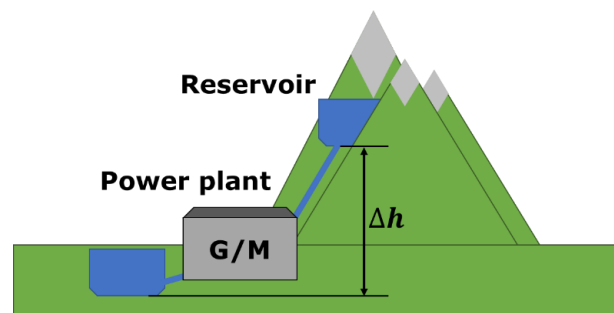


Figure 1.11 Schematic of a pumped hydro power plant

Another mechanical energy storage system is compressed air energy storages (CAES). While charging, air is compressed and pushed into big tanks. In the tanks, the energy is stored as the pressured air. For discharging, the air is expanded again. The expanded air is directed to a turbine which is connected to a generator. A schematic of the CAES is shown in Figure 1.12. During the compression, a lot of heat is generated. Hot pressured air cannot be stored. Therefore, the air is cooled down before storing [29]. The in 1978 installed CAES in Huntorf, Germany releases the heat to the environment. While discharging, heat is necessary for expanding. The CAES in Huntorf uses natural gas to heat the air while expanding. These releases CO_2 , which is bad for the climate. To reduce the effect on the environment, heat storages systems could be used [29]. The heat storages are charged with the heat produced during the compression of the air and are discharged again and release the heat energy again while expanding. This would also increase the overall efficiency of the CAES. Other solutions would be the use of hydrogen or methane produced with renewable energy sources or the connection to a heat network, which uses the heat from other industrial processes, to decrease the CO_2 emissions. So far only two grid-scale CAES are installed, but big players like MAN Energy or Siemens Energy have CAES in their portfolio [34, 35]. One drawback of CAES is the geological circumstances it needs for big storages. The idea is to use underground caverns as storage, but they are not everywhere available. Some project were already stopped due to the geological circumstances [19]. Compared with pumped hydropower plants the benefit of CAES is that air is available everywhere for free. Due to the lower efficiency of CAES, so far hydropower plants are wider used. Research in the last decades increased the efficiency of CAES. Currently, the goal of research on CAES is to make it carbon neutral and increase the efficiency further [36].

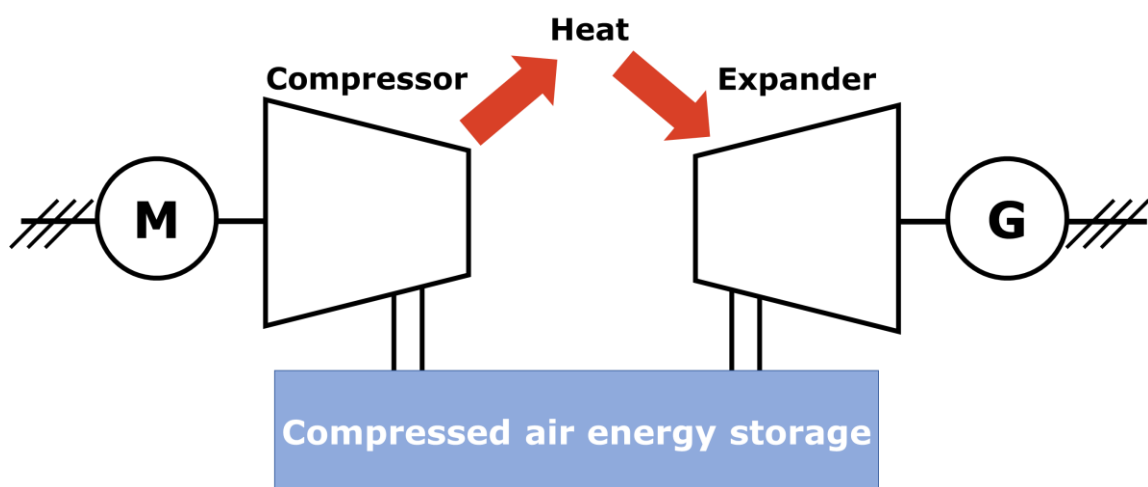


Figure 1.12 Schematic of a compressed air energy storage

One energy storage system where the energy is stored as electrical energy are supercapacitor energy storage systems (SESS). Supercapacitors are a special form of capacitor. The energy is stored in the electric field between the two electrodes. A schematic of a normal and a supercapacitor is shown in Figure 1.13.

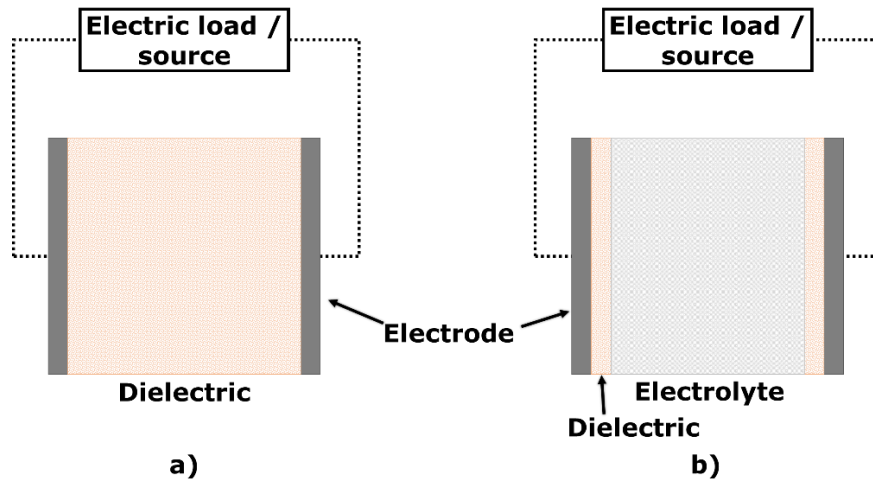


Figure 1.13 Schematic of a) „normal“ capacitor b) supercapacitor, based on [29]

The normal capacitor a) has two electrodes, separated by a dielectric layer. The supercapacitor b) has only a small dielectric film on its electrodes and an electrolyte between the electrodes. The capacity C of a plate capacitor can be calculated with equation (1.7). For the calculation, the plate area A , the permittivity of the dielectric ϵ , and the distance between the plates d is necessary. The stored energy of a capacitor can be calculated with equation (1.8). The voltage V influences the stored energy in square.

$$C = \epsilon \frac{A}{d} \quad (1.7)$$

$$E = \frac{1}{2} C \cdot V^2 \quad (1.8)$$

The use of the electrolyte in super capacitors reduces the distance between the plates significantly. As result, the capacity C increases and therefore the stored energy E . Since the electrical energy is not converted to another type of energy, it can be charged and discharged very fast, in a very efficient way. Compared with a battery, it withstands a lot of cycles without degradation, and it has a lower impact on the environment, since no harmful chemicals are used in supercapacitors. The drawbacks of supercapacitors are its self-discharge rate, the non-linear voltage drop while discharging and the high price [37].

1.2.2 Flywheel energy storage system (FESS)

A FESS is an energy storage system which converts electrical energy into rotational energy while charging. For the conversion, an electrical drive is used. The drive is directly connected to a rotational mass. Due to acceleration of the rotational mass, energy is stored in the system. The charging cycle is stopped when the rotational mass is not accelerated further. As long as the rotational mass has a velocity, energy is stored in the system. To discharge the FESS, the rotational mass is decelerated with the electrical drive and the rotational energy is converted back to electrical energy. The electric drive is the most important component of the system, since it is responsible for the charging and discharging of the system.

FESSs are one of the oldest energy storage systems. In the middle age, higher oscillating weights were used to smooth the output force of water- or windmills. With the industrial revolution in the eighteenth century, flywheels were used to balance the rotating motion of steam engines. In these constructions, the belt drive and flywheel were one component. Without flywheels which convert the linear motion of the piston of a drive to a rotational motion, the development of combustion engines would have failed [29]. The first modern FESS was developed in Switzerland. An electric bus used its braking energy and the electrical energy it charged at every station to accomplish its daily route[29]. Compared with the early flywheels, the modern FESS shares the basic principle, but due to technical improvements in the last years, their design, storage capacity, self-discharge rate, and power density differ significantly.

A schematic of a basic FESS is shown in Figure 1.14. The electrical drive, visible on top of the figure, is connected to an inverter. The drive can either be a three-phase asynchronous or synchronous induction motor, or a DC motor. Some FESSs have an extra fan to cool down the electric drive. Depending on the control signal, the inverter increases, holds, or decreases the rotational speed of the drive. This corresponds to an addition, storage, or extraction of energy. The drive is connected to a rotational mass via the shaft. The shaft must withstand high torques, produced by the drive or the rotational mass. The mass is fixed with bearings to the chamber, so it does not start to vibrate or swing while rotating. The chamber is completely closed for modern FESS. This helps to increase the safety of the system since nothing can disturb or damage the FESS while spinning. The size of a FESS can vary between the size of a small fridge, up to the size of room [38, 39]. Some companies build stacks out of several flywheels to increase their storage capacity [40, 41].

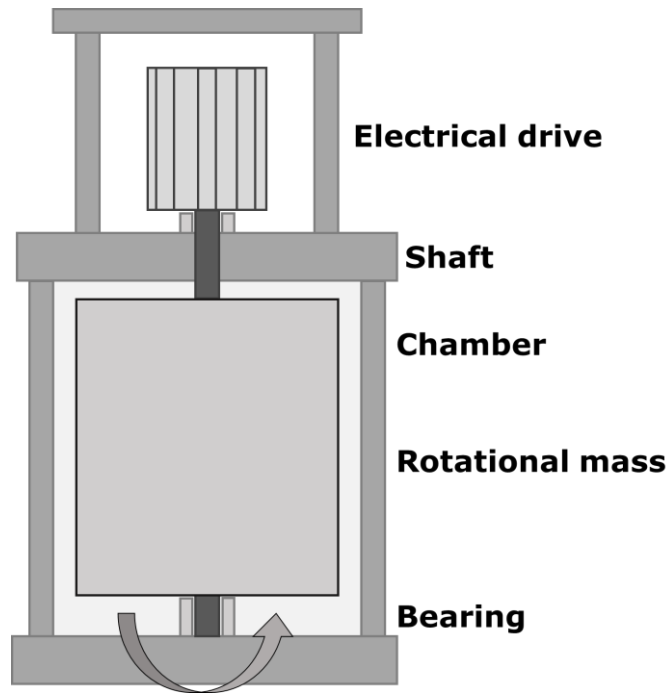


Figure 1.14 Schematic of a FESS, based on [38]

One main reason for the self-discharge of FESS is friction, either mechanical friction at the bearings or air friction on the rotational mass. To reduce the friction at the bearings, magnetic bearings can be used instead of ball bearings. To reduce the air friction, it is necessary to apply a vacuum in the chamber. Both measures reduce the friction significantly and therefore the self-discharge of FESS. The stored rotational energy E_{rot} is proportional to the square of the rotational speed ω of the FESS, see equation (1.9).

$$E_{rot} = \frac{1}{2} \cdot J \cdot \omega^2 \quad (1.9)$$

While the moment of inertia J can be calculated with:

$$J = \sum_i m_i \cdot r_i^2 \quad (1.10)$$

To increase the stored rotational energy, two measures are available. Either the electrical drive must increase the rotational speed or, due to design changes at the rotational mass, the moment of inertia is increased. Equation (1.10) describes the general calculation of the moment of inertia. It uses several point-masses m_i with a distance r_i to the rotating axis. Assuming there are two point-masses m_p , which are connected with a weightless bar with the length $2r$, the moment of inertia changes, depending on the rotational axis. In equation (1.11), a rotation around the central axes of the system is given. If the rotation is performed through one of the mass points, the mass point does not influence the moment of inertia. Due to the increase in distance of the other mass point, the moment of inertia increases, see equation (1.12).

$$\text{Central rotational axis: } J = m_p \cdot r^2 + m_p \cdot r^2 = 2m_p r^2 \quad (1.11)$$

$$\text{rotational axis at one end of bar: } J = m_p \cdot 0^2 + m_p \cdot (2r)^2 = 4m_p r^2 \quad (1.12)$$

The example shows that the same setup can have different moment of inertia depending on the position of the rotational axis. The increase of moment of inertia with non-centralized rotational axis comes with an increase of mechanical stress on the systems. The mechanical stress outvotes the increase with non-centralized rotational axis and is therefore not used.

Developments in recent years made it possible to increase the maximum possible rotational speed and increasing the moment of inertia with new materials. With higher rotating speeds, the centrifugal forces F_{cf} attacking the rotor increase quadratic, see equation(1.13).

$$F_{cf} = m \cdot r \cdot \omega^2 \quad (1.13)$$

Fiber-reinforced plastics are one new material used in rotational mass construction. It increases the potential energy storage compared to steel, see Table 1.1. Another benefit of reinforced plastics is their behavior if the rotational mass breaks due to a malfunction. While masses out of steel build a dangerous bullet, the reinforced plastics crack up in lighter, less dangerous pieces [29].

Table 1.1 Material properties for rotational masses of FESS [29]

Material	Tensile strength in N/mm²	Density in kg/m³	Specific strength in kNm/kg	Max. circumferential speed in m/s	Possible energy density in kJ/kg
Steel	1300	7800	167	410	106
Titan	1150	5100	225	570	143
Glass-fiber reinforced plastics	1300	1900	680	820	335
Carbon-fiber reinforced plastics	6300	1546	2470	1570	1570

FESS can be manufactured without any rare materials. They have a very long lifespan with only small amount of maintenance. The technology of the energy storage system is very simple compared with other storage solutions. It is possible to charge and discharge the FESS very fast. This makes it suitable for balancing the power of renewables [9].

The potential of FESS is limited due to the self-discharge rate of 3 % to 20 % in an hour [29]. This limits the system significantly. It can only be used as a short-term energy storage. The benefits of FESS are a long lifetime, very low influence of charging cycles, environmentally friendly materials and low maintenance [42]. Since FESS can be charged and discharged without degradation, it can be used to smooth the grid power or reduce the charging and discharging cycles of other energy storage systems. This could increase the life span of batteries or fuel cells [9, 10]. Due to an increase of renewable energy sources, the grid could get more and more instable. Wind gusts increase the output of a wind power plant for a short period of time, clouds reduce the output power of photovoltaic panels for a short moment. It is proven that FESS can help to stabilize the grid [43]. These fluctuations in power output can be smoothed very well with FESS, since they can be discharged or charged very fast and very often.

Companies which produce FESS are for example ABB, Amber Kinetics or Beacon POWER. They already operate several grid scale FESS in Asia and the USA. Siemens Energy reported in May 2021 that they are going to install the world's largest FESS. It is used for grid stabilization in Ireland [44].

1.2.3 Comparison between energy storage systems

In Table 1.2 all the introduced storage systems are compared. Since this thesis focuses on electrical energy, the use of thermal energy while discharging is not included in the shown efficiencies. Compressed air energy systems are not widely used so far and therefore some values currently cannot be determined.

Li-ion battery storages show with the super capacitors and the FESS the best efficiency. The lowest efficiency can be found for fuel cells. For self-discharge, Li-ion batteries and pumped hydropower perform best. The worst storage systems regarding the self-discharge rate are FESS, since due to the rotation and the occurring friction, it is harder to keep the charge. Pumped hydropower stops the pumps and closes the pipe, and the system stays charged. By far, FESS last most cycles, followed by super capacitors. Li-ion batteries perform worst in this category. In case of costs, FESS perform best again, while super capacitors and fuel cells are the most expensive storage systems. Li-ion batteries and pumped hydropower storages perform best for long term storage. However, Li-ion batteries have a big problem with the amount of cycles, they can withstand. Pumped hydropower always needs fitting geological locations and result in a big influence of the local environment. Since FESS can be cycled without ageing and compared to other storage systems their price is low, the use of FESS in microgrids as short-term energy storage is analyzed in this thesis. For short-term energy storages, FESSs are in a competition with supercapacitors. Compared with supercapacitors, FESS

are cheaper, have a longer life span and withstand more cycles[45]. The biggest drawback for FESS is their high self-discharge rate. Due to the development in the last years, this drawback is shrunk significantly. For medium- or long-term energy storages, other storage systems like batteries, hydrogen, pumped hydropower or CAES are more suitable.

Table 1.2 Energy storage comparison [29, 46]

Storage	Li-Ion	VRB	FC	PHES	CAES	SESS	FESS
Efficiency [%]	90-97	70-79	34-51	70-82	70	90-95	83-93
Selfdischarge [%/day]	0.008-0.041	0.3	0.03	0-0.5	n.a.	0.004-0.013	72-100
Cycles [n]	400-6000	7000-15000	n.a.	12800-33000	n.a.	1Mio.	>1Mio.
Costs	Medium	High	High	Medium	Medium	High	low

1.3 FESS control scenarios

Since FESSs are able to charge and discharge with high power without ageing, FESS can be used in several control scenarios. This subchapter introduces some scenarios, which will be analyzed in the end of this thesis with the developed power hardware in the loop test setup (P-HIL).

1.3.1 Load levelling of building with moving average controller

The load profile of a building depends on the size and the usage of the building. Industrial buildings have a very different power profile compared to residential buildings. However, in all profiles demand peaks can occur, due to use of different machines in the building. Some common machines which introduce a big power peak and are not used a lot over the day are coffee machines, vacuum cleaner or in the industrial area overhead cranes which lift heavy things. They are all only used over a short period of time. If the power of the building is supplied by batteries, the power peaks introduce heating of the batteries. The heat reduces the batteries lifespan. By levelling the load of the building with a FESS, the peak power is supplied by the FESS and the battery is not heated. The load levelling scenario was already analyzed with simulations in [9]. For the simulation, a load sequence with a length of two minutes. The sequence was measured from the NRG building of Tallinn University of Technology. The load profile is

shown in Figure 1.15. It consists of two peaks of around 4kW with a time distance of around one minute. A moving average filter with the length of 30 seconds is used to calculate the levelling signal for the FESS, which smooths the load of the building. Since the FESS also consumes energy for keeping itself charged, two test runs are performed. The first test run is performed without charge retention. It will indicate how well a perfect FESS could perform without self-discharge or if the FESS is charged with previously unused power. The second test run will be performed with charge retention. Modern FESS will perform better than the in the laboratory present FESS, however their load levelling behavior will not be better than the behavior of the present FESS without charge retention.

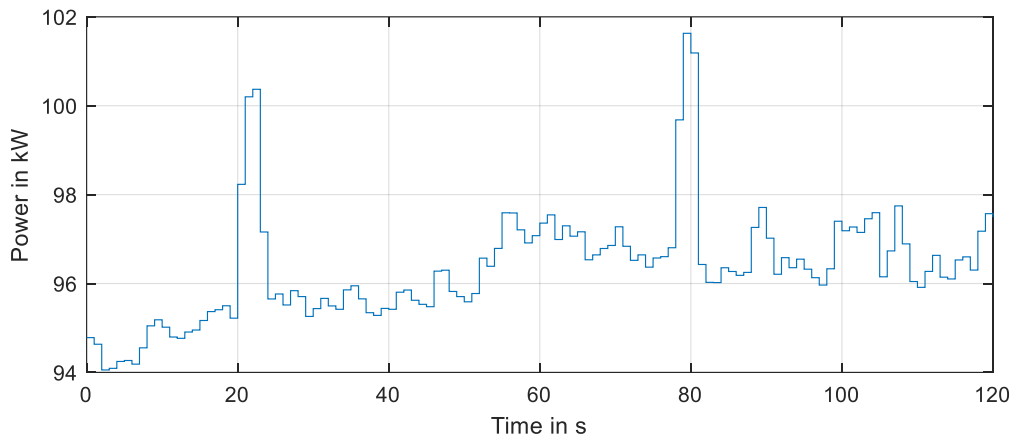


Figure 1.15 Two minutes load profile window of NRG building

The FESS is controlled with a cascaded controller design. The control structure is shown in Figure 1.16. A moving average controller (MAC) is used to determine the power which is balanced by the FESS. It builds the outer controller. As inner controller, the FESS power controller converts the power signal to the input signal of the inverter. The output power P_{out} of the inverter is fed back to calculate the error $P_{err.}$ between the aimed grid balancing power $P_{bal.}$ and the actual measured power.

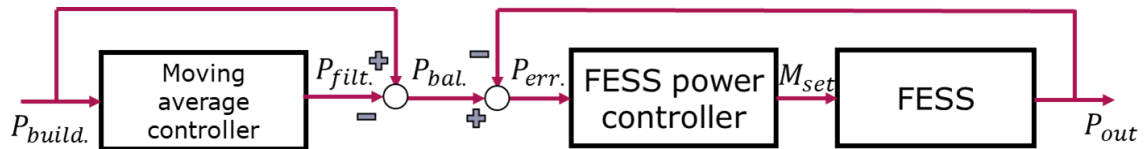


Figure 1.16 Cascaded control structure with MAC and FESS controller

The moving average control algorithm uses the previous and the current load of the building $P_{build.}[k]$ of the system and divides them by the number of values n to calculate the filter output $P_{filt.}$, see equation(1.14) [10].

$$P_{filt.}[k] = \frac{\sum_{i=k-n}^k P_{build.}[i]}{n} \quad (1.14)$$

Figure 1.17 shows the behavior of two moving average filters, one with the length five in orange and one with the length of ten in yellow. The input signal is a step function with a single impulse disturbance. The input signal is shown in blue. In total, this calculation acts like a low pass filter. Fast changes like single peaks get smoothed out, while changes over several values influence the result. The higher the number of values, the smaller one single peak influences the result. A high number of values also slows down the reaction time of the controller.

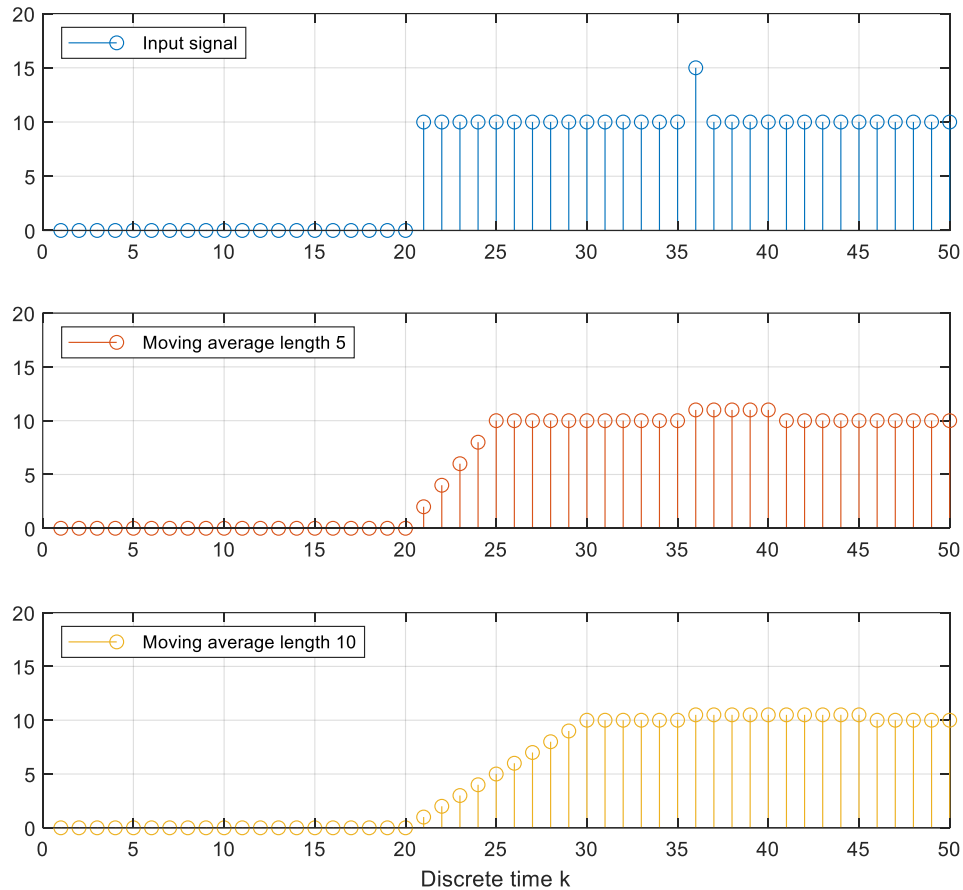


Figure 1.17 Overview of moving average filter behavior

A moving average filter helps to filter out disturbances and noise. The power which is balanced by the FESS $P_{bal.}$ is calculated by subtracting the moving average filter output $P_{filt.}$ from the current power of the load $P_{build.}$, see equation (1.15) [10].

$$P_{bal.}[k] = P_{build.}[k] - P_{filt.}[k] \quad (1.15)$$

Since this scenario was already analyzed in simulations, this scenario is used to validate the developed power hardware in the loop test setup.

1.3.2 PV output levelling

Power peaks cannot only occur in buildings, but due to the volatility of nature, the output of PV sources can vary significantly too. The same load levelling control algorithm of the previous scenario can be used to smooth the output power of an open area photovoltaic systems under volatile weather conditions. For the validation with the P-HIL, a sample of one hour between 1pm and 2pm is used. The sample profile is shown in Figure 1.18. Power smoothing of load and PV sources can also be performed simultaneously in microgrids to increase the overall power balance.

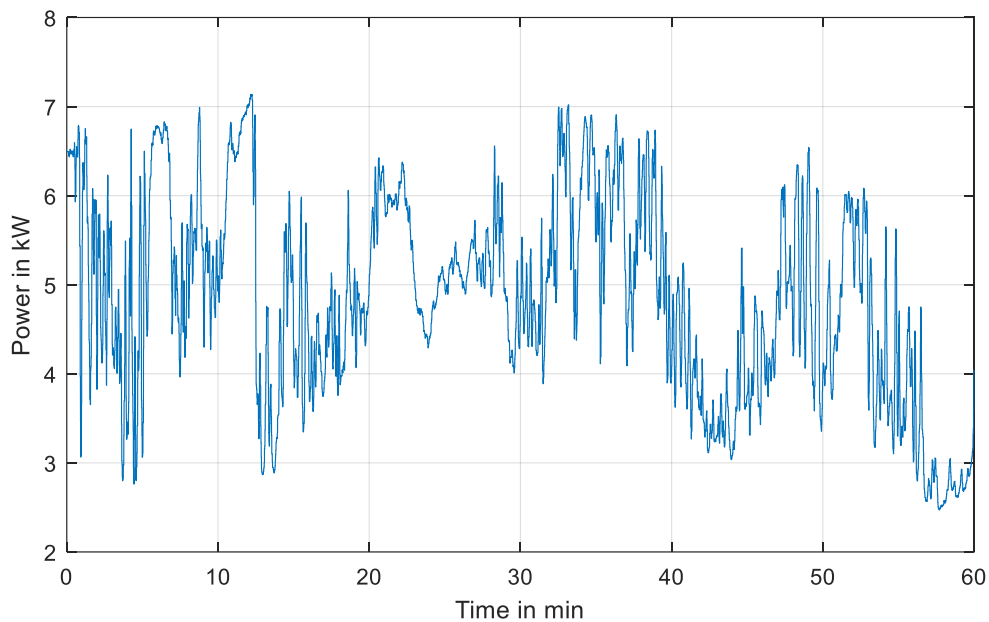


Figure 1.18 One hour PV power output profile volatile day

1.3.3 FESS as power buffer in microgrid applications

Battery storages and the existing transmission lines have a physically limited maximum power due to their design. By introducing a lot of renewables, their maximum power has to be scaled up to suit the maximum output of the renewable sources. However, since renewable sources are volatile, their output is often far below the peak power. Instead of scaling up the transmission lines or using bigger battery storages, a FESS can be installed to buffer the power. With the surplus of power, the FESS can be charged and discharged when the output of the sources is below the limits of the transmission lines or the battery storage. Additionally, the grid side inverter of the FESS can operate as static compensator (STATCOM). Here, the FESS compensates reactive power in the grid. Transmission lines must be designed according to the transported apparent power. The apparent power consists of active and reactive power. The reactive power is necessary for energizing capacitors and inductances. A STATCOM decreases the phase

difference between voltage and current. This reduces the apparent power on the transmission line and allows the existing infrastructure to carry more power. The given inverter Unidrive SP is not able to operate at STATCOM, since the reactive power cannot only be set manually. In this thesis, only a hybrid storage system consisting of a battery storage system and a FESS is analyzed. The FESS will act as buffer, when the physical charging limits of the battery are reached.

1.3.4 FESS as buffer for fast charging of electric vehicles

Fast charging of electric vehicles requires high powers from 100kW up to 350kW over several minutes. With renewable sources it is not possible to supply this power on demand since their power production is not controllable. FESS can be used as short-term buffer storage to enable fast charging of electric vehicles with renewable sources. The FESS is charged constantly with a low power from renewable sources. When the charging cycle of the electric vehicles is started, the FESS is discharged with high power. This not only enables fast charging with renewable sources, but also reduces the stress on the grid. The FESS could be positioned close to bus stations, so that the electric bus is charged from the FESS while people leave or enter the bus. One company who develops FESS for this purpose is Adaptive Balancing Power [47]. To analyze a FESS as buffer storages for fast charging, a MATLAB Simulink simulation is performed before running the P-HIL simulation. A simplified model of the FESS from Adaptive Balancing Power [47] is used for the MATLAB Simulink simulation, since this FESS is designed for powers up to 100kW. With a maximum charge of 12kWh. As electric vehicle, the Volkswagen ID3 is used with its fast charging capability of 100kW and a battery of 45kWh [48]. The used models for the battery and the FESS are similar with the models used in the setup shown in Figure 5.10. Only the parameters of the stationary battery are exchanged with the parameters of the electric vehicle, and the parameters of the FESS are exchanged with values of a different FESS.

1.4 Power hardware in the loop test setup

In software in the loop (SIL) test, the test is run on a virtual device under test (DUT). During classical hardware in the loop (HIL) tests, a hardware DUT is used and the communication between the simulation environment and the DUT is performed in real time. However, normal HIL tests do not include conducting the DUT with high power and measure the signals under real time conditions. A power hardware in the loop (P-HIL) test setup is a real time test bench, where the DUT is analyzed under real conditions. During the test, the DUT is conducted with high power and real physical signals are measured [49]. In this thesis, the device under test is the flywheel energy storage system. The previously described control scenarios are analyzed during the

tests. In Figure 1.19, a schematic of the planned setup is shown. The power profiles and the used battery models are simulated by the PLC. The models are not part of the DUT. The focus of this thesis is on the FESS. The FESS control algorithm also runs on the PLC. The PLC is controlling the inverter. The inverter is connected to the induction motor of the flywheel energy storage and to the grid. In the following chapter, the hardware setup is described in detail.

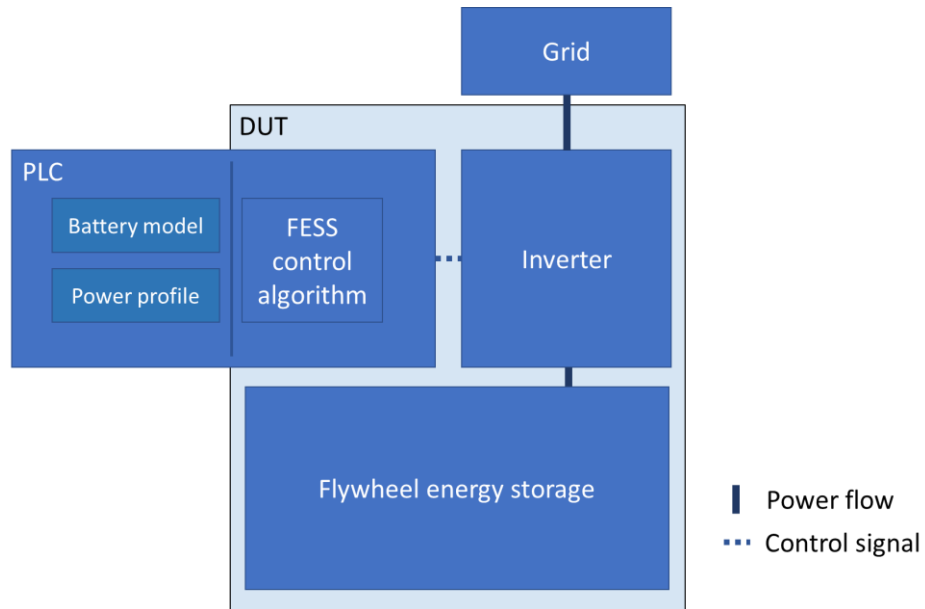


Figure 1.19 Schematic of P-HIL setup

2. Development of P-HIL test setup

To analyze the introduced control scenarios with real components, in this thesis a P-HIL test setup is developed. As base structure, an existing FESS is used. In the following subchapter, the previous hardware setup of the existing FESS is introduced. The setup was out of function due to its limited application areas. In the second subchapter, the system is modernized. The modernization enables a much more flexible use of the FESS since it allows the implementation of different control scenarios. In the third subchapter, smaller utility programs are introduced. They are necessary to perform the desired analyses of the scenarios.

2.1 Previous hardware setup

The FESS T3-15 is a system from the company Rosseta Technik GmbH. It uses two Unidrive SP 2403 inverter from control techniques, which are connected in regen drive mode. This means, that one inverter is connected to the grid, while the other is used to control the induction motor. The two inverters are connected via the DC bus. The DC bus voltage is set to 700V. The DC-link of the inverters is not connected to any external device and has no DC-link capacitor. In the previous setup the motor side inverter is connected to a basic PLC from Delta Electronics. Their communication is carried out via analog and digital control signals. The FESS has a maximum charging and discharging power of 15 kW with a usable energy of 300 kW [38]. The grid side inverter is connected directly to the grid. A schematic of the previous setup is visible in Figure 2.1.

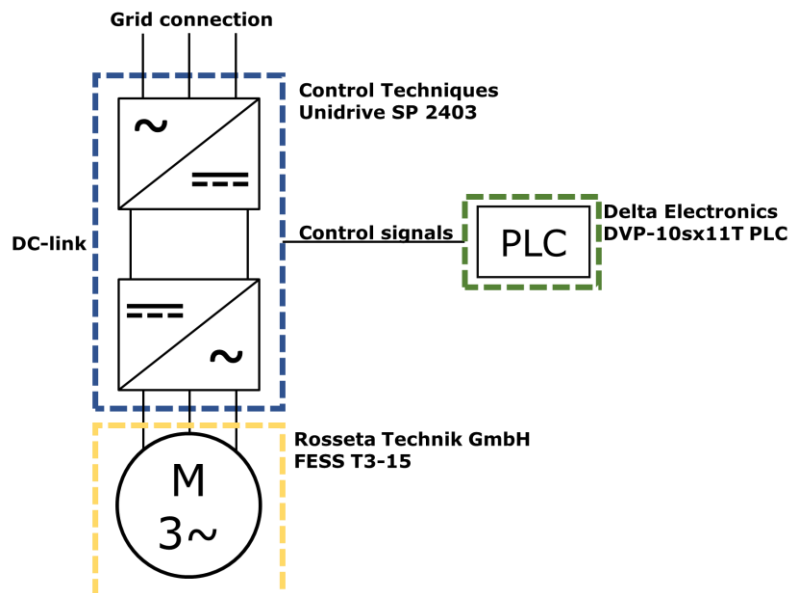


Figure 2.1 Schematic of old FESS setup

2.2 Modernized hardware setup

The modernized FESS setup will use a new PLC. To communicate with the inverter, the following requirements must be fulfilled by the new PLC:

Hardware requirements

- 2xAnalog input
 - resolution: at least 10bit
 - cycle time < 250 μ s
 - range: $\pm 10V$
- 1xAnalog output
 - resolution: at least 16bit
 - cycle time < 250 μ s
 - range $\pm 10V$
- Optional: 2xDigital input
 - range: 0-24V
- Optional: 5xDigital output
 - range: 0-24V
- 2xRJ45 port

Software requirements

- Real-time capable interface between MATLAB Simulink and PLC programming environment for control algorithms
- Cycle time < 250 μ s for control algorithms
- Communication protocol (IEC61850 or real-time TCP / UDP)

The requirements are based on the user manual of the frequency inverter EPA Unidrive SP 2403 [50], the installation guide for regen mode of the inverter [51], and the planned setup in the lab. The analog output of the PLC is connected to the analog input of the inverter which controls the induction motor. The communication is performed with a differential $\pm 10V$ 16bit analog signal. Depending on the settings of the motoring inverter, the signal is either the set rotational speed or the motoring torque. The inverters have two analog outputs. The output signals can be selected by changing the inverter settings. Commonly used signals are the active current, active power or the rotational speed. The manufacturer of the FESS installed several sensors in the setup. The sensors measure the temperature of the induction motor, the vibration of the FESS, the rotational speed of the induction motor and one phase current of the grid side inverter. All the signals are sent as analog signals. In this thesis, not all the signals are necessary and therefore not all the sensors are connected to the PLC. By adding further analog modules, it would be possible to analyze these signals additionally. It is planned to include the FESS into a network with a battery energy storage system (BESS) and a

real time digital simulator (RTDS). The communication with the RTDS should be performed with IEC61850 or real-time TCP / UDP. An overview of the planned setup is shown in Figure 2.2.

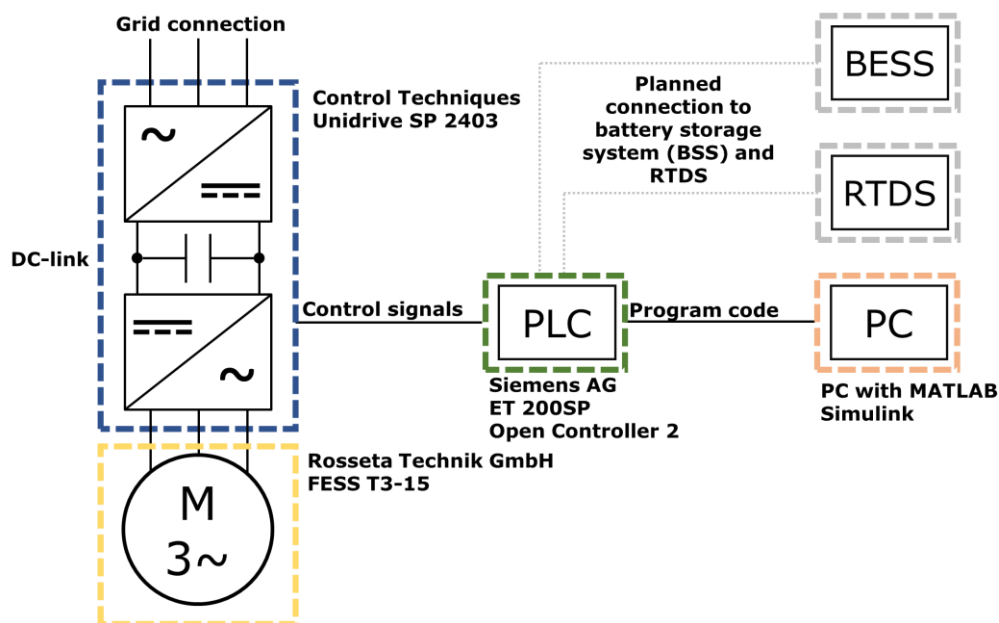


Figure 2.2 Schematic of modernized FESS setup

A request for a suitable PLC was sent to the companies located in Tallinn: ABB, Beckhoff and Siemens. In their responses, they offered their products Automation PC 910, CX5240, and ET200SP Open Controller Second Generation. An overview of the systems with a rating to the mentioned requirements is presented in Table 2.1. The table shows that only two PLC manufacturers can supply a PLC which fulfills all requirements. For the Automation PC 910 from B&R, an ABB company, it is not possible to connect analog signals. It requires an extra I/O module to connect analog signals. The available modules are too slow for the communication from the Automation PC 910 to the analog output port. A change to a field bus communication with the motoring inverter is more expensive, since an extra module connected to the inverter is necessary. The Beckhoff CX5240 is suitable for the application. The communication to the RTDS is performed via TwinCAT3 TCP/UDP Realtime. The CX5240 is powerful enough for the necessary control algorithms. As interface to MATLAB Simulink, the function TwinCAT 3 Target for Simulink can be used. It generates PLC code, which performs the in MATLAB Simulink designed control algorithm. The Siemens ET 200SP Open Controller Second Generation is ranked first since it fulfills all requirements to the lowest price. The ET 200SP Open Controller combines the functions of an ET 200SP with the benefits of an industrial PC (IPC) [52]. The used analog modules, digital modules, and bus module fulfill the requirements. The communication with the RTDS can be done via Modbus TCP or IEC61850. The IEC61850 protocol is included in the software package OPC UA. The SIMATIC Target 1500S for

Simulink function fulfills the requirements for implementing the control algorithms designed in Simulink[52, 53]. As programming environment, the Totally Integrated Automation (TIA) portal from Siemens is used. The TIA portal will run on a separate computer. The separate computer will also run MATLAB Simulink. With the Target 1500S function, the Simulink code will be converted to a function block in the TIA portal.

Table 2.1 PLC comparison

hardware requirements	ABB/B&R	Beckhoff	Siemens
Analog input	-	+	+
Analog output	-	+	+
Digital input	-	+	+
Digital output	-	+	+
RJ45 port	+	+	+
Software requirements			
MATLAB Simulink interface	+	+	+
Cycle time control algorithm	+	+	+
Communication protocol	+	+	+
Others			
Price	0	0	+
Availability	0	0	+
Ranking			
	3	2	1

+ better, 0 average, - worse

The bundle offered by Siemens has one analog output, four analog inputs and several digital output and input ports. Most of the digital ports are not used. They could be used if the energy storage is expanded, and the PLC has to control other storage system too. The differential analog output is connected to the motoring inverter as input signal. The analog input ports of the PLC are connected to the two analog output ports of the motoring inverter, to one analog output port of the grid side inverter and to the rotational speed display sensor. The motoring inverter sends the power consumption and the rotational speed. If the inverter is disabled via the disable-switch while the FESS is still rotating, the power and rotational speed signals are set to zero. The rotational speed display sensor still shows the real speed of the system. Disadvantage of the rotational speed sensor is its very slow sampling rate. The grid side inverter sends its measured power.

The cabinet of the FESS is shown in Figure 2.3. On the topside, the 24 V power supply and the new PLC are located. In the row below, some fuses and relays are located. A detailed description of the contact plan and the cabinet components can be found in Appendix 1. The cabinet in which the PLC is positioned has two RJ45 ports which can be

used for the connection to further periphery. The planned connections to RTDS and BESS are not existing so far. During the time this thesis was generated, the FESS was stored in a different location than the RTDS and the BESS setup was still in planning phase.

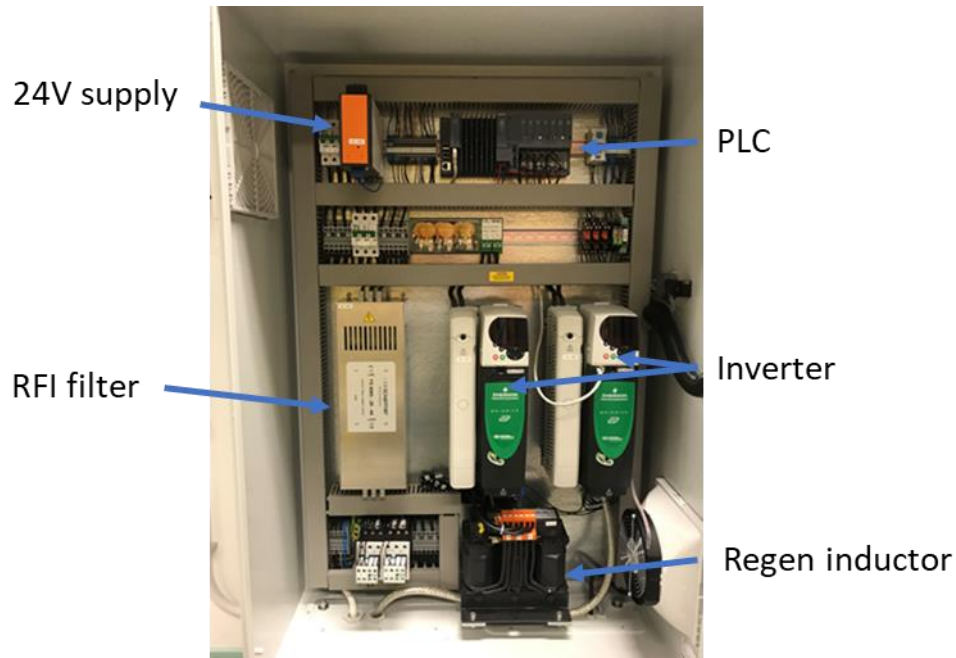


Figure 2.3 Cabinet with installed PLC

For setting the parameters of the inverter as desired, first the inverter was reset to factory settings. The parameters of the inverters were set with some minor changes according to the program-description of the ENERGIATEHNIKA 15 kW Rosseta Technik GmbH - technical documentation [54].

2.3 Implementation of utility programs

The following three subchapters give a short overview over the used utility programs. First, the data logging of the measured signals is explained. Afterwards, the MATLAB Simulink Target 1500S function from Siemens is introduced. For a detailed explanation it is recommended to take a look at [55] for data logging and at [56] for the Target 1500S functions. At last, the transformation from analog signal values to real physical signal values is explained on the PLC.

2.3.1 Datalogging of signal

To validate a test, it is necessary to log the data for later analyzes. The PLC gives two possibilities to log the data. For high sampling frequencies, the trace function of the TIA portal is used. With the trace function it is possible to sample signals with a sampling rate of up to 10 kHz. However, the amount of data processed by the trace function is

limited. Therefore, the data logger library elements are used to analyze slow signal changes over a longer period of time. For the data logger blocks, the amount of processed data is also limited, but since the data is written into a CSV file with every repetition of excusing, the TIA portal does not start to lag, and it is even possible to disconnect the programming computer for measurement. It is also possible to use several CSV files which enables almost unlimited storage of data. The sampling frequency of the data logger blocks is much smaller compared to data logging with traces. A precise value for the sampling frequency with the data logger library cannot be given, since it depends on the complexity of the overall performed algorithm on the PLC.

2.3.2 Implementation of MATLAB Simulink code

To implement MATLAB Simulink code on the PLC, first it is necessary to build a functional Simulink model. This is described in Appendix 2. With the Target 1500S function it is possible to build C code from the Simulink model, which can be executed by the PLC. The implementation into the TIA project can either be performed automatically or manually. The manual implementation is more reliable, but it also includes more tasks for the operator. For the manual implementation it is necessary to generate the function blocks out of the first source file, generated by the Target 1500S function. The other file must be uploaded to the web server of the PLC. By generating the function blocks out of the source file, at least three function blocks are created. The load and unload function blocks are necessary to load or unload the Simulink model into the memory of the CPU. It is also possible to change the control parameters of the controller in Simulink, while the control algorithm is running on the PLC. This mode is called external mode. It needs further function blocks for the implementation.

2.3.3 Transformation from physical to signal values

Since for the introduced power control algorithms physical values are used, but the communication is performed with analog values, a transformation is necessary. The communication between PLC and inverter is performed via the ± 10 V analog interface. No offset between the positive and negative side of the signal is used. An offset could be used to detect open wires or short to ground. For simplification of the calculation and since none of the devices in the cabinet is moving, the offset is not used. The analog signals between the PLC and the inverters, and PLC and the rotational speed sensor are scaled with the following formulas. The scaling is performed in the cyclic organization block (OB). The PLC interprets a voltage of 10 V with the integer 27648. For the transformation from integer to physical values, the 27648 is an essential number and is used in every calculation. It is below the maximum possible resolution of the 16 bit

analog digital converter. The higher bits are used to determine errors. The rotational speed of 5030 rotations per minute (rpm) is set as clamping speed. It is a value defined by the manufacturer of the FESS and is a set parameter of the motoring inverter.

Calculation of measured speed in repetitions per minute from inverter [50]:

$$rpm_{meas.,inverter} = \frac{value_{meas.}}{27648} \cdot 2 \cdot 5030 \text{ rpm} \quad (2.1)$$

Calculation of measured speed in repetitions per minute from display sensor:

$$rpm_{meas.,display} = \frac{value_{meas.}}{27648} \cdot 6000 \text{ rpm} \quad (2.2)$$

Calculation of measured power in W from inverter [50]:

$$P_{FESS} = \frac{value_{meas.}}{27648} \cdot P_{max} \quad (2.3)$$

$$P_{max} = \sqrt{3} \cdot V_{AC \ max} \cdot I_{Drive \ max} = 62546.279 \text{ W} \quad (2.4)$$

Calculation of measured DC-link voltage from inverter [50]:

$$V_{DC-link} = \frac{value_{meas.}}{27648} \cdot V_{DC \ max} \quad (2.5)$$

$$10V_{PLC} = 27648, \quad V_{AC \ max} = 650 \text{ V}, \quad I_{Drive \ max} = \frac{25}{0.45} \text{ A}, \quad V_{DC \ max} = 830 \text{ V}$$

The implementation of the code is shown in Appendix 3. Since the analog input signals contain a lot of noise, the signals are filtered with multiple different PT1 filter. The difference between the PT1 filters, are their parameters. The filter parameters are chosen in a way, so that their signal quality is improved, but the focus is on a short filter delay. The filter helps to reduce the noise in the measured signal, but also introduce a delay and therefore slow down the system. For setting the acceleration torque, no physical value is calculated. The only manipulation on the output signal of the controller is transformation from a real value to an integer value.

2.4 Analyzes of measured signal quality

Since both inverters share the same DC-link, the measured signal should be identical. To verify this, the inverter outputs are set to send the DC-link voltage signal. The analog input signal for the torque of the motoring inverter is set to zero.

The measured signal can be seen in Figure 2.4. The DC-link voltage signal from the grid side inverter shows a different behavior compared to the motor side inverter. The grid side inverter signal contains a regular sequence. The DC-link voltage measured with the

motor side inverter is constant at the desired value of 700 V. A measurement with a disabled motor side inverter show a similar behavior.

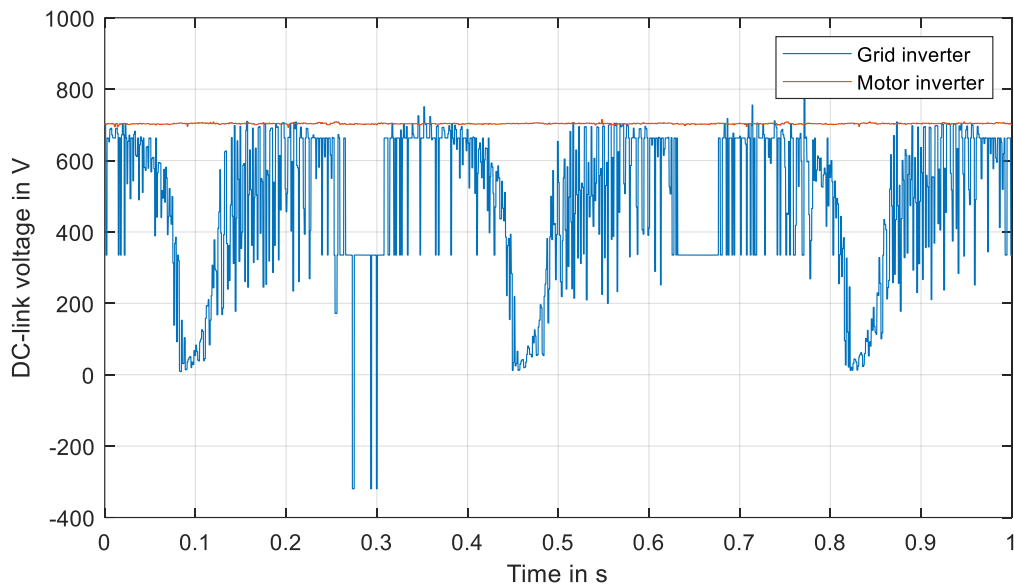


Figure 2.4 DC-link voltage measurement on both inverters

To understand the root of the sequence in the DC-link voltage of the grid side inverter, the power of the motoring inverter and the power of the grid-side inverter are measured simultaneously. Since only one connection is wired to the grid side inverter, the DC-link voltage is measured with the motor side inverter. The set torque during this test is zero and no control algorithm is used. The FESS is not rotating.

A window of the measured signal is shown in Figure 2.5. In the first plot, the grid side inverter power, in the second the DC link voltage and in the third plot the motor side inverter power are shown. If the power of the grid side inverter is positive, the DC-link is charged, if the power is negative, power is transferred from the DC-link to the grid. The grid side inverter power shows a periodic behavior. First, the power stays constant at zero for around 200 ms. Afterwards, it starts to switch a lot between maximum and minimum power. At some point it stays constant for around 50 ms before it continues to switch again a lot. In the DC-link signal, an increase in voltage during the 50ms sequence can be observed. In total, the DC-link voltage is oscillating around the desired voltage of 700 V. The motor inverter power shows a triangular signal with some peaks. The triangular signal has a similar frequency compared to the grid side inverter sequence. When the grid side inverter power stays constant, the power of the motoring inverter decreases. During the switching of the grid side inverter, the motoring power rises. With a disabled motoring inverter, the same behavior can be observed, see Appendix 4.

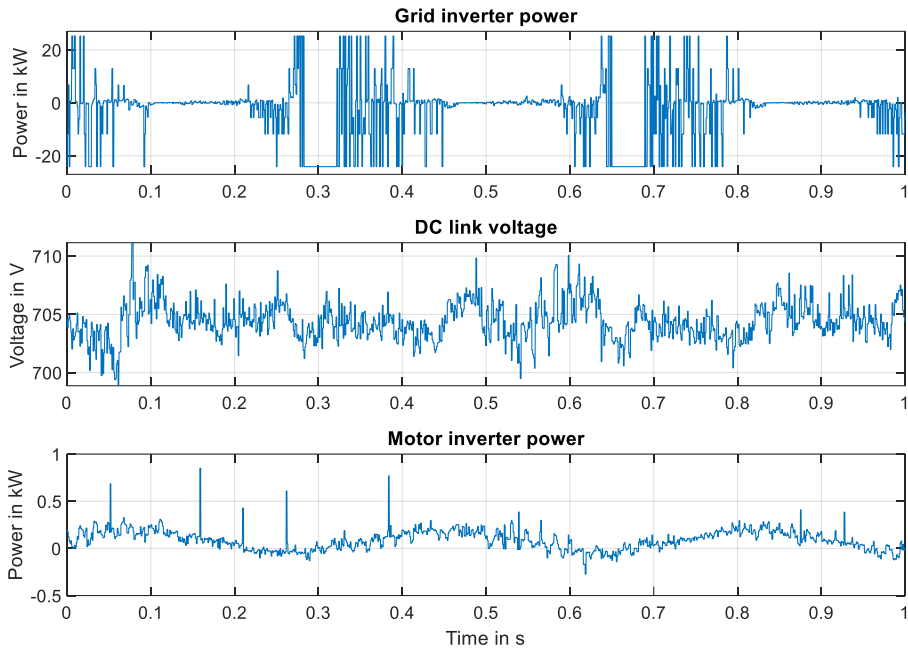


Figure 2.5 Ringing investigation with different signals

A spectral analysis on the measurement of the grid inverter power and the FESS motor power is performed with MATLAB. A description of the spectral analysis is shown in Appendix 5. In Figure 2.6 the analyzed ringing power signals are shown on the left side. The spectral analysis on the right side shows, that both signals are ringing with a frequency of around 2.7 Hz. For the grid side inverter power, several harmonics of the interfering signal are visible in the spectrum.

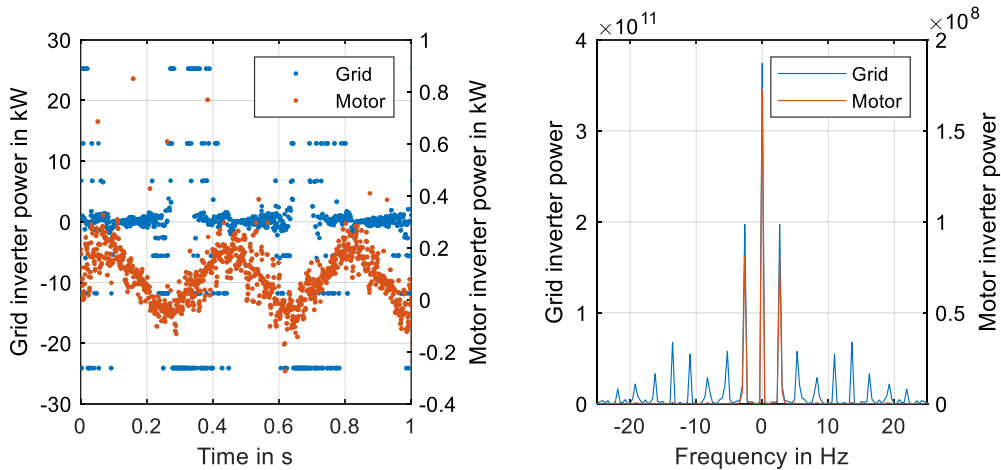


Figure 2.6 Ringing in measured power signals (left) and its spectral analysis (right)

Since the DC-link voltage is measured with both inverters, it is estimated that the analog output port of the grid side inverter is damaged. Independent of the selected signal, the output produces a signal with a lot of disturbances. Further, the signal shows a lot of changes from the maximum to the minimum signal.

The ringing can be measured with both inverters. The amplitude at the motor side inverter is much smaller. The measured average power of the motor side inverter at stand still is around 80 W. It is estimated that the ringing is caused by the power supply for the inverters. Since the inverters are not connected to the 24 V power supply of the cabinet, they take their necessary power from the DC-link or the grid. None of the inverters is working with a frequency of 2.7 Hz.

In the following chapters, the power measured with the motor side inverter is used for the calculations and control of the FESS. The losses between the grid connection and the DC-link cannot be investigated with the motor side inverter power. However, most of the losses of the FESS will occur at the mechanical side due to friction. Therefore, the electrical losses in the grid side inverter are negligibly small.

3. Development of FESS power control strategy

A FESS power controller is necessary to set the appropriate input signal to the motoring inverter. As input signal, the motoring torque is used. The FESS controller uses a PI control structure to adjust the output power of the FESS to the desired power. To choose the controller parameters, a good understanding between the set torque and output power relationship is necessary. To understand how the system behaves, several steps are applied on the inverter input, and the power and rotational speed are measured. The measured data is used to determine the system behavior. Afterwards, the controller is designed in MATLAB Simulink and implemented on the PLC.

3.1 FESS system identification

To understand the system behavior in torque control, various steps with different heights are applied on the inverter input. The torque is set as integer value on the PLC for 25 %, 50 % and 75 % of the maximum possible torque.

The measured signals of the step functions show a relationship between the set torque, the power output and the actual rotational speed, see Figure 3.1. The higher the set torque, the higher the final power output. If the rotational speed is below 3000 rpm, the output power is limited. This is a desired behavior by the manufacturer of the FESS and mentioned in the data sheet. In this thesis, it is desired to reach the necessary power as fast as possible. It is not possible to wait till the FESS accelerated to 3000 rpm so that the relationship between set torque and desired power is valid.

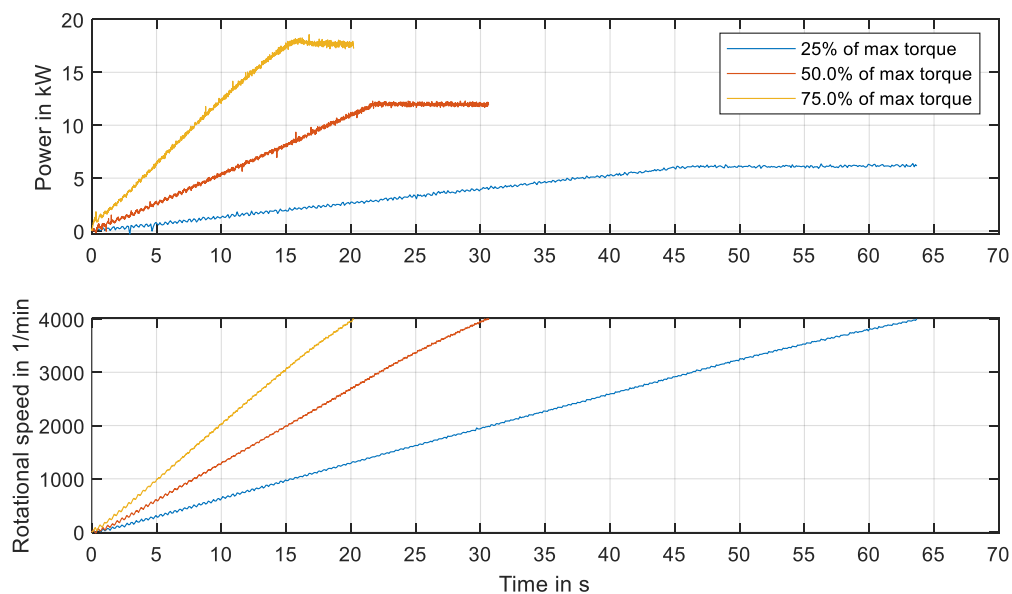


Figure 3.1 Relationship between set torque, measured power and measured speed over time

3.2 Approximation of FESS system behavior

To approximate the system behavior below 3000 rpm, several torque steps are applied to the motoring inverter. This time, the measurement is started with zero rotational speed. It is necessary to have a better system understanding for low rotational speeds, so that the desired power can be reached in a fast and efficient manner.

In Figure 3.2 the power of the FESS is plotted over its rotational speed with different set torque values. All measurements show a linear behavior between the power and the rotational speed. A trend line through zero is used to determine the slope of all curves.

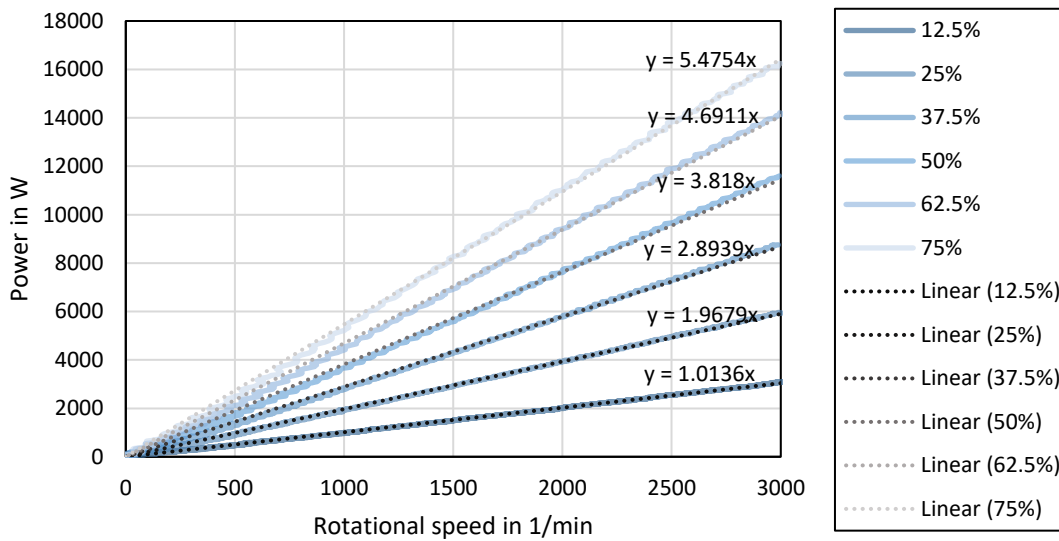


Figure 3.2 Relationship between power and rotational speed below 3000rpm

The gradient - set torque relationship is shown in Figure 3.3. Since the curve with 75 % of maximum set torque shows already signs of the systems limits, this gradient is not used in the curve. The figure shows in the area from 12.5 % to 62.5 % a linear relationship between torque and gradient.

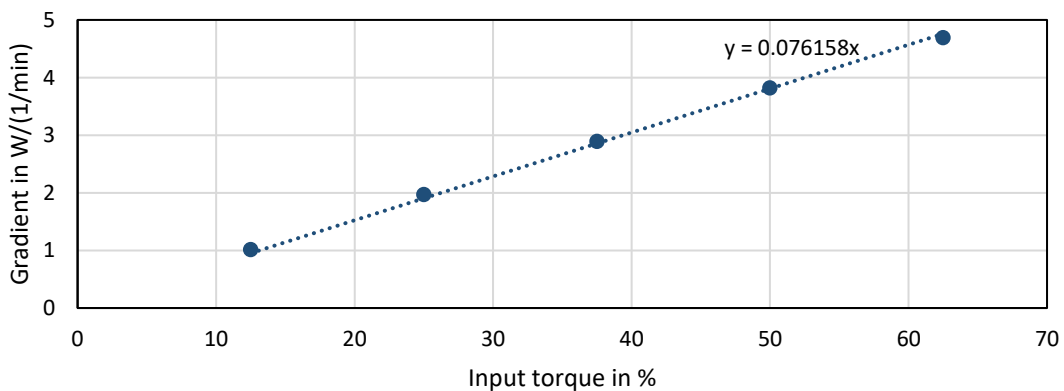


Figure 3.3 Gradient of power-speed relationship over set torque

Out of Figure 3.2 it is possible to determined equation (3.1). If the slope $k_{P,\omega}$ is known, it is possible to calculate the output power P with the rotational speed ω . Figure 3.3 shows that the slope $k_{P,\omega}$ is linear depending on the set input torque τ_{set} . With equation (3.2) the slope $k_{P,\omega}$ can be calculated out of the constant k_τ and the set torque. By inserting equation (3.2) into (3.1), equation (3.3) is derived. With this equation it is possible to calculate the output power of the system, depending on the rotational speed and the set torque.

$$P(\omega, k_{P,\omega}) = k_{P,\omega} \cdot \omega \quad (3.1)$$

$$k_{P,\omega}(\tau_{set}) = k_\tau \cdot \tau_{set} \quad (3.2)$$

$$P(\omega, \tau_{set}) = k_\tau \cdot \tau_{set} \cdot \omega \quad (3.3)$$

With $k_\tau = \frac{0.0762 \frac{\text{min}}{\% \text{int}} \cdot 100\%}{27648} = 0.000275456 \frac{\text{min}}{\text{int}}$

To verify equation (3.3), the previous measurement is compared to results of the calculation. In Figure 3.4 one the left side, the result is shown. The approximated values are indicated with a dotted line. For all set values, the calculation and real value are close to each other. On the right side, the difference between approximation and measurement is shown. For the used curves, the maximum difference is never bigger than ± 400 W. This is equal an error of 10 %. With the developed equation it is possible to calculate the necessary torque value. The rotational speed is measured continuously. The set torque value is calculated by reshaping (3.3) to τ_{set} , see equation (3.4).

$$\tau_{set}(P, \omega) = \frac{P}{k_\tau \cdot \omega} \quad (3.4)$$

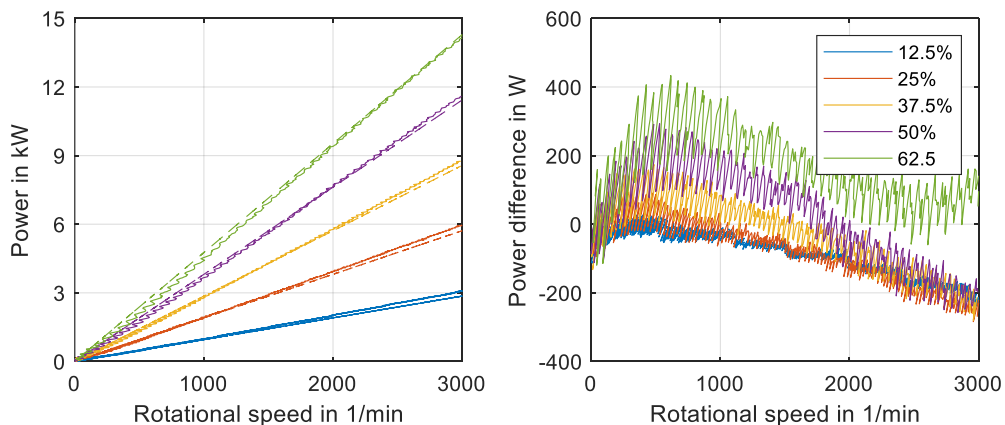


Figure 3.4 Comparison between measurement and approximation (left) and difference between measurement and approximation (right), approximation as dotted line

3.3 Verification of approximation

To analysis if the approximated equation (3.4) can be used to control the power, the equation is implemented on the PLC and a constant power is set as input. The implementation is shown in detail in Appendix 6. The FESS will start from zero rotational speed and tries to accelerate with the set amount of power. The test is performed several times with different powers.

The results of the tests are shown in Figure 3.5. The figure includes all set power values and the acceleration with maximum torque. In the beginning, all curves accelerate with the same power. The closer the measured power gets to the set power, the curve drifts off from the maximum torque curve and approaches the set value. There is always a small mismatch between desired and actual power. Further, an overshoot occurs at the beginning of the convergence.

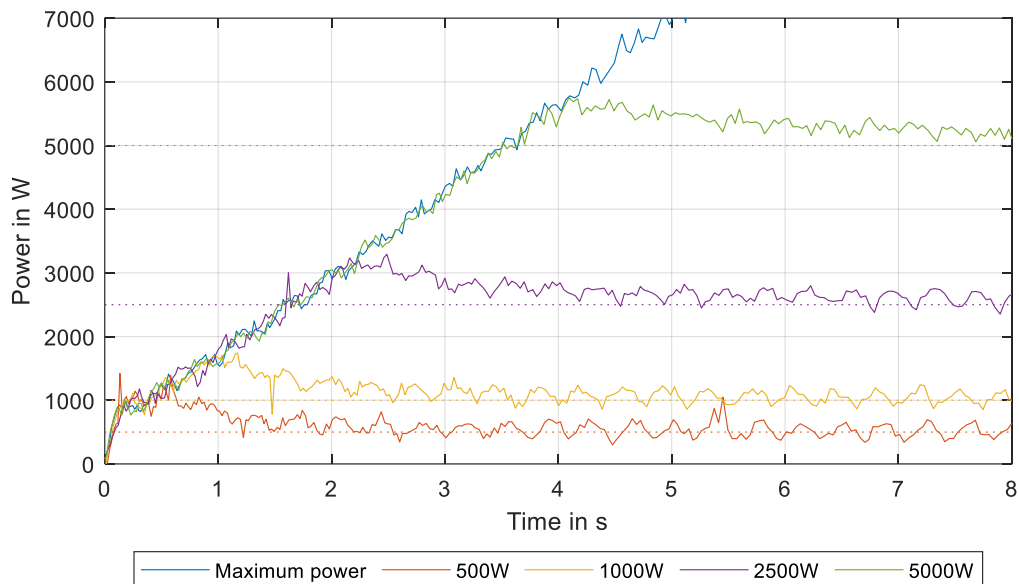


Figure 3.5 Measurement results - set power, measure power, start from zero rotational speed

3.4 Development of FESS power controller

To control the FESS power to the set power and reduce the power overshoot, a PI controller is implemented. For the parametrization of the controller, more knowledge of the system is necessary. To the input of the approximation, several steps will be applied. This time the FESS is accelerated to 2000 rpm before applying the steps.

The measurement results are shown in Figure 3.6. While the system is already spinning, no overshoot occurs. Depending on the set power, a gain error can be observed. The time till the power reaches a steady value is independent of the set value.

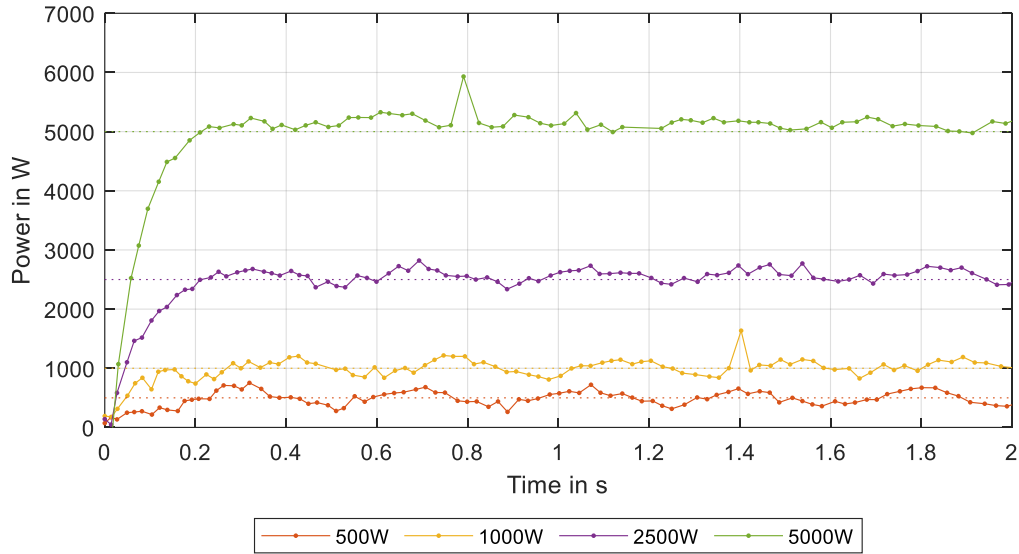


Figure 3.6 System behavior with approximation while already spinning at around 2000rpm

The result of the 5000 W test run is used to characterize the system behavior. Out of the measured graph, the gain error and time constant are determined. The power settles at around 5103 W, which results in a gain error g_{error} of 1.02. The time constant describes the time the system needs to reach 63.2 % of the set value. For the settling power P_{settle} of 5103 W, the time constant is located where the system reaches 3225 W. Since the measurement is performed with samples, linear interpolation is used to calculate the time constant. The measurement result is shown in Table 3.1 while the calculation is shown in equation (3.5).

Table 3.1 system behavior 5000 W

Sample	Time since start in s	Measured power in W
5	0.075	3074.4
6	0.095	3696.5

$$\begin{aligned}
 P_{\tau} &= P_{settle} \cdot 63.2 \% = 3225 \text{ W} \\
 m &= \frac{t[k] - t[k-1]}{P[k] - P[k-1]} = 3.21 \cdot 10^{-5} \frac{\text{s}}{\text{W}} \\
 n &= t[k] - m \cdot P[k] = -0.02384 \text{ s} \\
 \rightarrow \tau &= m \cdot P_{\tau} + n = 0.0798 \text{ s}
 \end{aligned} \tag{3.5}$$

As result, the transfer function of the system is described as in equation (3.6).

$$G(s) = \frac{b}{s+a} = \frac{g_{error} \cdot \tau^{-1}}{s + \tau^{-1}} \tag{3.6}$$

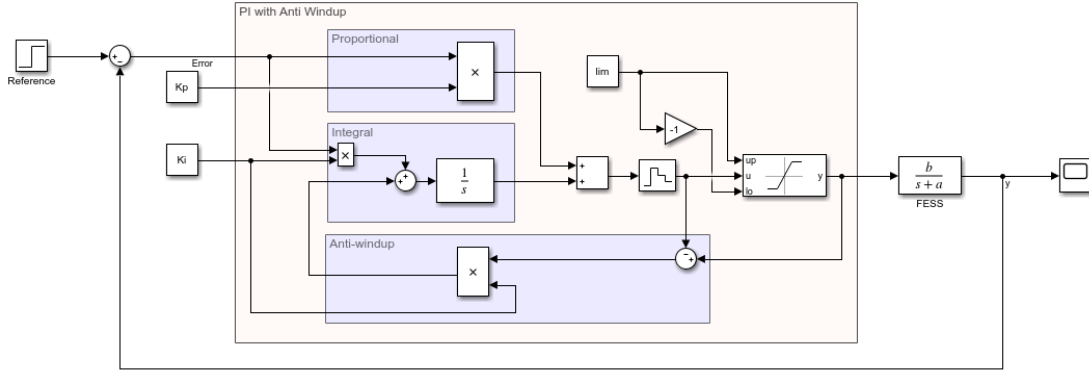


Figure 3.7 Simplified model of FESS with PI power control structure

In Figure 3.7 the model of the whole system out of PI power controller and FESS is shown. The open loop transfer function $G_0(s)$ describes the model from the error to the output signal y . Therefore, the feedback path is not included. The system transfer function $G(s)$ describes the function from the references to the output y including the feedback path. To determine the open loop transfer function, the anti-windup structure is ignored. This simplifies the equation. The open loop transfer function is given in (3.11).

$$G_0(s) = \left(K_p + \frac{K_i}{s} \right) \cdot \frac{b}{s+a} = \frac{b \cdot (K_p \cdot s + K_i)}{s^2 + a \cdot s} \quad (3.7)$$

The closed loop transfer function $G(s)$ can be determined with equation (3.11).

$$G(s) = \frac{G_0(s)}{1 + G_0(s)} = \frac{b \cdot (K_p \cdot s + K_i)}{s^2 + s \cdot (a + b \cdot K_p) + b \cdot K_i} \quad (3.8)$$

To calculate the controller parameters via pole placement, the denominator of the resulting closed loop transfer function is compared with the denominator of the wished behavior of a transfer function of second order. The denominator of the wished transfer function is given with:

$$s^2 + s \cdot 2 \cdot D \cdot \omega_0 + \omega_0^2 \quad (3.9)$$

As last, the control parameter K_p and K_i are calculated:

$$a + b \cdot K_p = 2 \cdot D \cdot \omega_0$$

$$K_p = \frac{2 \cdot D \cdot \omega_0 - a}{b} \quad (3.10)$$

$$b \cdot K_i = \omega_0^2$$

$$K_i = \frac{\omega_0^2}{b} \quad (3.11)$$

With $D = 1$ and $\omega_0 = 10$ the controller parameters are given with:

$$K_p = 0.5851 \text{ and } K_i = 7.8276$$

3.5 Implementation of FESS power controller

As shown in Figure 3.7, the FESS power controller consists of an PI-controller with anti-windup structure. The controller structure was designed in MATLAB Simulink, since simulations were used to determine the system behavior before the code was implemented on the PLC. For the implementation, the constant controller parameters K_p , K_i and the saturation limits are exchanged with input ports. This gives the user the possibility to change the parameters easily in the TIA portal without adding further function blocks or generating new source files repeatedly. The back calculating anti windup structure ensures, that the integrator output does not continue rising when the system reaches its limits. For the back calculation, the parameter K_i is used. Due to the zero-order hold block before the saturation block, the controller output is a discrete signal and can be used in a TIA project. With the Target1500s function the PI controller structure is implemented in the project.

The whole FESS power control structure is implemented in a function (FC). The FC is executed in cyclic OB and consist of several networks which perform the necessary calculations. First, the control error between desired power and measured power is calculated. Due to the on-site power of the FESS, the measured power at stand still is already around 200 W. With a reference value of zero, the error is always negative. The integrator part of the PI controller will run to its limit. To prevent this, a function called integral stop is positioned between the error signal and the PI controller. If the rotational speed is below 200 rpm and a power below 200 W is desired, the input value of the PI controller is zero. This enables the charging of the FESS but limits the discharging below 200 rpm. Above 200 rpm, the error is fed through the function. The output of the integral stop function is used as input of the PI controller. The controller parameters are chosen as described in chapter 3.4. The saturation limits are selected at 17 kW. The FESS is designed for 15 kW, however for a short period of time more power can be supplied. This is visible in Figure 3.1 for the 75 % curve. The PI controller output is used as input for the approximation FC. The approximation of chapter 3.2 is only performed if the rotational speed is below 3000 rpm. For rotational speed between 3000 rpm and 5100 rpm, the input signal is fed through the FC without manipulation. If the rotational speed is above 5100 rpm, the approximation FC sets a torque of zero. This limits an acceleration above the system limits. An increase above the limits could damage the FESS and must be avoided. Since the FESS is also able to spin in reverse direction, the approximation FC sets a torque of zero if the rotational speed is below 200 rpm and a negative power is applied. A detailed description of all the used functions, function blocks (FB) and organization blocks can be found in Appendix 7.

3.6 Validation and optimization of FESS power controller

To analyze the performance of the developed FESS power controller via torque, a constant power of 10000 W is applied for charging the FESS.

The measured result is shown in Figure 3.8. It is visible that a big overshoot in power occurs before settling to the set value. The power slope stays constant also after passing the set value. This indicates that the integrator part of the PI controller reached its limits. Until the measured power passed the set power, the error is in positive direction and the integrator increases. After the measured power passes the set power, the integrator starts to decrease from its limits. Further, a decrease in the measured FESS power can be observed when the rotational speed reaches 3000 rpm. Since the approximation is only performed below 3000 rpm and its multiplication factor is not equal to one at 3000 rpm, a step in the set torque can be observed.

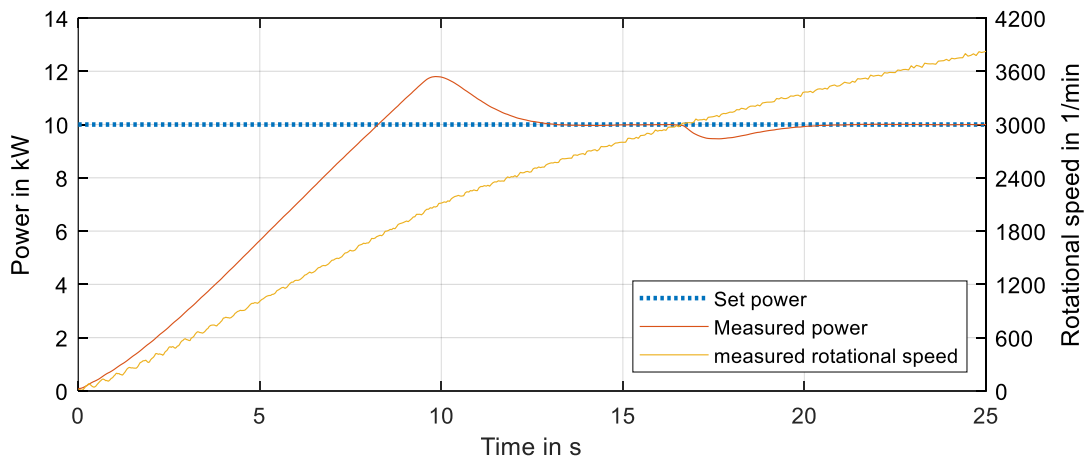


Figure 3.8 Power controller validation

To remove the step at 3000 rpm, it is necessary to multiply the desired set torque with the constant factor occurring at a rotational speed of 3000 rpm. The factor is calculated with equation (3.12), derived from equation (3.4). The multiplication with the factor is included into the approximation FC in the range between 3000 rpm and 5100 rpm.

$$a_p = \frac{1}{k_t \cdot \omega} = 1.150977 \quad (3.12)$$

By using flexible saturation limits, the windup of the integrator can be reduced. This should remove the occurring overshoot. For a rotational speed below 3000 rpm, the limits are calculated depending on the measured rotational speed. For the calculation, the trend line with maximum set torque is used. The graph with maximum torque is shown in Figure 3.9. The trend line slope is used as factor m for the calculation. Since

the power calculation for a rotational speed of zero is a power of zero, no acceleration of the system would be possible. Therefore, a constant power limit of ± 1200 W is set at a rotational speed below 200 rpm. The implementation on the PLC is shown in Appendix 7.

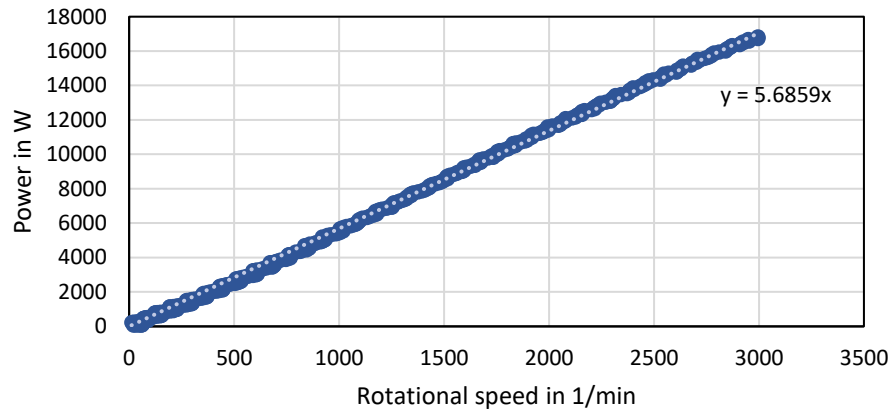


Figure 3.9 Relationship between maximum power – rotational speed below 3000rpm

The results of the optimization are shown in Figure 3.10. The tuning with the trend line removed the overshoot. However, the slope of the power curve decreased compared to the first measurement. The goal of the controller is to reach the desired power as fast as possible. To increase the slope, the factor m is increased from 5.69 to 6 and 6.5. With a factor of 6.5 the previous curve and the curve with removed overshoot fit almost all the time until the set power is reached. The factor 6.5 will be used for all the further work. Due to multiplication with the factor of (3.12), the decrease in power at 3000 rpm is removed completely.

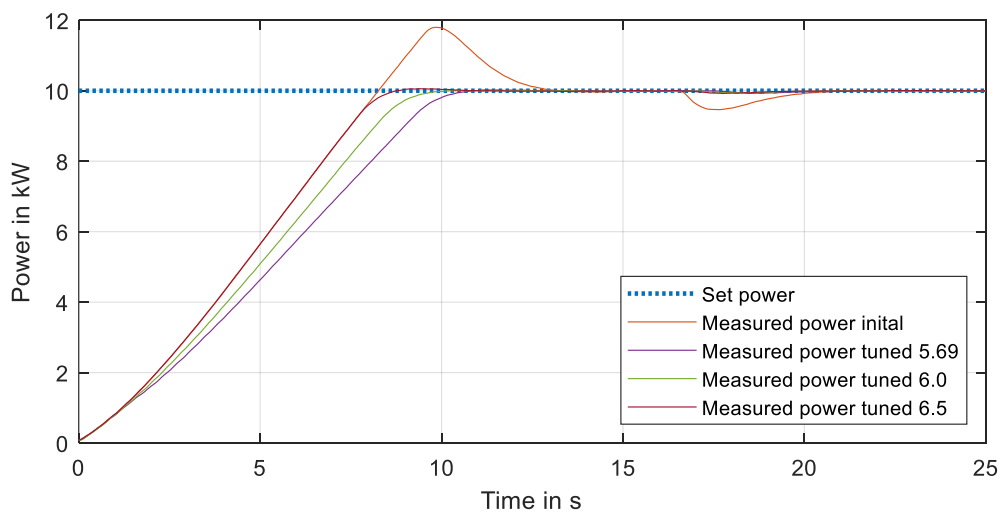


Figure 3.10 Results of controller optimization

The final performance of the FESS power controller is shown in Figure 3.11. Here a step is performed from zero power to 5 kW power while the FESS is already pre-charged. It is visible that the system takes around 0.5 s to settle around the set value. To decrease the settling time, the PI controller parameters are tuned. By changing the integral part to 13.5 and the proportional part to 0.8, the controller takes around 0.2 s till it settles. Based on the developed control algorithm, a laboratory training was produced. It can be found in Appendix 8.

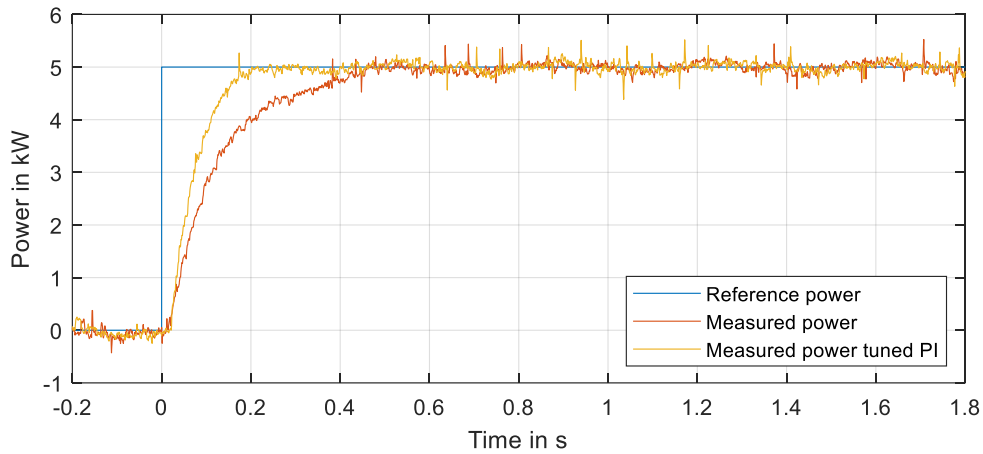


Figure 3.11 FESS power controller - step response

To analyze the accuracy of the controller, a constant power of 5000 W is set for charging the system. The power is measured from a rotational speed of around 850 rpm up to 5000 rpm.

The system needs around 75 s for the acceleration with 5000 W to 5000 rpm. The average measured power over this test is 5000.5 W, while the median is 5006.5 W. The maximum power is 5197.2 W while the minimum is 4809.5 W. The standard deviation is around 64.7 W. The noise distribution stays constant over the full measurements in time, see left side of Figure 3.12. The rotational speed has no influence on the noise, see right side. More measurements points are located at higher speed since the energy increases by the square of the rotational speed, see equation (1.9).

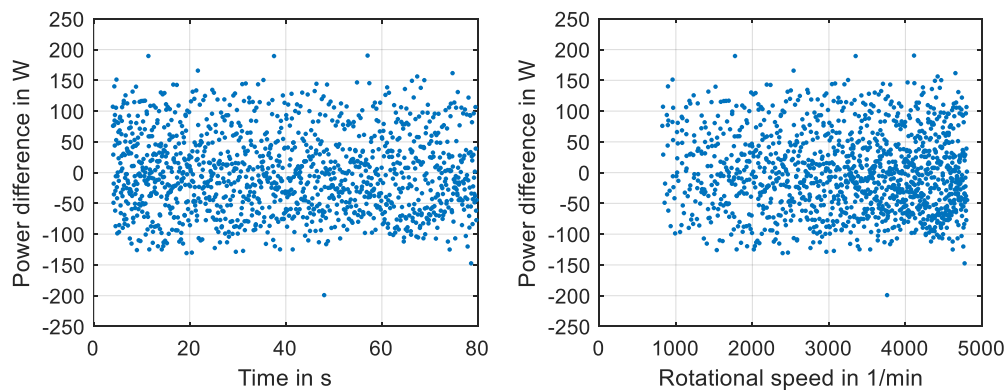


Figure 3.12 Power difference over time (left) and over rotational speed (right)

4. Modernized setup performance study

This chapter includes several tests which indicate the overall performance of the P-HIL test setup. First, the self-discharge behavior and the charge retention are analyzed. Afterwards, the repeatability and the round-trip efficiency are investigated. The repeatability shows how reliable the system is following the set signal. The round-trip efficiency indicates how efficient the FESS is working.

4.1 FESS self-discharge behavior

Since the FESS is used as energy storage, the self-discharge behavior is an important property. In the following, three different scenarios are applied to the inverter. Before starting the self-discharge scenarios, the FESS is accelerated to 5000rpm. In the first scenario, the output power of the motoring inverter is controlled to 0W. During the second scenario, the PLC applies a torque input signal of zero to the inverter. In the last scenario, the inverter disable switch is in disable position, so that the inverter stops to control the motor. In all scenarios the rotational speed is measured with the PLC and the state of charge is calculated.

Figure 4.1 shows the results of the self-discharge measurement. It is visible that the zero-torque and the zero output power scenarios discharge the FESS much faster than in the disabled inverter scenario. With zero power, the FESS is completely discharge already after 7 min. With zero torque, it takes around 10 minutes till the FESS self-discharged itself. In case with zero power, the FESS supplies the 200 W self-consumption of the inverter. Therefore, the FESS is actively discharged in this scenario. In the disabled scenario, the FESS still has a charge of around 30 % after one hour.

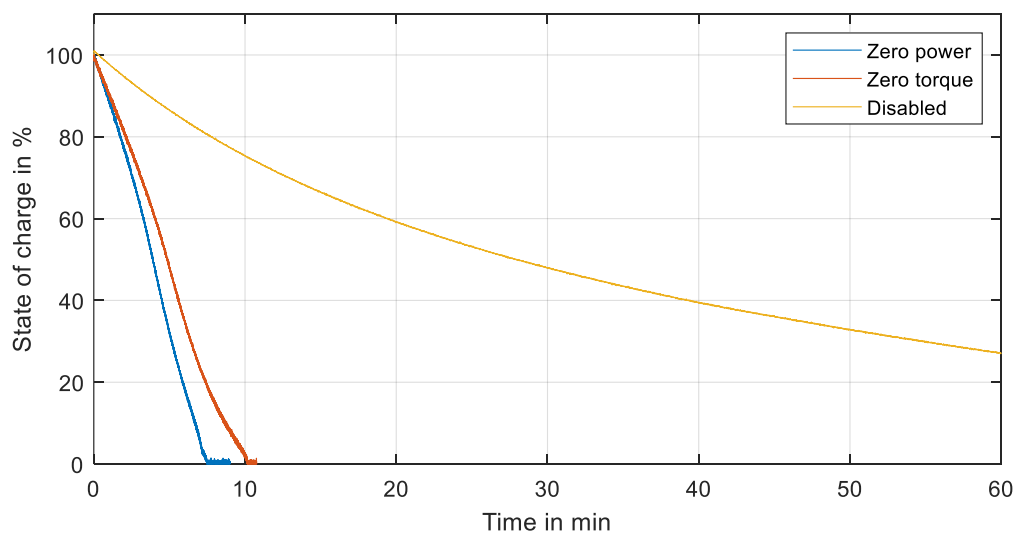


Figure 4.1 Self-discharge of FESS during different conditions

In Figure 4.2, the power flow of the motoring inverter during the zero torque and zero power scenarios is shown. It is not possible to measure the power flow during the disabled scenario, since the inverter stops to deliver the power signal in disabled mode. It is visible that during the zero-power scenario, the measured power is oscillating around zero as long, as the FESS contains some charge. When the FESS is completely discharged, its power is increasing to a power of around 200 W. This is the same value which can be measured for the FESS at stand still without control. During the zero-torque scenario, the power first stays constant. After around four minutes at a state of charge (SOC) of around 60 %, the power is reduced to the same power as if the FESS is at standstill.

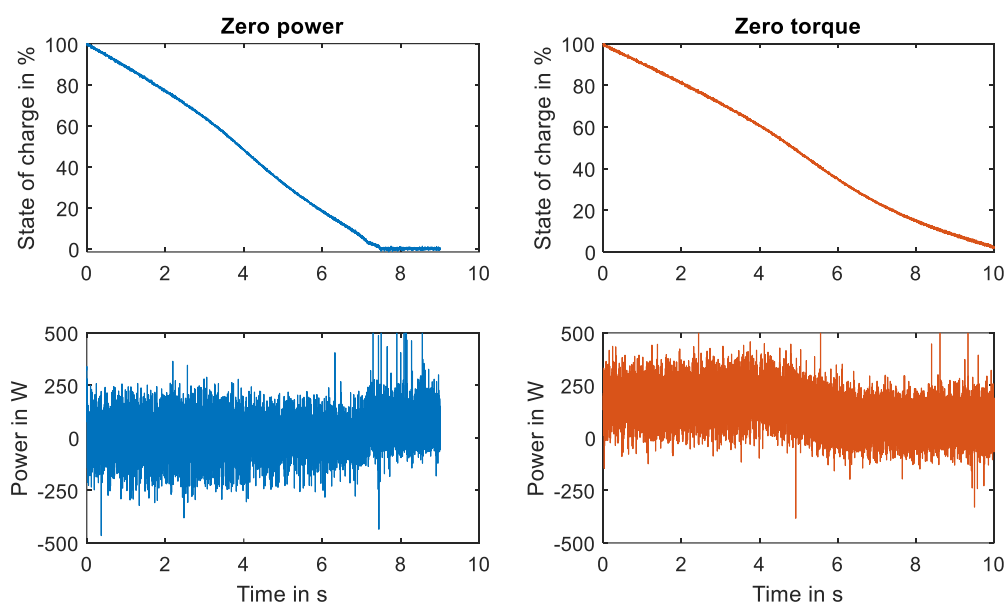


Figure 4.2 FESS power during self-discharge measurement

So far, it is not possible to implement the disabled inverter scenario. For the test, the disable switch was operated manually. Further periphery is necessary to implement the scenario and therefore reduced the self-discharge of the FESS. The available digital output ports are not able to control the enable inverter port of the motoring inverter. It is estimated that the power output of 0.5 W is not enough for the port. Either a relay module which is added in the current structure of the switch or another digital output module with higher current output could enable the control of the motoring inverter with the PLC. Since the disabled motoring inverter would not send any measured signals, using the display signal for rotational speed would give information about the SOC of the FESS.

4.2 Charge retention

To keep the FESS charged with a constant value, it is necessary to keep the rotational speed constant. Due to the self-discharge, it is necessary to supply power to the system to keep a constant SOC. The necessary power is depending on the present SOC. To analyze how much power is needed for which SOC, different constant power values are applied on the FESS over a longer period of time, and the charge is measured. Since it takes a while till the FESS settles at a constant charge, the power is supplied for around 30 min before the rotational speed is measured. Out of the rotational speed, the SOC is calculated.

Figure 4.3 shows the results of the measurement. With a power of 300 W, the FESS settles at a charge of around 5 %. By increasing the power, the FESS settles at a higher SOC. With a power of 1200 W the FESS settles at a charge of around 63.3 % of the maximum charge which is equal to 190 kW.

Depending on the used case of the FESS, the charge retention power must be selected. The given equation helps to estimate the settling power of the FESS. Keeping the SOC on a high level does not seem reasonable, since the charge retention power must be applied over the whole operation time. With a smaller charge, the FESS is still able to supply power for a short period of time. However, due to the limited power below 3000 rpm, the accessible power is reduced too.

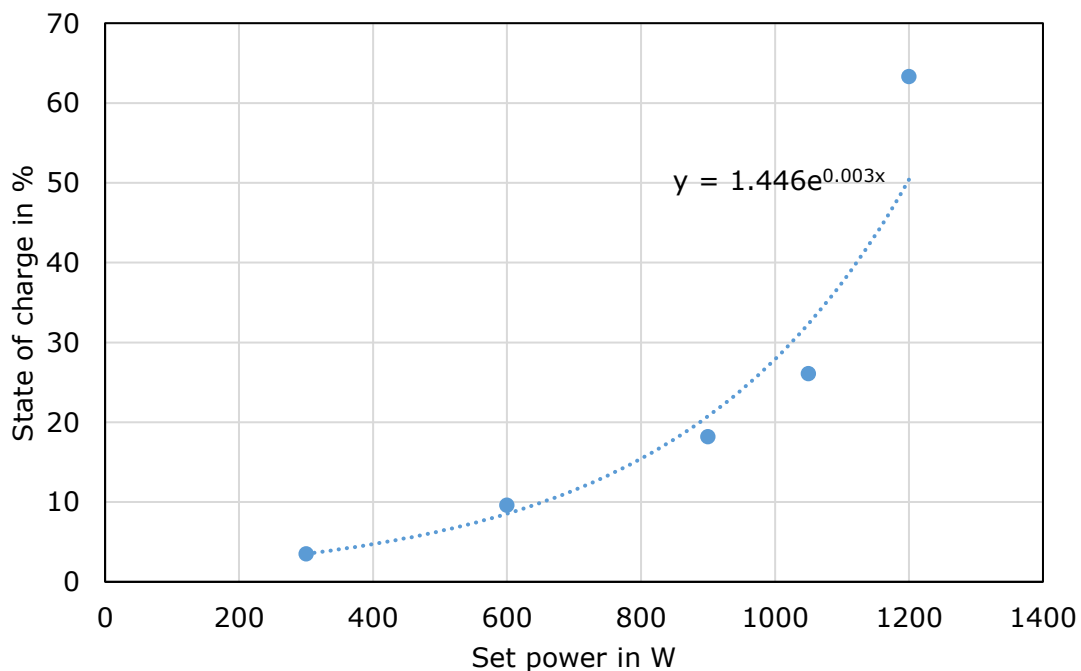


Figure 4.3 Charge retention power - SOC relationship

4.3 Repeatability of FESS power control

Since the FESS is used for analyzing control scenarios, it is necessary to know how repeatable and accurate the controller is charging and discharging the FESS. Therefore, a ramp in power is applied. The same test is performed five times and its deviation from the set ramp is analyzed. The test is always started from stand still. The set power signal is shown in Figure 4.4. The power increases from zero to 3000 W in one minute and decreases with the same slope again.

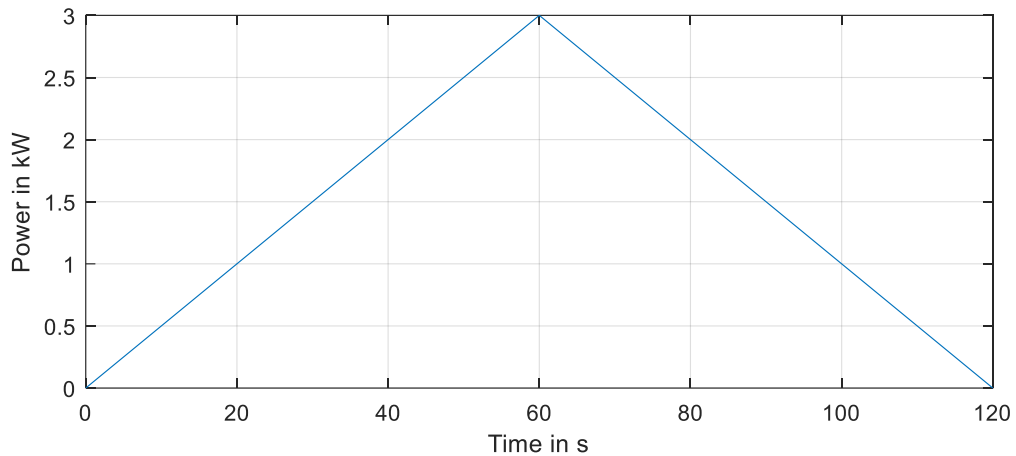


Figure 4.4 Ramp signal for repeatability analysis

To analysis the accuracy, the difference between set power and measured power is calculated for all five test runs. Overall, the average difference between set and measured signal is -0.09 W and the median -3.97 W. The maximum and minimum occurring power difference are 1206.13 W and -493.24 W. The extremes occur during the beginning of the measurement, when the FESS just starts to spin. It is assumed that these are only measurement errors and not real occurring power values. For all five curves the root mean square (RMS) error is calculated. It is an indicator for the mismatch between set power and measured power over the whole measurement. On average, the RMS error is 97.74 W.

Table 4.1 Repeatability analysis

Test run	1 st	2 nd	3 rd	4 th	5 th	Overall
Average	-1.63W	0.25W	0.58W	0.00W	0.26W	-0.09W
Median	-4.68W	-0.83W	-3.40W	-7.14W	-5.46W	-3.97W
Maximum	250.36W	625.67 W	682.20W	478.47W	1206.13W	1206.13W
Minimum	-493.24W	-393.15W	-393.82W	-279.38W	-324.19W	-493.24W
RMSE	94.06W	96.66W	98.25W	95.57W	100.91W	

4.4 Round trip efficiency

The round-trip efficiency is an indicator which shows how efficient the charging and discharging of the energy system works. To determine the round-trip efficiency, the system is charged with a constant power and discharged with the same power again. In the end, the quotient between charging energy and discharging energy is calculated. The FESS round-trip efficiency analysis is performed with two different powers. First, a constant power of ± 5 kW is used. This power is chosen since it is closer to the real use case, compared to the second measurement. For the second measurement, maximum power is used. During the test, the system accelerates continuously until it reaches 5000rpm. When reaching the 5000 rpm, the discharging starts. For the calculation of the used charging energy E_{charge} , the power $P[k]$ is multiplied by the difference in time and sum up till the time step x , the system starts to discharge with the same power. To remove noise in the power signal, the average between the present and the previous measured is calculated, see (4.1). For the calculation of the discharging energy, the same equation is used.

$$E_{charge} = \sum_{k=1}^x \frac{P[k] + P[k-1]}{2} \cdot (t[k] - t[k-1]) \quad (4.1)$$

Figure 4.5 shows the measurement results of the first test run with 5 kW. It is visible that the charging cycle takes more time compared to the discharging cycle. These results in a much higher charging energy of 427.7 kW compared to the discharging energy of 251.0 kW. The round-trip efficiency of the FESS is 58.7 %. The maximum charge of the is 300 kW. With a power of 5 kW, 127.6 kW of energy was lost during charging of the FESS.

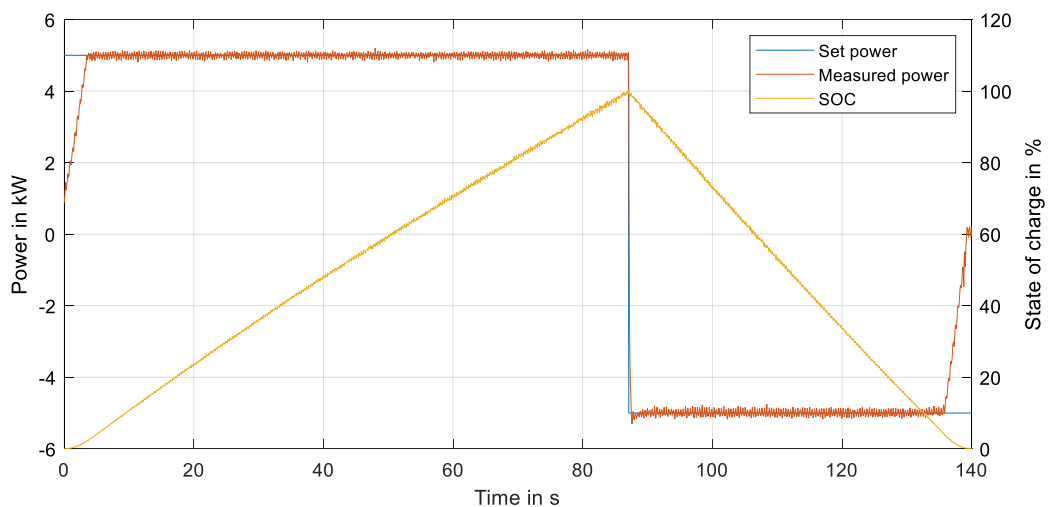


Figure 4.5 Round-trip efficiency measurement with 5 kW

For the second test run with 15 kW power, the total test duration is shorter. This reduces the influence of the FESS self-discharge significantly. The second measurement is shown in Figure 4.6. The limited power access below 3000 rpm has a higher influence on the test with 15 kW power. After 3.5 s the system is able to charge with 5 kW while it takes up to 12 s till charging with 15 kW is possible. During the discharging cycle, the FESS has to reduce its power after half of the discharging time, while for the 5 kW measurement, the power is only limited for around the last 10 %. The test duration with 15 kW is around 54 s. Compared with the 137 s with 5 kW, the 15 kW power test is much shorter. In total, during the second test run with 15 kW, 375.3 kW are charged into the FESS while 269.3 kW are discharged. This is equal to around 12 % less charging energy and 7 % more discharging energy compared to the test with 5 kW. The round-trip efficiency is 71.8 % with 15 kW power. The round-trip efficiency for smaller power is lower due to the self-discharge. The more time is necessary to reach the turning point of 100 % charge, the more energy is lost due to self-discharge.

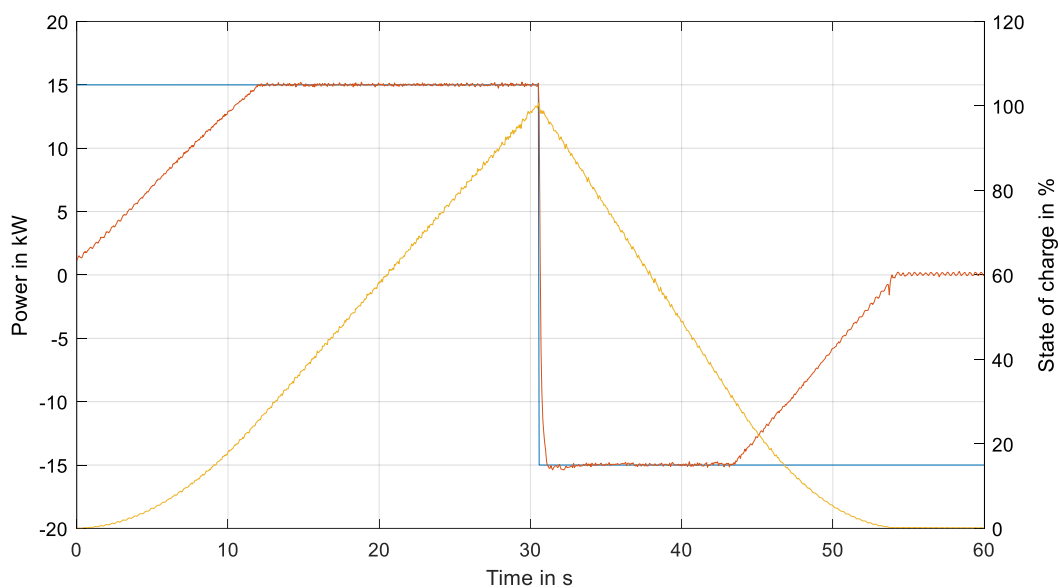


Figure 4.6 Round-trip efficiency measurement with 15 kW

In the data sheet of the FESS, the same test is described. The FESS is accelerated with maximum power to 5000 rpm and afterwards decelerated again to zero. While fore charging an energy of 222 kW is given, for discharging 172 kW were measured. This results in a round-trip efficiency of around 75 %. The lower round-trip efficiency in the measurement of this thesis occurs due to ageing processes. Performing maintenance like exchanging the oil for the bearings could increase the round-trip efficiency again.

5. Research on control scenarios with P-HIL

This chapter analyzed the different use cases of FESS, which were introduced in chapter 1.3. Since the present FESS is an old model and has its limits in case of stored energy and power, some additional simulations are performed with up-to-date FESS. As modern products, the FESS from ADAPTIVE Balancing power [47] or the FESS from Amber Kinetics are used [57].

5.1 Load levelling of buildings

To perform the load levelling control of buildings, first the moving average controller must be implemented. This is done in the TIA portal. After the implementation of the moving average controller, the test setup is introduced. Two test runs will be performed with the P-HIL. For the first test, no charge retention is used, while for the second test, the FESS stays charged. In both cases, the FESS is pre-charged before starting the test. After analyzing the measurements, the load levelling control is optimized.

5.1.1 Implementation of moving average controller

The moving average controller, described in chapter 1.3.1, is implemented directly in the TIA portal. The code is programmed in a function block (FB). The FB uses one input signal to calculate one output signal. A static history array is used of the length of the filter to store the occurred measurements. The static variable sum stores the sum of the all the values in the history array. Using a variable for the sum reduces the calculation time compared to a calculation of the sum in every execution of the code. A pointer is used to always point to the oldest value in the history array. While executing the code, first the oldest value is stored in a temporary variable. Afterwards, the new input value is positioned at the location of the oldest value. To update the actual sum of the array, the new input value is added, and the oldest value is subtracted from the saved previous sum. The new sum is then divided by the length of the array, to calculate the moving average value. As last step the pointer is increased until it reaches the array length. If it reaches the array length, the pointer is set to zero. The length of the filter is fixed to 30. To change the length, the array length of the history, the division by the array length and the reset value of the pointer must be changed.

The moving average FB is called in a cyclic OB. The cyclic OB consists of four networks. Its cycle time is set to 1s since the load profile is sampled with the same cycle time. In the first network, the load profile of Figure 1.15 is read. With every repetition, the new value is transmitted for the simulation. To generate the load profile, a function block is generated with the target1500s function. The load profile was implemented as timeseries in MATLAB Simulink before building the code for the TIA portal. In the second

network, the output of the load profile FB is fed into the moving average FB. To build the balancing signal for the FESS, the output of the moving average FB is subtracted from the load profile in the third network. The last network is used for the charge retention. Depending on the FESS charge retention scenario, a constant amount of extra power is added to the balancing signal. A detailed description of the implementation is shown in Appendix 9.

5.1.2 Test setup for moving average load levelling

For performing the load levelling tests, the moving average filter is initially filled with the first occurring load signal. This is necessary, since without it, the moving average controller would take 30 repetitions till it performs as desired. In the first test run, the load levelling is analyzed without charge retention. Therefore, the FESS is charged up to around 4500 rpm, which is equal to around 240 kW before the test is started. When the test is started, the FESS performs the load levelling. Due to the self-discharge of the FESS and the necessary power for levelling, the charge of the FESS decreases. The second test run is performed with a constant extra power of 600 W, applied to the FESS. The extra power increases the total load power of the building. With the power of 600 W, the FESS is charged to around 1550 rpm or around 29 kW. Due to the self-discharge of the FESS, the FESS settles around this charge. A controller to keep the FESS charged to a constant value is not developed, since a higher SOC requires a higher power to compensate the self-discharge. It is necessary to analyze for every use case which SOC is required and if a SOC controller would be beneficial.

5.1.3 Results of moving average load levelling

The measured signal of the test run without charge retention is shown in Figure 5.1. The FESS smooths the signal as desired. Smaller changes in the load profile are removed completely by the FESS. The measured signal contains more noise, compared to the load profile. Since the load profile is generated with a dataset which is sampled every second, while the measured signal is sampled every 100 μ s, it is not possible to compare the amount of noise in the signals. The two load peaks are smoothed out in the measured signal. However, when the power peaks occur and when they disappear, small and short peaks are shown in the measured signal. Further, 30 s after the peak occurs, a drop in the load leveled signal is visible.

The drop in the load levelled signal is caused by the moving average filter. The impulse response of a moving average filter has a rectangular shape. The shape is depending on the peak height and the filter length.

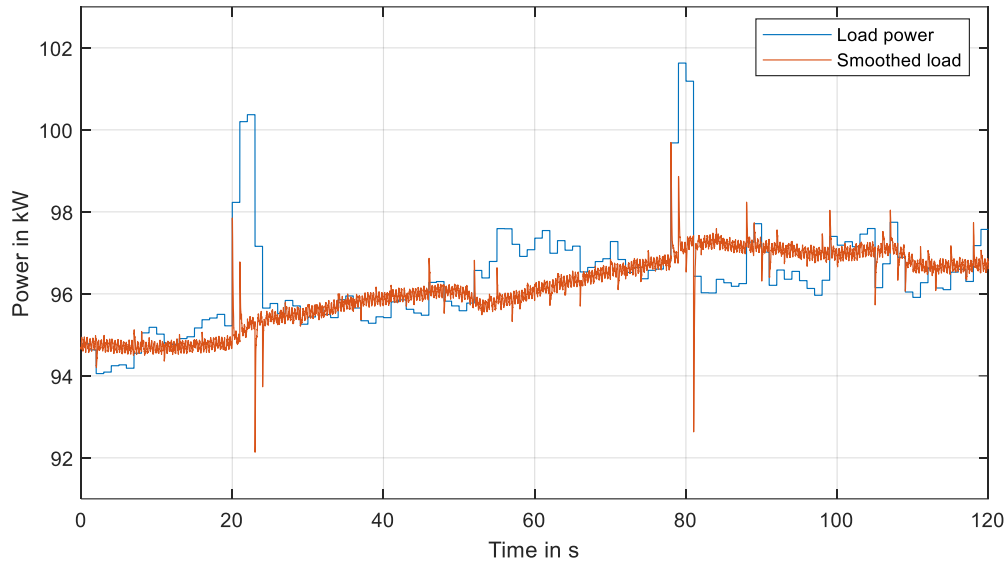


Figure 5.1 Measurement load levelling without charge retention

Figure 5.2 shows a detailed view of the first peak at around 22s. In the first subplot, the load profile and the smoothed signal are shown, while the second subplot shows the FESS power. It is visible that the FESS needs around 200 ms to smooth out the load change. This is the time which the FESS power controller needs to adapt the set signal to the output signal. The peaks occur in positive and negative direction since in both cases the FESS power controller needs to react to change in the set signal.

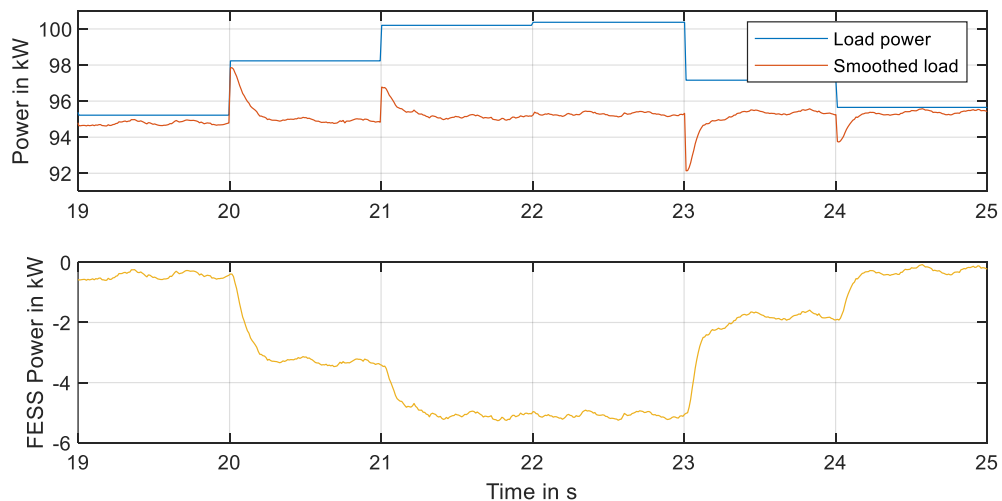


Figure 5.2 Detailed view of measured load peak at around 22s

In Figure 5.3 the measurement with charge retention is shown. The signal looks similar to the one without charge retention. The drop in the load levelled signal and the small power peaks due to the reaction time of the power controller are visible as well. On average the load power is increased by around 0.6 kW over the full test duration. If the FESS is used for load levelling over a full day, the FESS would consume 14.4 kWh.

Compared with the compensated peaks of around 4 kW which occur once a minute, this is a lot of energy used to level the load of the building.

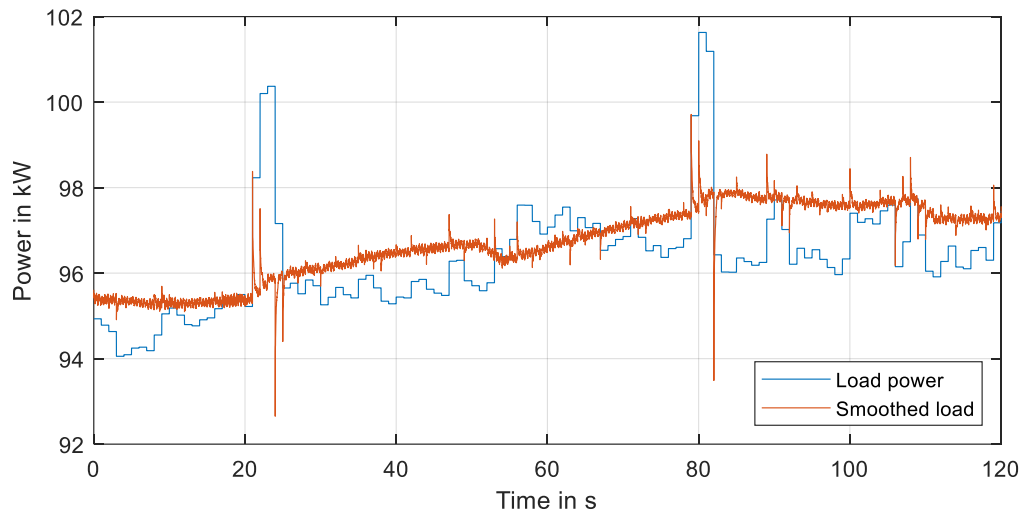


Figure 5.3 Measurement load levelling with charge retention

5.1.4 Optimizing of load levelling algorithm

To optimize the load levelling controller, the use of a Butterworth filter instead of the moving average filter is analyzed. Both filters are low pass filter. Compared to the moving average filter, a Butterworth filter is less influenced by one single disturbance, but also reacts faster if the system stays constant for a while. Butterworth filters achieve a fast roll-off of the signal, but allow ripples in the frequency response. A Butterworth filter is a special form of a Chebyshev filter with 0 % ripple in the pass band [58]. In Figure 5.4 an impulse response of a moving average filter and a Butterworth filter is shown. The moving average filter has a length of 30 samples. The Butterworth filter is designed as a second order filter with a sampling frequency of 1 Hz and a cut off frequency of 1/60 Hz.

It is visible that the moving average filter reacts first to the impulse. With every further time instance, the output of the moving average filter stays constant till the impulse passes the full filter. The Butterworth filter reacts less aggressive to the impulse, compared to the moving average filter. After some seconds, the Butterworth response overshoots the moving average response. The Butterworth filter is the first filter which starts to decrease and aligning to zero. The slope of the moving average filter reaches zero first.

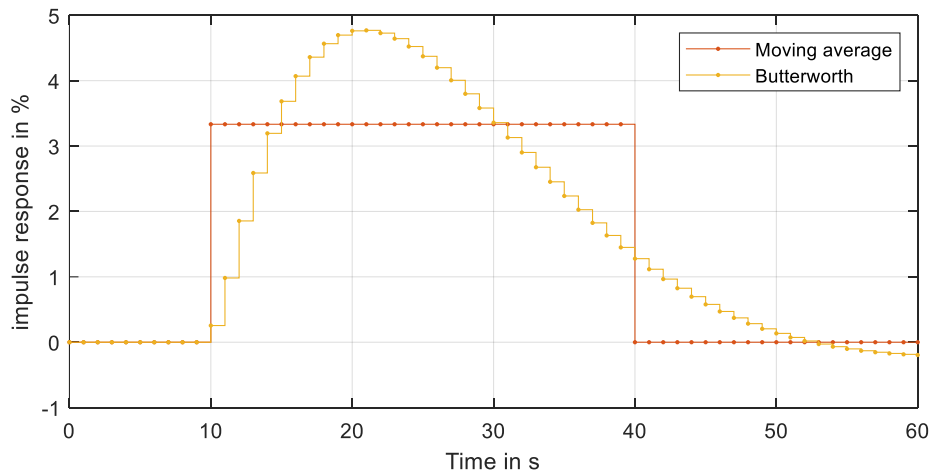


Figure 5.4 Impulse response of moving average and Butterworth filter

To further investigate the Butterworth filter for load levelling, the filter is applied to the load profile of Figure 1.15 in a simulation. The controller parameters are chosen similar to the impulse response explained above. Since the goal of the load levelling is a smooth output signal, the signal gradient is calculated.

Figure 5.5 shows on the left side the load power signal and the filtered outputs. Both filters reduce the load peaks of the signal significantly. Only small differences can be observed in the signals. When the load peak occurs, the moving average controller reacts first. After some seconds, the Butterworth signal overshoots the moving average signal. On the right side, the power gradient between the signals is plotted. The graph shows a higher peak for the moving average filter compared to the Butterworth filter. Especially the negative peak, when the load peak is leaving the moving average filter after 30 repetitions, is visible. This kind of behavior cannot be observed in the Butterworth signal. The code for the simulation is shown in Appendix 10.

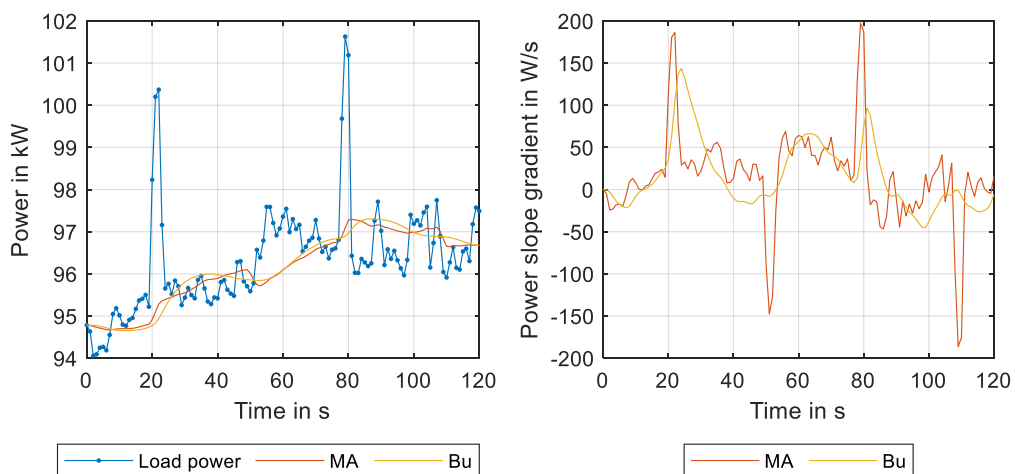


Figure 5.5 Power signals with different filters (left) and their slope gradients (right)

To verify, if the simulation data fits the real application, the Butterworth filter is implemented on the PLC. The filter is designed in Simulink with the digital filter design toolbox. The filter parameters are the same as for the simulation. The toolbox is able to build the filter with basic Simulink components. With the Target 1500S function, the filter is implemented in the TIA portal project and replaces the moving average filter. As test signal the same signal is used as in previous measurements.

The results are shown in Figure 5.6. It is visible that the measurement result fits the simulation. With a Butterworth filter, it is possible to smoothen the load signal further. The peaks in load power, caused by the reaction time of the FESS power controller can be observed again in the measurement.

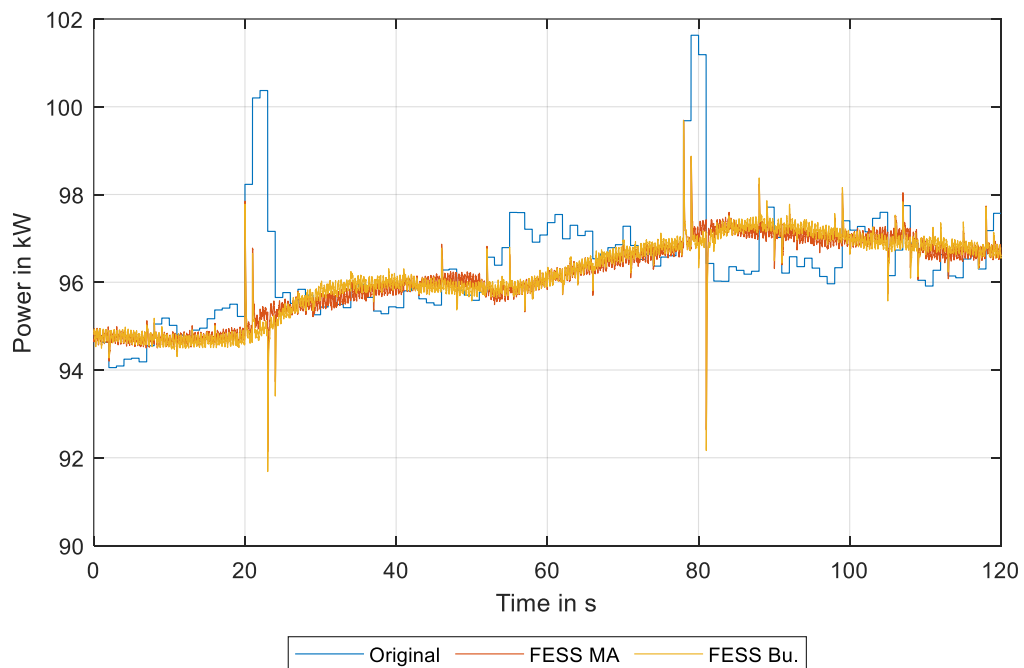


Figure 5.6 Analysis with different filters for FESS control

5.2 PV power levelling with P-HIL

In subchapter 1.3.2, the use of the levelling algorithm was already introduced to smooth the output power of PV sources. In this chapter, the developed Butterworth filter is used to smooth the PV profile shown in Figure 1.18. The P-HIL test is performed once without any power to pre-charge or charge retention and once with extra power.

In Figure 5.7 the SOC of the FESS during the tests is shown. It is visible that the FESS is completely discharged very often for the test run without charge retention power. When the FESS is completely discharged, it is not able to perform any further PV power smoothing and the output of the system behaves, as if there is no FESS used. When 300 W of the PV output power is used to keep the FESS charged, the FESS settles at a SOC of around 5 %. With the extra charging power, the FESS is completely discharged only five times in the analyzed hour, while without extra charging power, the FESS is discharged completely around 50 times.

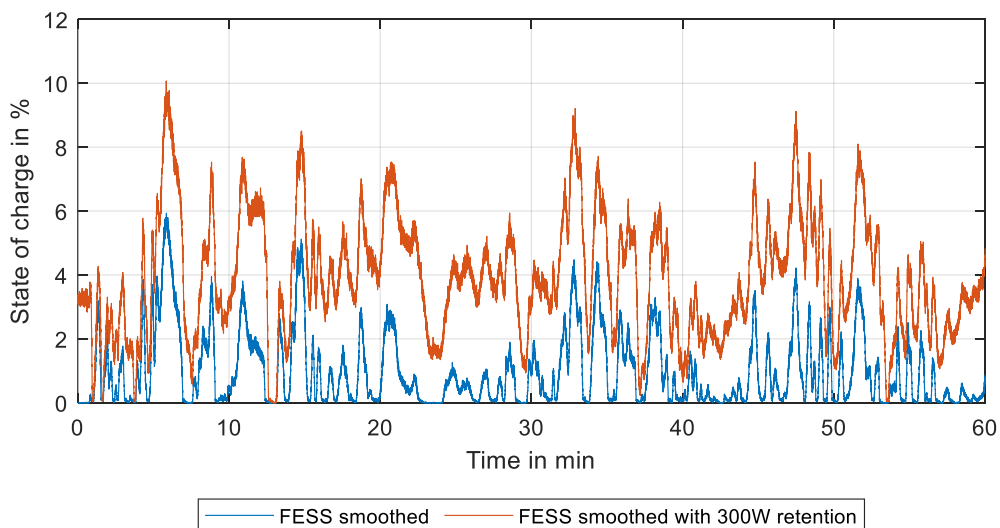


Figure 5.7 FESS state of charge over one hour PV power levelling

In Figure 5.8 the FESS power under both scenarios is plotted in a time window of five minutes. The measurement with charge retention power shows higher peaks in positive and negative direction. Further, it is able to provide the desired power at 37 min and 39 min due to the higher SOC. In the scenario without charge retention power, the FESS stops to supply power since it is completely discharged. The maximum charging and discharging power supplied by the FESS during the one-hour test is +2.5 kW and -2 kW without charge retention, and ± 3 kW with charge retention power. The present FESS could level the power output of up to five PV power production plants with the given size.

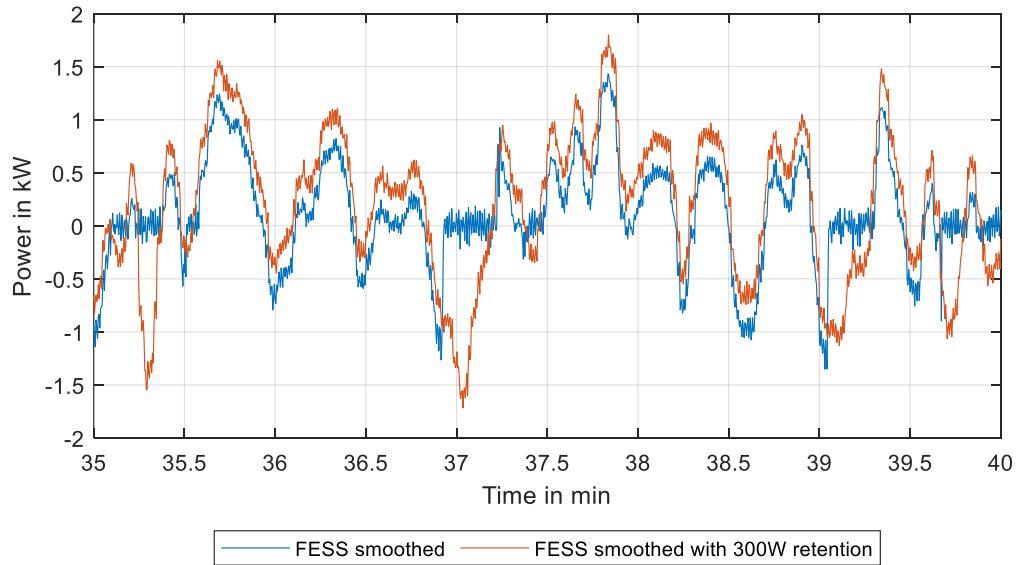


Figure 5.8 FESS power in five minute window

The power output of the PV source with FESS storage system of the five-minute time window is shown in Figure 5.9. The signal level with charge retention power is 300 W below the signal without retention power. However, it is much smoother since the FESS is able to provide the desired power all the time. For the other test run, the output power starts to follow the PV profile several times. This can be observed at the time stamps between 35 and 35.5 s, at around 37 s and 39 s. In general, without the extra power, the FESS is not able to provide power for smoothing the PV output. In most of the cases only positive peaks are smoothed out.

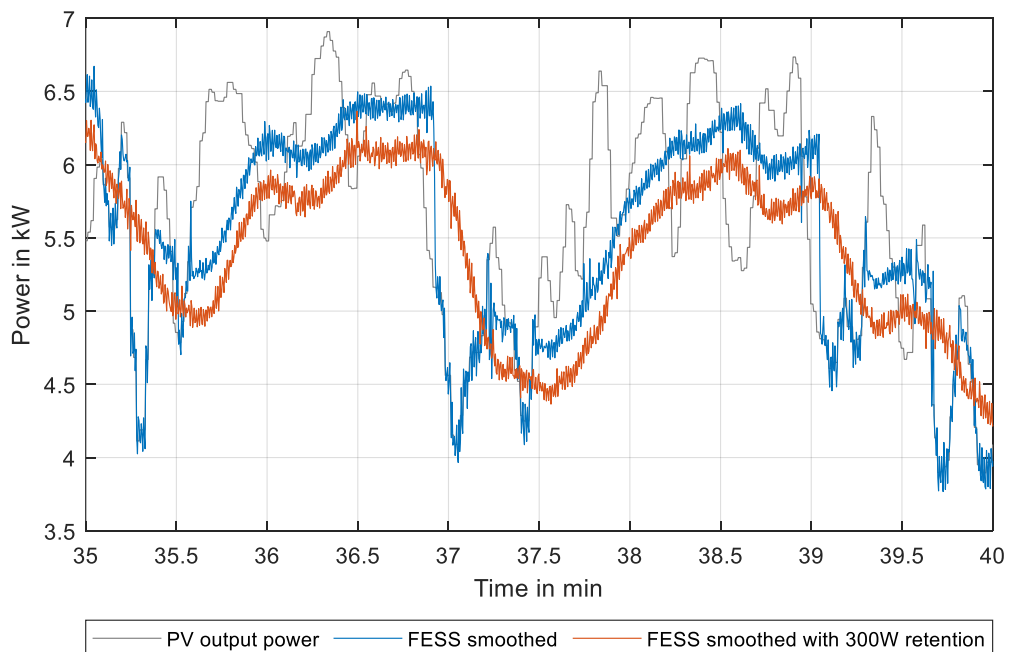


Figure 5.9 Levelled PV power output in five minute window

5.3 FESS as buffer in hybrid storage

Depending on the balance between the specifications of the installed battery storage inverter, the battery storage capacity and the PV source it can happen, that not all the produced power in a settlement can be used on site. Therefore, some power must be sold to the grid. In the FESS as buffer in hybrid storage scenario, the FESS is charged with the surplus of power and discharged when a suitable situation is given.

5.3.1 Hybrid storage simulation

For the simulation, a simplified model of the battery storage Sonnenbatterie 10 is used [59] and a simplified FESS model based on the data sheet of Amber Kinetics [60]. The inverter of the battery storage has a limited power of 4.6 kW. The FESS achieves a self-discharge rate of less than 100 W per second and has a capacity of 32 kWh[57]. Its charging and discharging power is limited to 9 kW. Depending on the power balance between load and production, the battery is charged. The goal of the FESS is to enable as much energy use on-site as possible without usage of the grid. If the balance exceeds the maximum power of the inverter, the FESS is charged. When the power balance is below the maximum inverter power, the FESS is discharged and energy is transferred from the FESS into the battery till the FESS is empty. If the battery storage is fully charged, all energy is stored inside the FESS. When the demand for power is higher than the production, the FESS starts to discharge first. Only when no energy is stored inside the FESS the battery is discharged. The Simulink model is shown in Figure 5.10. A detailed view of all subsystems is available in Appendix 11.

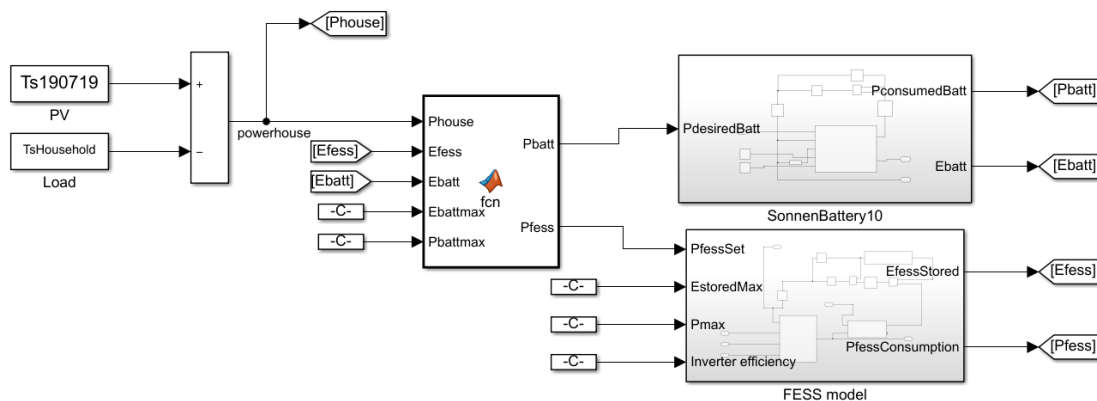


Figure 5.10 Simulink model for FESS power buffer simulation

The power profiles are shown in Figure 5.11. On the left side the PV production of a settlement in the south of Germany [61] is shown, on the right side the generated load profile of a settlement [62]. It is visible that due to a lot of clouds, the PV power output has not a steady value. Further, it exceeds the maximum power of the battery storage

regularly. The load profile consists of several peaks which indicate the usage of different household appliances. The storage system reacts to the balance between production and consumption.

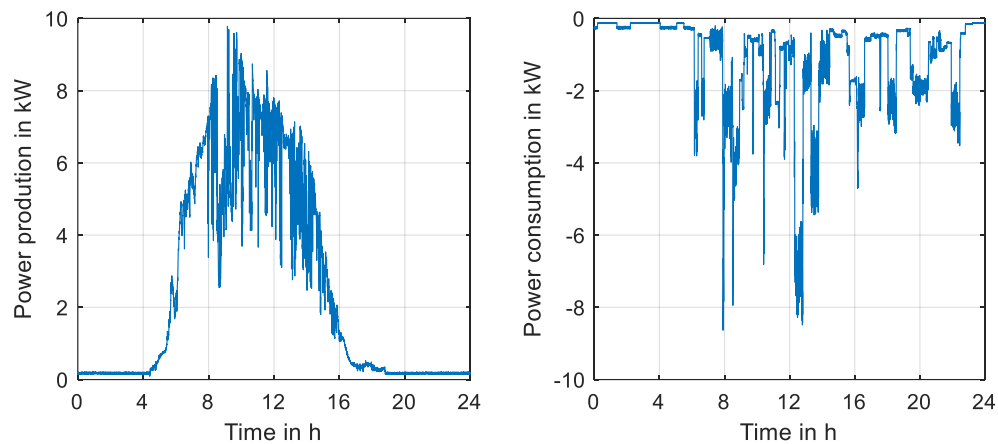


Figure 5.11 PV supply (left) [61] and house load profile (right)[62]

The result of the hybrid storage simulation is shown in Figure 5.12. First, all power is supplied or consumed by the battery storage system. When the power balance is above the maximum charging power of the battery, the FESS is charged. If the power of the house drops below maximum charging power, the FESS is discharged and the charging power of the battery stays constant until the FESS is completely discharged. The FESS smooths the battery power to maximum power. It is visible that after some time the battery is fully charged and all power is used on the FESS. When the FESS is completely discharged, the power is supplied by the battery again. The time in which the FESS can supply power depends very much on the self-discharge rate of the FESS.

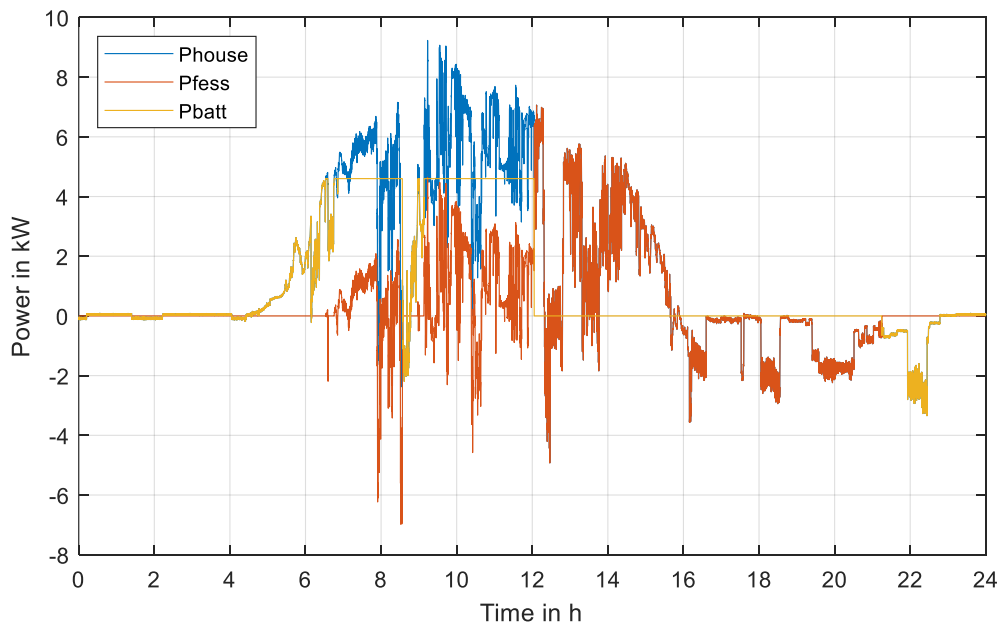


Figure 5.12 Simulation result of FESS as buffer in hybrid storage system

During this test, the model of the Amber Kinetics FESS was charged up to 30 % of its maximum capacity. This would allow the use of the FESS for different households at the same time, which increases the runtime of the FESS. However, the FESS from Amber Kinetics is only designed for a power of up to 8 kW. The peak load power at around 8am could not be supplied by this FESS for several households at the same time. This problem could be fixed either with demand scheduling, so that the power intensive household appliances do not work at the same time or with a change in the FESS design.

To increase the lifespan of the battery, it is possible to combine the load levelling controller with the hybrid storage power buffer controller, to reduce peak power during charging of the FESS and reduce the maximum power of the inverter. Less power leads to lower temperatures and increases the life expectancy of the battery storage [63].

5.3.2 Hybrid storage simulation with P-HIL

The developed control algorithm for the system is implemented and tested on the real setup with the older generation of FESS. Therefore, a big difference between simulation and real setup is expected. For analyzing the control algorithm, the present setup still can be used. The battery storage model is implemented on the PLC. It is similar to the model used in the simulation and exported from MATLAB Simulink to the TIA portal via the Target 1500S function. The sequence between seven am and eight am is used to analyze the behavior of the system, since in that time, the FESS is charged for a while and afterwards discharged.

The test result with the real setup is shown in Figure 5.13 on the left graphs. In the beginning of the test, all the power is used to charge the battery. When the power balance of the house exceeds the maximum charging power of the battery, the FESS is charged. The in the FESS stored energy is shown in the bottom subplot. After around 13min of the test run, the FESS power is reduced, but still is positive. In the energy plot, a decrease in charge can be observed. The charging power of the FESS is smaller than the self-discharge power of the FESS. This happens several times during the test run. When the house power is below the maximum battery power, the FESS starts to discharge itself and the battery power stays at maximum power. If the FESS is discharged completely, the battery starts to supply the house with power. On the right side of the figure, the discharging is shown in detail. It is visible that the hybrid storage controller is not performing well while discharging the FESS completely. Due to the noise in the measured rotational speed signal, which is used to calculate the in the FESS stored energy, the battery power is set for charging instead of supplying the power of the house two times for time intervals of around one second. A better filter for the rotational speed signal or a timer with set and reset block, at which the battery starts

to supply the house with energy could increase the performance. Further, the limited power of the FESS is neglected by the battery charging power. By calculating the efficiency of the setup, the used energy for charging and discharging are calculated. From the used energy for charging, 9.8 % is discharged again. During this test, 90.2 % are lost.

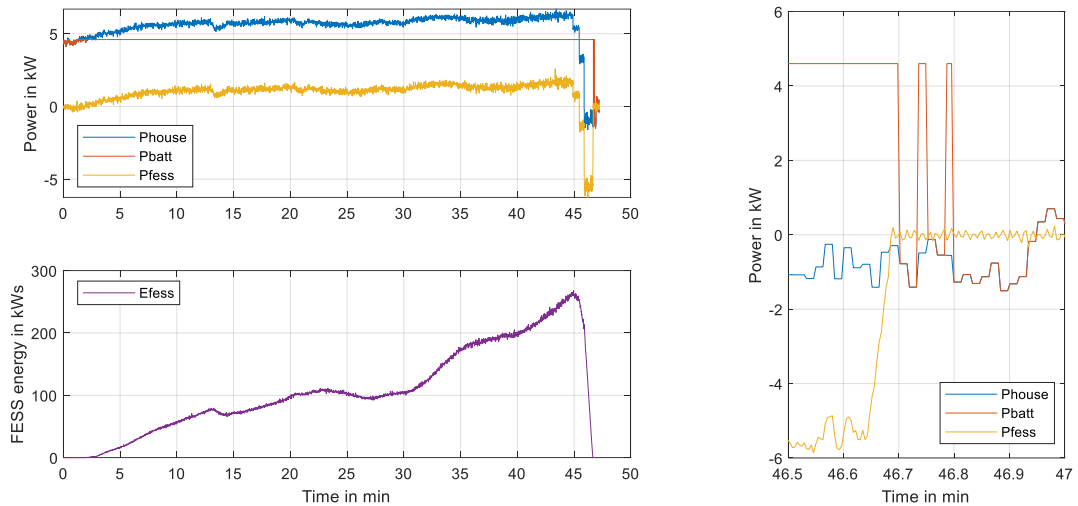


Figure 5.13 Hybrid storage P-HIL test result (left) and turn off behavior (right)

To solve the undesired charging of the battery while turning off, a timer is implemented in the controller. If an energy of less than 500 Ws is stored in the system, the battery starts to supply the house with energy. If the to balance energy is above the maximum power of the battery inverter, the FESS starts to charge. The limited power supply of the FESS at certain SOC was include the hybrid storage controller. A description can be found in Appendix 12.

A test run of the discharge behavior is performed to investigate the change. The result of the discharge test is shown in Figure 5.14. The problem with the undesired charging of the battery was solved with the timer and the changed hybrid storage controller code.

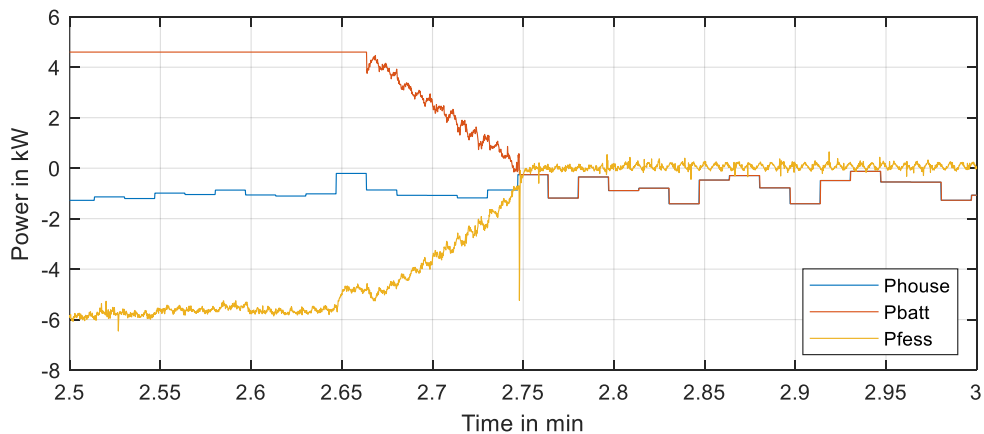


Figure 5.14 Hybrid storage improved discharge behavior

5.4 FESS as buffer for EV fast charging

As described in chapter 1.3.4 fast charging for EVs is getting more and more common. In the following subchapters, first a more modern FESS is simulated to buffer the power required for fast charging. Afterwards, the P-HIL is used to demonstrate the control algorithm's performance.

5.4.1 Simulation of FESS as buffer for EV charging

For the MATLAB Simulink simulation, a grid load of 15 kW is assumed. First, the 15 kW are used to charge the FESS. It is assumed, that the EV charging cycle starts when the FESS is completely charged. The load to the grid stays constant, while the FESS starts to discharge, so that the battery of the EV is charged with maximum power. The complete control algorithm is given in Appendix 13. The modelled FESS has a capacity of 12 kWh and a charging / discharging power of 100 kW. The FESS vacuum and magnetic bearings, to reduce the self-discharge rate. It is assumed the self-discharge rate is close to the previously modeled FESS with 100 W.

In Figure 5.15 on the left side the power flow during the simulation is shown. On the right side of the figure, the stored energies in the electric vehicle and the FESS are shown. At time step zero, the charging of the EV starts. It takes up to 56min till the FESS is charged with the constant grid power of 15 kW. The discharging takes around 9 minutes till the FESS is completely empty. The electric vehicle is charged with around 13.8 kWh in these 9 minutes which is enough energy for around 100 km.

To increase the loading power, it is possible to use several of the FESS in parallel. This would increase the power output and the accessible energy depending on the amount of FESS in parallel. It is also not necessary to charge the FESS completely before charging the EV.

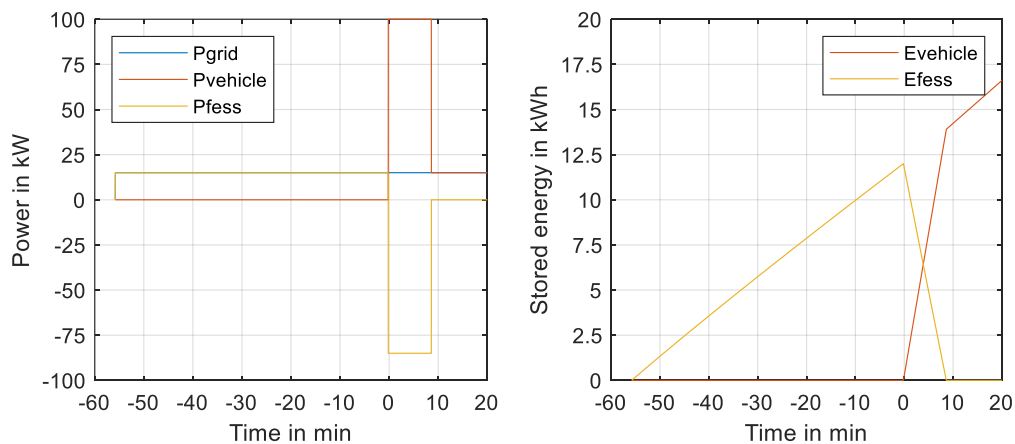


Figure 5.15 Power flow (left) and charge (right) during EV charging with FESS buffer

5.4.2 P-HIL simulation of FESS as buffer for EV charging

To prove that this kind of concept works also with real setups, a demonstration is performed on the developed P-HIL. Since the present FESS has a lower charging power, different values must be chosen. During the test, the FESS is charged with a constant power of 5 kW. The fast charging cycle starts when the FESS is completely charged. Then the FESS is discharged with the power of 15 kW till it is empty. These powers are much lower compared to the simulated FESS. Further, the capacity of the simulated FESS is also much higher than the FESS for test in the laboratory. The implementation is shown in Appendix 14.

The results of the fast charging P-HIL simulation are shown in Figure 5.16. The FESS needs some seconds until it can charge with the desired power of 5 kW. The charging power stays constant till the EV charging phase starts, which is after around 80s. The FESS is able to switch from charging to discharging with 15 kW in less than half a second. After 13s of discharging with 15 kW, the rotational speed is below 3000 rpm and the output power of the FESS is limited. The total discharging cycle takes around 23 seconds.

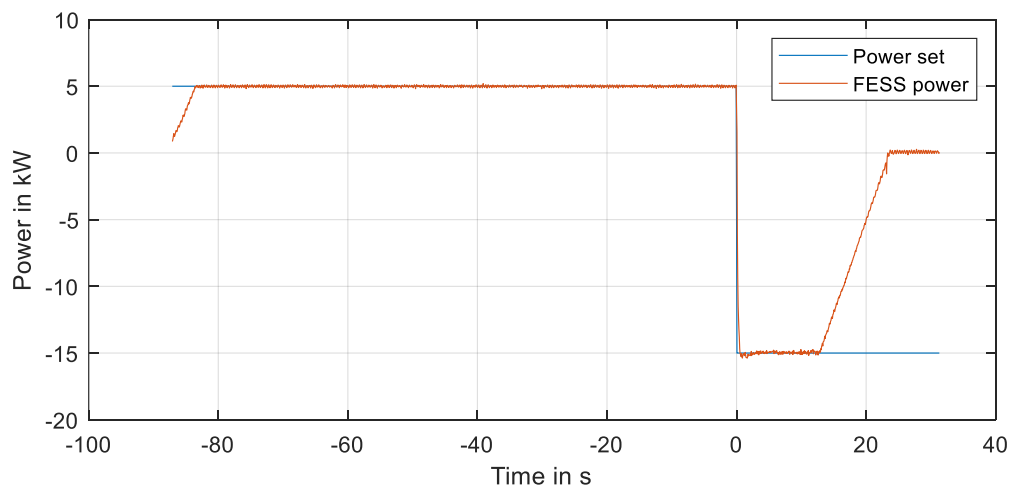


Figure 5.16 P-HIL simulation of FESS as buffer for fast charging

The present FESS has not enough capacity to function as a buffer for fast EV charging. In this control scenario, the FESS is spinning for a long time. This increases the losses of the system, since the higher the rotational speed of the FESS and the longer it keeps spinning with this speed, the higher the losses are. Putting several of the present FESS in series would increase the capacity of the storage system, but the losses would increase too and the power would be limited for all the devices after some seconds. However, the simulation with a more modern FESS shows that the use of a FESS to enable fast charging without peak loads is possible.

SUMMARY

In this thesis, a power hardware in the loop test setup was developed. The main component of the setup is a flywheel energy storage system. Flywheels are beneficial over other energy storages in case of the amount of charging and discharging cycles they can withstand without degradation. For flywheels, the maximum capacity depends on the moment of inertia of the rotating mass and the maximum rotational speed. Both parameters are not influenced by cycling of the energy storage. The test setup enables research on different control scenarios of flywheel energy storages in microgrids. To verify the functionality of the power hardware in the loop test setup, different controllers were developed and analyzed with the setup.

For the development of the test setup, an existing setup was modernized. The modernization includes the implementation of a state-of-the-art PLC. The new PLC enables the fast implementation from different MATLAB Simulink controller. Further, it is possible to implement different load profiles for investigating the system behavior of the controlled flywheel energy storage.

For the control of the energy storage, a power controller was developed. As input signal of the motoring inverter, the accelerating torque is used. The power of the flywheel energy storage is limited, if the rotational speed is below 3000 rpm. To enable accurate power control at low rotational speeds, a function to approximate the relationship between measured power – measured rotational speed – set torque is established. The approximation enables the flywheel energy storage to reach the desired power faster. A PI controller is used to remove the gain error of the flywheel energy storage and control the power to the desired value. After the implementation of the complete flywheel power control structure, the parameters of the controller were optimized. Based on the developed control algorithm, a laboratory training was produced.

A performance study was performed on the modernized setup. The performance study includes the characterization of the self-discharge of the flywheel energy storage system, the necessary power for keeping the level of charge, the repeatability of the control and the round-trip efficiency. If the flywheel is controlled to a power of zero watts, it is completely discharged from full charge in less than 500 s. If the motoring inverter is completely disabled during this test, it takes around 3500 s till the flywheel is discharged. The power which the flywheel needs to keep its state of charge depends on the state of charge. For a charge of around 65 %, 1.2 kW are necessary. The controller is able to follow a given ramp signal by an RMS error of 97.74 W. The modernized system has a round trip efficiency of around 71.8 %. This is a value close to the round-trip efficiency of around 75 %, given by the manufacturer of the flywheel.

To verify the functionality of the power hardware in the loop test setup, a load profile of a building was leveled with a moving average filter. One scenario was analyzed without charge retention, while in the second scenario, the average load was lifted to keep the flywheel charge. The extra charge enables the levelling in both directions. Due to the sharp edges of the impulse response of a moving average filter, the filter was exchanged with a Butterworth filter. The Butterworth filter smooths the signal further.

An investigation of the Butterworth filter for power smoothing of a PV source on a very volatile day is performed. In the analyzed one-hour window, the PV source produces on average 5500 W. By using 300 W of the produced power to keep the flywheel charged, the output power can be smoothed in the demanded form. The levelling controller could be used in a hybrid storage out of a battery and a flywheel. The flywheel levels the power, while the battery is responsible for the long-term power supply. The combination would increase the lifespan of the battery due to a lower amount of cycles performed by the battery.

Since the power with which a battery storage can be charged is limited, a flywheel controller for power buffering was developed. The controller enables the use of the produced power on-site without selling the power to the grid. If less power is available than the maximum charging power of the battery, the flywheel is discharged and the energy is stored into the battery. During this test, around 10 % of the charged energy in the flywheel could be used again while discharging. Since the flywheel was accelerated with a low amount of power, at some points the charging power and charge retention power were equal, and no further acceleration was performed.

The potential use of flywheel energy storages as power buffer for fast charging of electric vehicle was shown. The existing flywheel cannot supply enough power for fast charging and has a very low capacity. Several of the present flywheels would be necessary in parallel. During the test, only 63 % of the charged energy is used for charging the electric car due to the self-discharge. Putting several of the flywheels in parallel would also increase the overall losses of the system.

The performed tests with the P-HIL test setup show that it is possible to analyze developed control scenarios. Flywheel energy storages have a lot of potential use cases in microgrids, since they can balance supply and demand without degradation or be used as short-term buffer storage. However, the tests also show, that the present flywheel has a very high self-discharge rate and its use is not lucrative in a lot of cases. More advanced flywheels have lower self-discharge rates. The future of flywheel energy storages is depending a lot on the performance regarding the self-discharge rate.

KOKKUVÕTE (SUMMARY IN ESTONIAN)

Käesolevas lõputöös arendati välja jõuelektronika riistavara silmuse (*hardware-in-the-loop*) süsteem, mille peakomponendiks on hooratasenergiasalvesti. Hooratase eeliseks teiste salvestusseadmete ees on laadimiste ning tühjendamiste kõrge tsükliline taluvus, ilma energiamahutavuse vähenemiseta. Hooratase energiamahutavus sõltub pöörleva massi inertsist ja maksimaalsest pöörlemiskiirusest. Mõlemad parameetrid ei sõltu tühjendamis- ja laadimistsüklite arvust. Katsesüsteem võimaldab uurida mikrovõrkudes kasutatavate hooratasenergiasalvestite erinevaid juhtimisstsenaariume. Jõuelektronika riistavara silmuse katsesüsteemi funktsionaalsuse kontrollimiseks arendati välja erinevad regulaatorid, mida analüüsiti katsesüsteemil.

Katsesüsteemi arendusega moderniseeriti olemasolev aegunud hooratasenergiasalvesti süsteem, mille käigus paigaldati süsteemi kaasaegne programmeeritav kontrolleri (PLC). Paigaldatud PLC võimaldab kiirelt rakendada MATLAB Simulink abil välja töötatud regulaatoreid. Lisaks on võimalik rakendada erinevaid koormusprofiile, et uurida süsteemi käitumist juhitava hooratasenergiasalvestuse puhul.

Energiasalvesti juhtimiseks arendati välja võimsusregulaator. Mootoripoolse vaheldi sisendsignaali kasutatakse hooratta kiirendusmomenti. Energiasalvesti väljundvõimsus on piiratud, kui selle pöörlemiskiirus on alla 3000 p/min. Võimsuse täpsemaks reguleerimiseks madalatel pöörlemiskiirustel koostati funktsioon, mis loob ligikaudse seose mõõdetud võimsuse, mõõdetud pöörlemiskiiruse ja seadistatud pöördemomendi vahel. Antud funktsioon võimaldab hoorattal jõuda kiiremini soovitud väljundvõimsuseni. Proportsionaal-integraal (PI) regulaatorit kasutati võimsusätte ja tegeliku väljundvõimsuse vea eemaldamiseks. Arendatud juhtimisalgoritmi alusel loodi laboratoorse töö juhend.

Moderniseeritud süsteemi jõudlust uuriti katsetuste teel. Katsetuste käigus tuvastati hooratasenergiasalvesti isetühjenemine, vajalik võimsus laetuse taseme (*state-of-charge*) hoidmiseks, juhtimise korratavus ja laadimis- ning tühjendamistsükli kombineeritud kasutegur. Kui hooratta väljundvõimsus on seadistatud hoidma null vatti, siis hooratas tühjeneb täisolekust vähem kui 500 sekundi jooksul. Samas, kui mootoripoolne vaheldi on välja lülitatud testi jooksul, siis tühjenemiseks kulub ligikaudu 3500 sekundit. Laetuse hoidmiseks vajaminev võimsus sõltub laetuse tasemest endast. Näiteks 65 % laetuse hoidmiseks on vaja tarbida 1,2 kW võimsust. Loodud võimsusregulaator suudab järgida lineaarselt kasvavat sätteväärtust ruutkeskmise (RMS) veaga 97,74 W. Moderniseeritud süsteemi laadimis- ja tühjendamistsükli kombineeritud kasutegur on ligikaudu 71,8 %, mis on ligidane hooratta tootja andmelehes toodud 75 %.

Jõuelektronika riistavara silmuse katsesüsteemi funktsionaalsuse kontrollimiseks tasandati hoone tarbimisprofiil liikuva keskmise (*moving average*) filtri abil. Ühel katsestsenaariumil teostati tarbimise tasandamine ilma laetustaseme hoidmiseta, samas teisel katsestsenaariumil tõsteti keskmist tarbimist laetustaseme hoidmiseks, mis võimaldab tarbimise tasandamist mõlemas suunas. Hüppekaja teravate servade tõttu asendati liikuva keskmise filter *Butterworth* filtriga, mis silus signaali veelgi.

Võimsuse tasandamist *Butterworth* filtriga uuriti PV allika alusel väga muutliku päeva puhul. Uuritud ühe tunni sees tootis PV allikas keskmiselt 5500 W. Kasutades sellest ära 300 W hooratta laetustaseme hoidmiseks, on võimalik väljundvõimsust siluda nõutud kujule. Tasandamise regulaatorit on võimalik rakendada ka aku-hooratas hübriid süsteemis, kus hooratas hoolitseb võimsuse tasandamise eest ja aku pikaajalise toite tagamise eest. Antud kombinatsioon suurendaks aku kasutusiga tänu väiksemale aku poolt sooritatavate tsüklite arvule.

Kuna akusalvesti laadimisvõimsus on piiratud, siis töötati välja võimsuse puhverdamiseks mõeldud hooratta regulaator, mis võimaldab kasutada toodetud energiat kohapeal seda võrku müümata. Kui aku maksimaalsest laadimisvõimsusest on saadaval vähem võimsust, siis tühjendatakse hooratas ja salvestatakse energia akusse. Selle katse käigus sai umbes 10 % hoorattasse laetud energiast uuesti kasutada tühjendamise ajal. Kuna hooratast kiirendati väikese võimsusega, siis mõnel ajahetkel olid laadimisvõimsus ja laetustaseme säilitamise võimsus võrdsed ja edasist kiirendamist ei toimunud.

Töös vaadeldi lisaks hooratta rakendust energiapuhvrina elektriautode kiirloomimisel. Käesolevas töös kasutatud hooratas ei suuda üksinda pakkuda kiirloomimiseks vajalikku võimsust ja selle energiamahutavus on madal. Kiirloomimise võimalust saaks pakkuda mitme hooratta ühendamisega rööbiti. Katsetuste käigus selgus, et isetühjenemisest tingituna kasutati ainult 63 % salvestatud energiat elektriautode loomimiseks. Mitme hooratta rööpühendus suurendaks ka süsteemi üldisi kadusid.

Läbiviidud jõuelektronika riistavara silmuse katsed näitavad, et katsesüsteemil on võimalik analüüsida välja töötatud juhtimisstsenaariume. Hooratasenergiasalvestitel leidub mikrovõrkudes palju potentsiaalseid rakendusi. Näiteks, neid on võimalik kasutada lühiajalise energia puhvrina energia tootmise ja tarbimise tasandamiseks, ilma energiamahutavuse vähenemiseta. Katsete käigus selgus, et käesolevas töös kasutatud hoorattal on suur isetühjenemine, mille tõttu ei ole selle kasutus paljude otstarvete puhul tulus. Hooratasenergiasalvestite tulevik sõltub paljuski nende efektiivsuses isetühjenemise kontekstis.

LIST OF REFERENCES

- [1] Bill Gates, "How to avoid a climate disaster: The solutions we have and the breakthroughs we need", Allen Lane, [UK edition], [London], 2021.
- [2] United Nations, "Paris Agreement", 2016.
- [3] "Plans for New Nuclear Reactors Worldwide - World Nuclear Association", <https://world-nuclear.org/information-library/current-and-future-generation/plans-for-new-reactors-worldwide.aspx>, accessed November 12, 2021.
- [4] Deutsche Welle, "A global nuclear phaseout or renaissance? | DW | 04.02.2021", <https://www.dw.com/en/germany-looking-for-final-repository-for-nuclear-waste-global-outlook/a-56449115>, accessed November 12, 2021.
- [5] Globaldata Energy, "Spain on track to complete nuclear power phase-out by 2035", Power Technology | Energy News and Market Analysis, 2021.
- [6] John Engel, "The role of small modular nuclear reactors in meeting climate goals", Power Engineering, 2021.
- [7] Kevin Morrissey, Salman Kahrobaee, Andrew Ioan, "Optimal Energy Storage Schedules for Load Leveling and Ramp Rate Control in Distribution Systems", 2020 IEEE Conference on Technologies for Sustainability (SusTech), 2020 IEEE Conference on Technologies for Sustainability (SusTech), Santa Ana, CA, USA, 4/23/2020 - 4/25/2020, IEEE, pp. 1–4, 2020 - 2020.
- [8] Energy Transformation Network of Ontario, "Structural Options for Ontario's Electricity System in a High-DER Future: Potential implications for reliability, affordability, competition and consumer choice", 2019.
- [9] F. Plaum, T. Häring, R. Ahmadihangar, A. Rosin, "Power Smoothing in Smart Buildings using Flywheel Energy Storage", Setubal, Portugal, 2020.
- [10] C. Nazli, "RESEARCH AND DEVELOPEMENT OF CONTROL STRATEGIES FOR ENERGY STORAGES IN AN ISLANDED MICROGRID", Master thesis, Tallinn, 2020.
- [11] EnBW AG, "Spannungsebenen".
- [12] Gretchen A. Bakke, "The grid: The fraying wires between Americans and our energy future", Bloomsbury, Paperback edition, New York, NY, 2016.
- [13] TenneT TSO GmbH, "Energy: from sea to land".
- [14] Elering AS, "Synchronization with continental Europe".
- [15] "NordLink - TenneT", <https://www.tennet.eu/our-grid/international-connections/nordlink/>, accessed November 8, 2021.
- [16] ENTSO-E, "ENTSO-E Transmission System Map", <https://www.entsoe.eu/data/map/>, accessed April 23, 2021.
- [17] Ministry of Industries and Innovation, "Energy".
- [18] "Map of European Transmission System Operators Organizations", <https://upload.wikimedia.org/wikipedia/commons/6/6d/ElectricityUCTE.svg>.

- [19] Bernd M. Buchholz, Zbigniew A. Styczynski, "Smart Grids - Fundamentals and Technologies in Electricity Networks: Fundamentals and technologies in electricity networks", Springer Berlin Heidelberg, Aufl. twentiethfourteenth, Berlin, Heidelberg, 2014.
- [20] Benjamin Dierks, "Atomkraftwerke müssen Leistung drosseln", 2018.
- [21] Brandon Clark, "Thermal Water Pollution from Nuclear Power Plants".
- [22] Bundesnetzagentur, "List of Power Plants", 2021.
- [23] Marcia Wendorf, "What caused the texas electricity blackout", Interesting Engineering, 2021.
- [24] Jesper Starn, Brian Parkin, Irina Vilcu, "The Day Europe's Power Grid Came Close to a Massive Blackout", 2021.
- [25] Siemens AG, "Warum Microgrids die Zukunft des Energiemanagements sind".
- [26] EnBW AG, "Wasser ist Energie: Heimische Wasserkraft".
- [27] European Commission, "Study on "Residential Prosumers in the European Energy Union"", 2017.
- [28] Papiya Ray, Monalisa Biswal, "Microgrid: Operation, Control, Monitoring and Protection", Springer Singapore, Singapore, 2020.
- [29] Michael Sterner, Ingo Stadler, "Handbook of energy storage: Demand, technologies, integration", Springer, [firstst edition], Berlin, Germany, 2019.
- [30] sonnen GmbH, "Technische Daten sonnenBatterie 10".
- [31] LG, "LG Energiespeichersysteme".
- [32] Mahammad A. Hannan, Md. M. Hoque, Aini Hussain, Yushaizad Yusof, Pin J. Ker, "State-of-the-Art and Energy Management System of Lithium-Ion Batteries in Electric Vehicle Applications: Issues and Recommendations", IEEE Access, Vol. 6, pp. 19362–19378, 2018.
- [33] Brockhaus Enzyklopädie Online, "Erdgas", NE GmbH | Brockhaus, 2021.
- [34] MAN Energy Solutions, "MAN turbomachinery: for compressed air energy storage (CAES)".
- [35] Siemens Energy, "Compressed Air Energy Storage Solutions: Comprehensive, proven, grid-scale energy storage".
- [36] Jidai Wang, Kunpeng Lu, Lan Ma, Jihong Wang, Mark Dooner, Shihong Miao, Jian Li, Dan Wang, "Overview of Compressed Air Energy Storage and Technology Development", Energies, Vol. 10, No. 7, p. 991, 2017.
- [37] Battery University, "BU-209: How does a Supercapacitor Work?: Discover how the supercapacitor can enhance the battery.".
- [38] Rosseta Technik GmbH, "Flywheel storage system T3-15", Technical documentation.

- [39] GE Power Conversion, "Rotating Stabilisers: CO2 free, high-inertia machines to help stabilise weak grids and enable higher penetration of renewable energy.", 2020.
- [40] STORNETIC, "Powerful Storage System for Grid Services", 2018.
- [41] Jim Arseneaux, Beacon Power LLC, "20 MW Flywheel Energy Storage Plant".
- [42] Laura Beltramin, "State-of-the-Art of the Flywheel/Li-ion Battery Hybrid Storage System for Stationary Applications", 2017/2018.
- [43] J. Li, J. Bi, G. Yan, Y. Ge, P. Jin, "Research on improving power quality of wind power system based on the flywheel energy storage system", 2016 China International Conference on Electricity Distribution (CICED), 2016 China International Conference on Electricity Distribution (CICED), pp. 1–6, 2016.
- [44] Siemens Energy, "Siemens Energy's grid stabilizer technology to help Irish grid exceed renewables penetration limit".
- [45] Mahdiyeh Khodaparastan, Ahmed Mohamed, "Flywheel vs. Supercapacitor as Wayside Energy Storage for Electric Rail Transit Systems", *Inventions*, Vol. 4, No. 4, p. 62, 2019.
- [46] Ahmad Rahmoun, "Mathematical Modeling and Analysis of a Battery Energy Storage System for Microgrids: THESIS ON POWER ENGINEERING, ELECTRICAL ENGINEERING, MINING ENGINEERING D85", 2017.
- [47] Adaptive Balancing Power, "Product - Adaptive Balancing Power", <https://www.adaptive-balancing.de/en/product/>, accessed October 9, 2021.
- [48] ADAC, "VW ID.3: Test, Reichweite, Elektroauto, Daten, Preise, Kosten | ADAC", <https://www.adac.de/rund-ums-fahrzeug/autokatalog/marken-modelle/vw/vw-id-3/>, accessed November 25, 2021.
- [49] Frank Puschmann, "Sicheres Testen durch Power-Hardware-in-the-Loop-Systeme", *ATZelektronik*, Vol. 16, 7-8, pp. 52–55, 2021.
- [50] EPA Antriebstechnik GmbH, "Usermanual Unidrive SP", twelfth edition.
- [51] Nidec Control Techniques Ltd, "Installation Guide Unidrive SP Regen: 200V, 400V, 575V, 690V", third edition, 2018.
- [52] Siemens AG, "SIMATIC ET 200SP Distributed I/O system: System Manual", 2019.
- [53] Siemens AG, "STEP 7 (TIA Portal) Optionen Target 1500S™ für Simulink® V4.0: Programmierhandbuch", SIMATIC, second edition, 2020.
- [54] Rosseta Technik GmbH, "Technical documentation: ENERGIATEHNIKA OÜ Flywheel 15kW".
- [55] Siemens AG, "Recording and monitoring process data", fourth edition, 2020.
- [56] Siemens AG, "STEP 7 (TIA Portal) options Target 1500S™ for Simulink® V4.0 Update 2: Programming Manual", 2020.

- [57] Amber Kinetics, "Amber Kinetics M32-DataSheet: The Industry's Only Long-Duration Kinetic Energy Storage System (KESS)—Enabling Highly Efficient Industrial and Commercial Applications".
- [58] Steven W. Smith, "The scientist and engineer's guide to digital signal processing", California Technical Publ, first. ed., San Diego, Calif., 1997.
- [59] sonnen GmbH, "Technische Daten sonnenBatterie 10".
- [60] Amber Kinetics, "Amber-Kinetics-DataSheet".
- [61] Philipp Hofbauer, AllgäuNetz GmbH & Co.KG, "Messung PV", 2019.
- [62] Noah Pflugradt, "LoadProfileGenerator", <https://www.loadprofilegenerator.de/>, accessed October 9, 2021.
- [63] Soo S. Choi, Hong S. Lim, "Factors that affect cycle-life and possible degradation mechanisms of a Li-ion cell based on LiCoO₂", Journal of Power Sources, Vol. 111, No. 1, pp. 130–136, 2002.

APPENDICES

Appendix 1 Electrical circuit description of FESS

Terminal plan X1

function text	Indication	Connection	Terminal	Bridge	Indication	Connection	Page
L1	A10	2	1		X2	1	P1-2B
L2	A10	4	2		X2	3	P1-2B
L3	A10	6	3		X2	5	P1-2B
N	A10	N	4				P1-2B
PE	A10	PE	PE		PE	several	P1-3B

Terminal plan X2

function text	Indication	Connection	Terminal	Bridge	Indication	Connection	Page
L1	X1	1	1		F1	1	P1-2B
MCB auxillary supply			2		F2	1	P1-2B
L2	X1	2	3		F1	3	P1-2B
MCB auxillary supply			4		F2	3	P1-2B
L3	X1	3	5		F1	5	P1-2B
MCB auxillary supply			6		F2	5	P1-2B

Terminal plan X3

function text	Indication	Connection	Terminal	Bridge	Indication	Connection	Page
L1	X2	1	1		A02	L1	P1-2C
Surge protection	A03	L1	2		A02	L1	P1-3C
L2	X2	3	3		A02	L2	P1-2C
Surge protection	A03	L2	4		A02	L2	P1-3C
L3	X2	5	5		A02	L3	P1-2C
Surge protection	A03	L3	6		A02	L3	P1-3C

Terminal plan X4

function text	Indication	Connection	Terminal	Bridge	Indication	Connection	Page
Charging contactor	K2	2	1		L1	U2	P1-2E
Current transducer	K1	2	2				P1-2F
Charging contactor	K2	4	3		L1	V2	P1-2E
Current transducer	K1	4	4				P1-2F
Charging contactor	K2	6	5		L1	W2	P1-2E
Current transducer	K1	6	6				P1-2F

Terminal plan X5 (0V)

function text	Indication	Connection	Terminal	Bridge	Indication	Connection	Page
auxiliary voltage ok			1		H1	x2	P2-3B
main contactor closed	H2	x2	1				P2-3B
display motor current	A09	2	1		X6	1	P2-5B
speed monitoring	A06	2	1				P3-3B
motor fan	X20	4	2				P3-6B
charging contactor	K2	A2	3				P2-3C
fan cabinet	M1	2	3		K2	A2	P3-7B
main contactor	K1	A2	4				P2-3C
coupling relay main contactor	K3	A2	5				P2-3D

Terminal plan X6 (Signals)

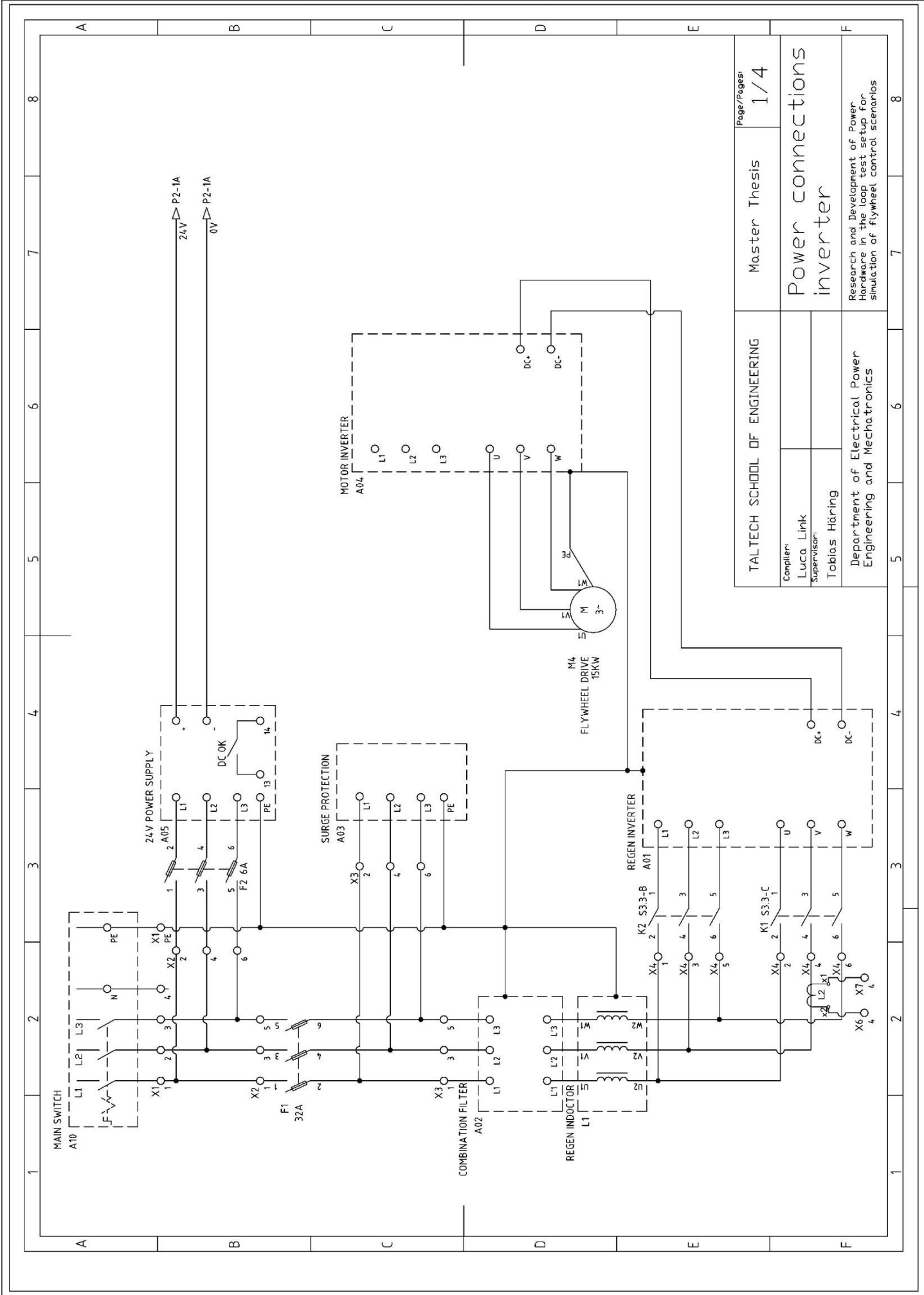
function text	Indication	Connection	Terminal	Bridge	Indication	Connection	Page
Current sensor 0V			1		A05	-	P3-2C
Temperature sensor 0V			2				P3-2C
Vibration sensor 0V			3				P3-2C
	A04	3	3		X20	13	P2-6C
Current			4		L2	x2	P1-2F
Temperature			5		A07	5	P3-2C
Vibration			6		X20	11	P3-4C
Speed display +	PLC	5.2	7		A06	16	P3-3C
Speed display -	PLC	5.4	8		A06	17	P3-4C
Inverter Analog input +	PLC	2.1	9		A04	6	P2-6D
Inverter Analog input -	PLC	2.5	10		A04	7	P2-6D
Enable motoring drive			11		A04	4	P2-6C
Speed monitoring -	A06	4	12		X20	8	P3-3C
Speed monitoring S	A06	5	13		x20	9	P3-3C
Speed monitoring +	A06	3	14		x20	10	P3-3C
Vibration sensor	K5	A1	15		x20	12	P3-4C
Motor thermistor	A04	8	16		x20	14	P2-5C
Motor inverter speed	A04	9	18		PLC	1.1	P2-6D
Motor inverter power	A04	10	19		PLC	1.2	P2-6D
Motor inverter 0V	A04	11	20		PLC	1.3 & 1.4	P2-6D

Terminal plan X7 (24V)

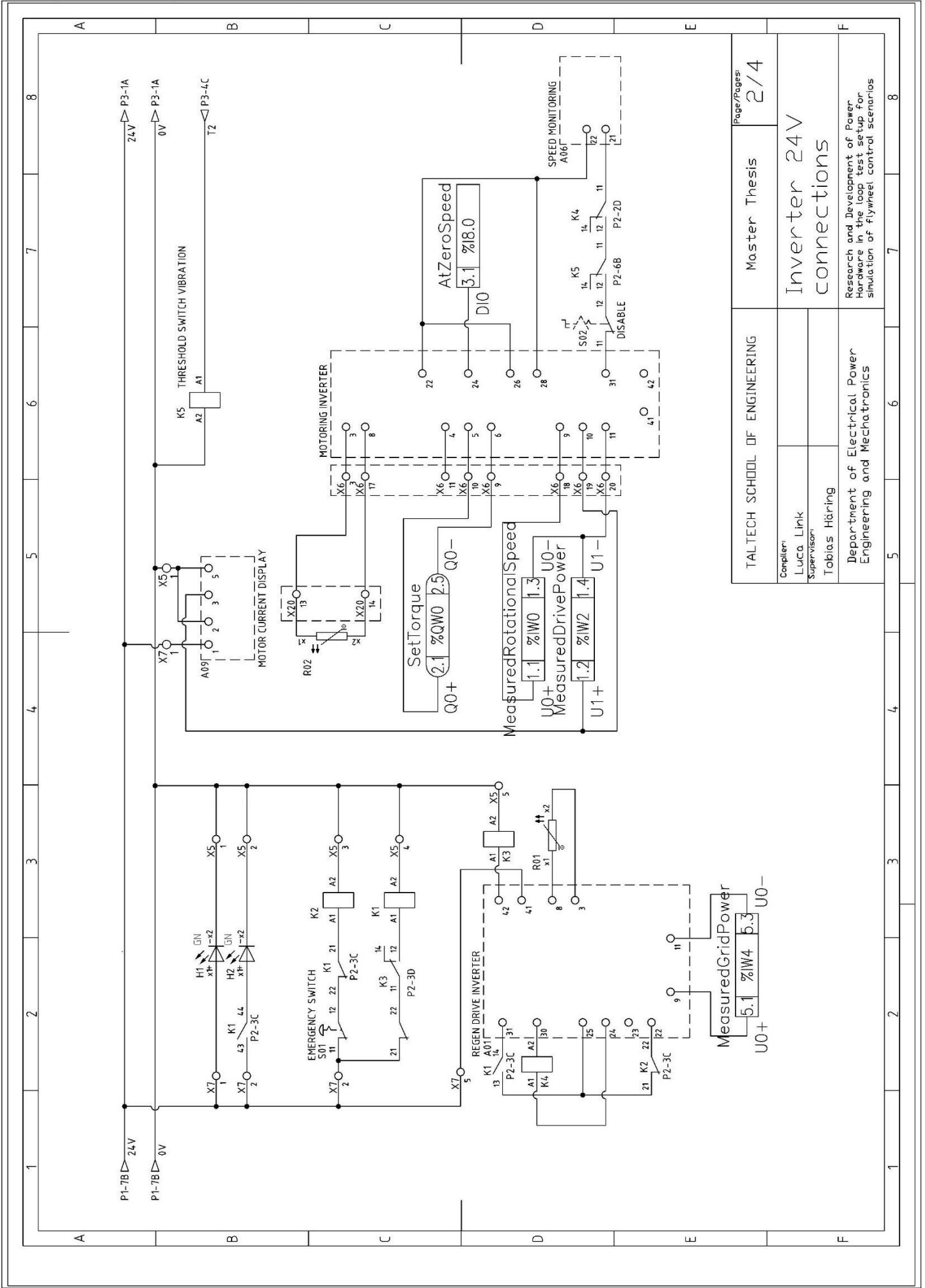
function text	Indication	Connection	Terminal	Bridge	Indication	Connection	Page
auxiliary voltage ok	A05		1		H1	x1	P2-2B
display motor current			1		A09	1	P2-4B
speed monitoring			1		A06	1	P3-3B
main contactor closed			2		K1	43	P2-2B
charging contactor			2		S01	11	P2-2C
motor fan			3		F4	1	P3-5B
fan cabinet			3		F3	1	P3-6B
From current transducer			4		L2	x1	P1-2F
Temperature transducer			4		A07	6	P3-2B
coupling relay for main contactor			5		A01	41	P2-2D

Terminal plan X20 (Motor)

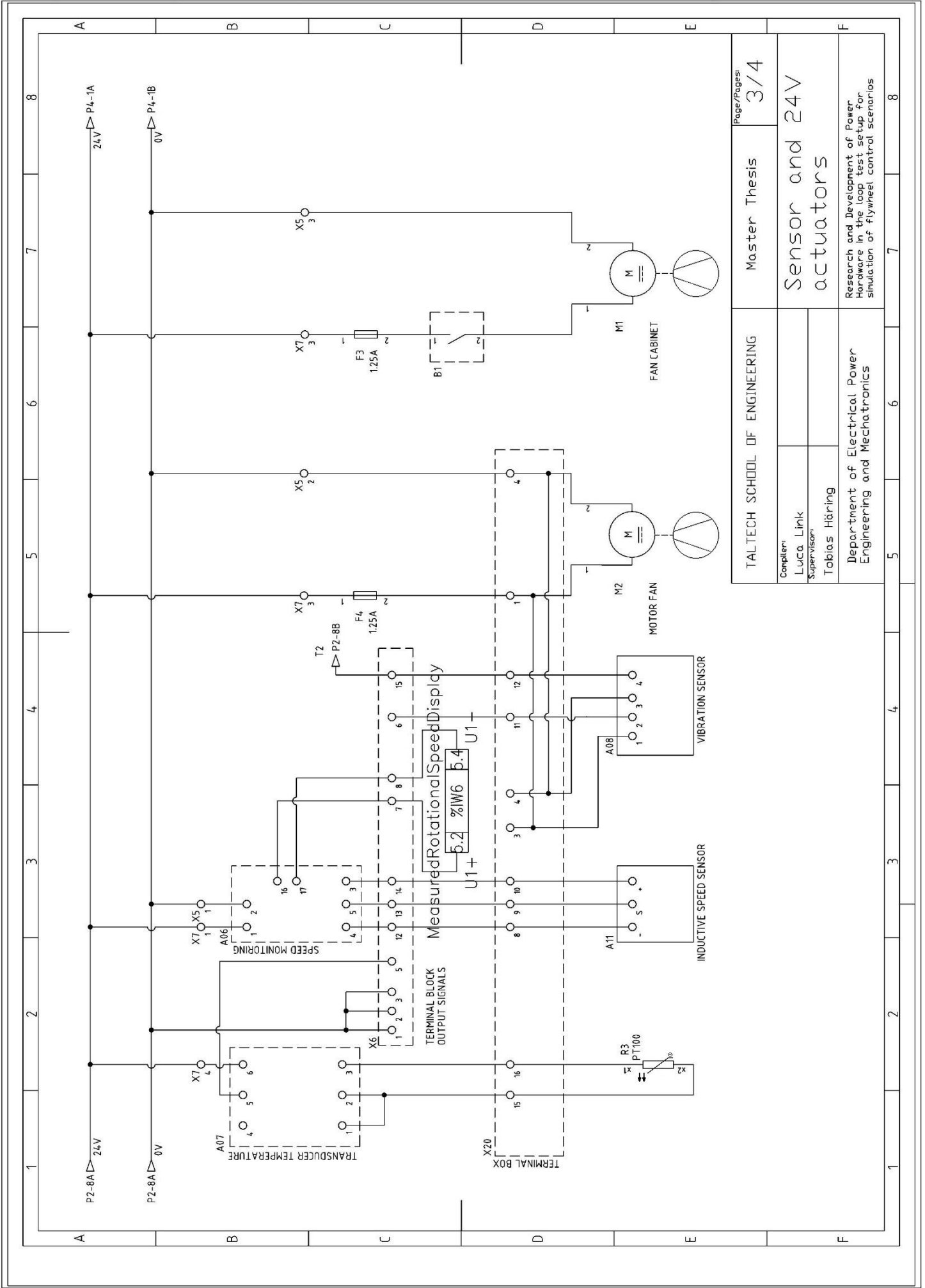
function text	Indication	Connection	Terminal	Bridge	Indication	Connection	Page
Motor fan	M2	1	1		F4	2	P3-5D
Vibration sensor 24V			3		A08	1	P3-3D
Motor fan	M2	2	4		X5	2	P3-6D
Vibration sensor 0V			4		A08	3	P3-3D
Speed monitoring -	X6	12	8		A11	-	P3-3D
Speed monitoring S	X6	13	9		A11	S	P3-3D
Speed monitoring +	X6	14	10		A11	+	P3-3D
Vibration sensor	X6	6	11		A08	2	P3-4D
Vibration sensor	X6	15	12		A08	4	P3-4D
Vibration sensor	X6	3	13		R02	x2	P2-5C
Vibration sensor	X6		14		R02	x1	P2-5C
Motor temperature	A07	2	15		R03	x2	P3-1D
Motor temperature	A07	3	16		R03	1	P3-2D



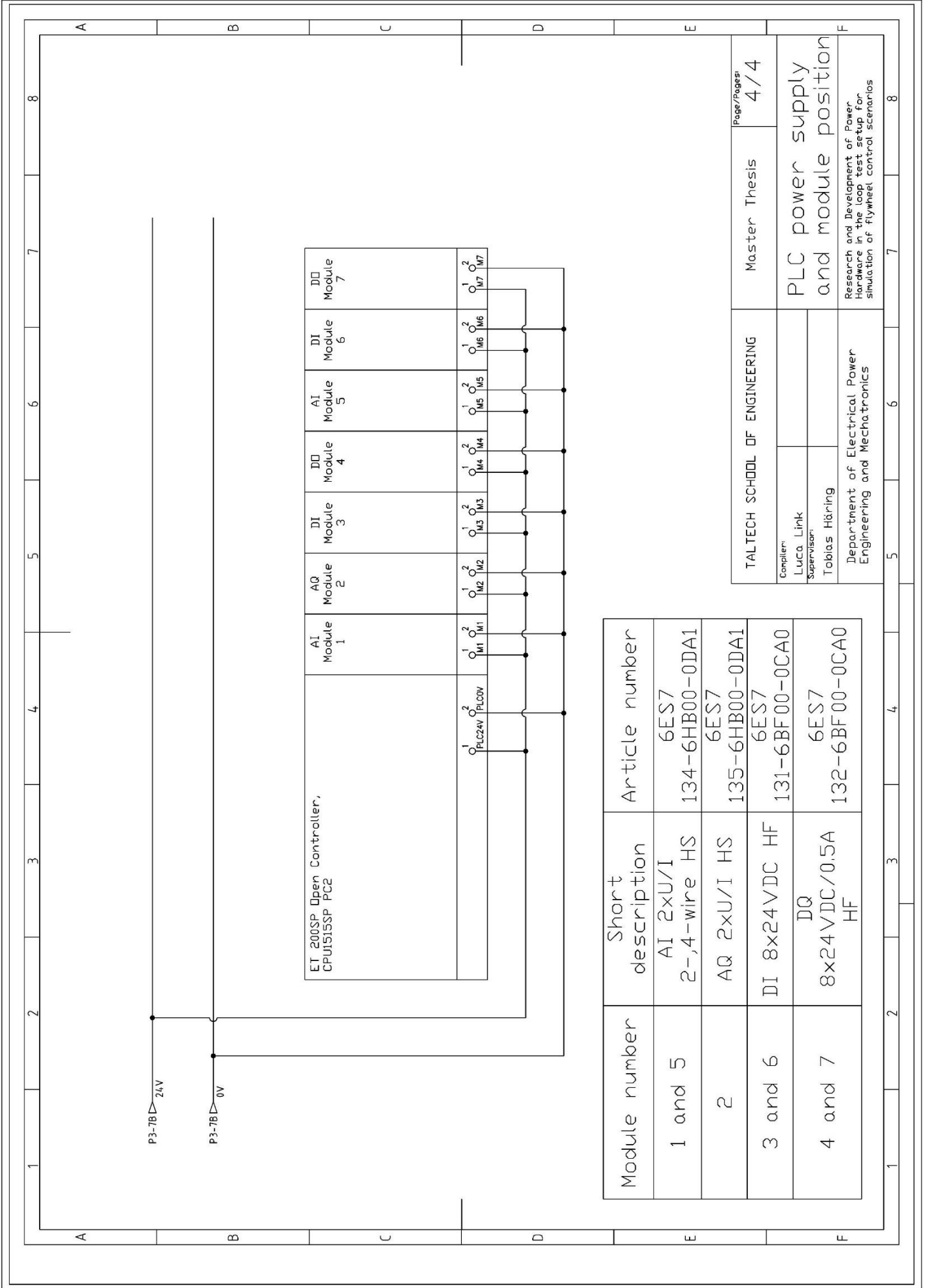
TALTECH SCHOOL OF ENGINEERING	Master Thesis	Page/Pages:	1/4
Complere: Luca Link	Power connections		
Supervisor: Tobias Häring	inverter		
Department of Electrical Power Engineering and Mechatronics	Research and Development of Power Hardware in the loop test setup for simulation of flywheel control scenarios		



TALTECH SCHOOL OF ENGINEERING	Master Thesis	Page/Pages: 2/4
Compiler: Luca Link Supervisor: Tobias Häring	Inverter 24V connections	
Department of Electrical Power Engineering and Mechatronics	Research and Development of Power Hardware in the loop test setup for simulation of flywheel control scenarios	



TALTECH SCHOOL OF ENGINEERING	Master Thesis	Page/Pages: 3/4
Compiler: Luca Link	Sensor and 24V actuators	
Supervisor: Tobias Häring		
Department of Electrical Power Engineering and Mechatronics	Research and Development of Power Hardware in the loop test setup for simulation of flywheel control scenarios	



Module number	Short description	Article number
1 and 5	AI 2xU/I 2-,4-wire HS	6ES7 134-6HB00-0DA1
2	AQ 2xU/I HS	6ES7 135-6HB00-0DA1
3 and 6	DI 8x24VDC HF	6ES7 131-6BF00-0CA0
4 and 7	DO 8x24VDC/0.5A HF	6ES7 132-6BF00-0CA0

TALTECH SCHOOL OF ENGINEERING	Master Thesis	Page/Pages: 4/4
Compiler: Luca Link		PLC power supply and module position
Supervisor: Tobias Häring		
Department of Electrical Power Engineering and Mechatronics		Research and Development of Power Hardware in the loop test setup for simulation of flywheel control scenarios

Appendix 2 MATLAB Simulink setup for build model

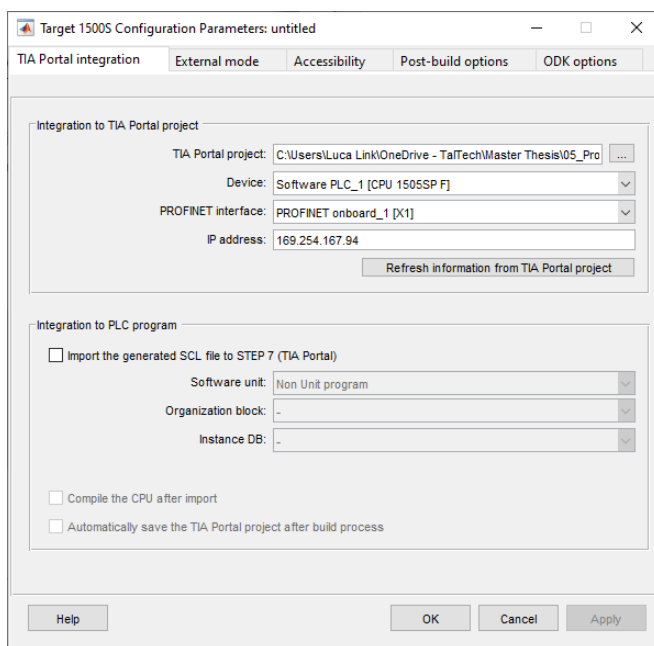
To build the executable function blocks from MATLAB Simulink, the following software must be installed on the PC. This includes the target 1500s:

- Microsoft Windows 10, 64bit
- SIMATIC ODK 1500S V2.0 or higher
- MATLAB 2020b (64bit) with the following configuration:
 - MATLAB 9.9
 - MATLAB Coder 5.1
 - Simulink 10.2
 - Simulink Coder 9.4

For all the software, a valid license is necessary.

Description of development of source code:

1. Open Model Settings in Simulink
2. Change under Code Generation the system target file to Target_1500S_V4_0_grt.tlc
3. Open the Target 1500S Options
4. Select the right TIA Portal project, Device and IP address



5. Apply the changes
6. By pressing ctrl and b, the building of the source code from the Simulink model is started.
7. In the diagnostics of Simulink, a link to the output files is shown

A detailed description of the implementation and further functions like the external mode is given in the manual of the Target1500s function [56].

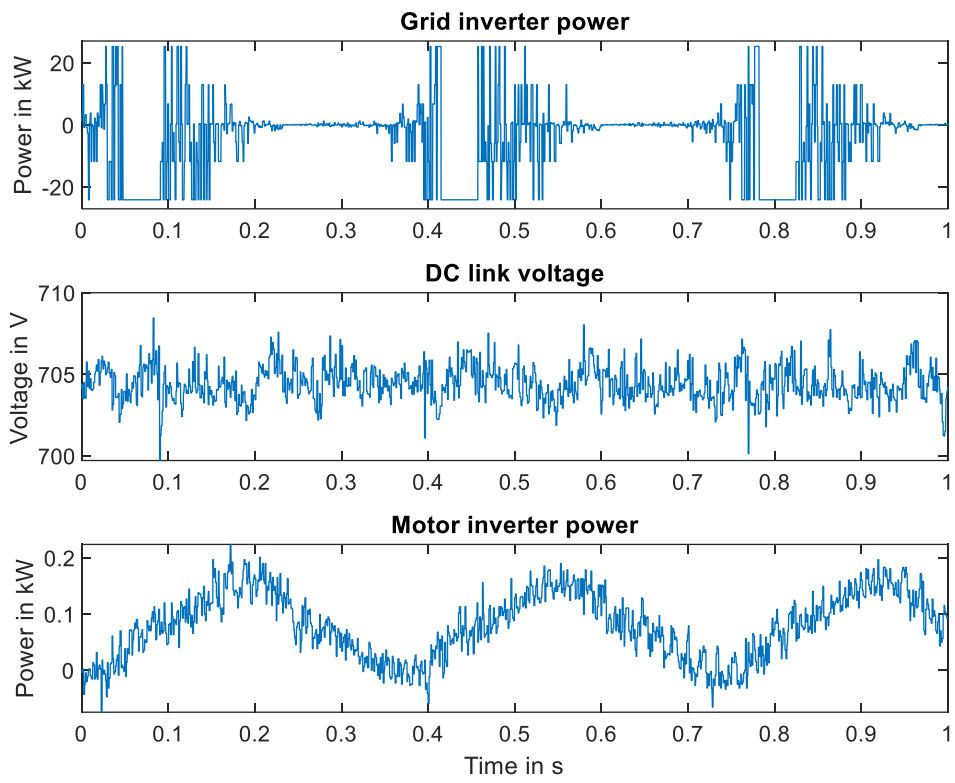
Appendix 3 Allocation function

The described function is executed in a cyclic OB with 100 microsecond cyletime.

First network

Description: Allocation and transformation of signals		
Constant variables		
PowerMax	Real	62546.28
MomentInertia	Real	2.15
PI	Real	3.14159
<pre>//-----Set analog output----- //Torque request "SetTorque" := REAL_TO_INT("FESS".Data.SetTorque); //-----Read Analog inputs----- //Rotational speed from drive inverter "FESS".Data.MeasuredRotationalSpeed :=(INT_TO_REAL("MeasuredRotationalSpeed") / 27648.0 * 2.0 * 5030.0); "Filter_PT1_DB_2"(Input:="FESS".Data.MeasuredRotationalSpeed, SubstituteOutput:=0.0, ErrorAck:=FALSE, Reset:=FALSE, Output=>"FESS".Data.MeasuredRotationalSpeed); "Filter_PT1_DB_2".CycleTime.Value := 0.0001; "Filter_PT1_DB_2".Lag := 0.002; //Calculation stored energy "FESS".Data.MeasuredStoredEnergy := #MomentInertia/2*(INT_TO_REAL("MeasuredRotationalSpeed") / 27648.0 *2.0 * 5030.0*#PI/30)**2; //Power from drive inverter "FESS".Data.MeasuredDrivePower := INT_TO_REAL("MeasuredDrivePower") / 27648.0 * #PowerMax; "Filter_PT1_DB"(Input:="FESS".Data.MeasuredDrivePower, SubstituteOutput:=0.0, ErrorAck:=FALSE, Reset:=FALSE, Output=>"FESS".Data.MeasuredDrivePower); "Filter_PT1_DB".CycleTime.Value := 0.0001; "Filter_PT1_DB".Lag := 0.001; //Power from grid inverter "FESS".Data.MeasuredGridPower := INT_TO_REAL("MeasuredGridPower")/ 27648.0 * #PowerMax; "Filter_PT1_DB_1"(Input:="FESS".Data.MeasuredGridPower, SubstituteOutput:=0.0, ErrorAck:=FALSE, Reset:=FALSE, Output=>"FESS".Data.MeasuredGridPower); "Filter_PT1_DB_1".CycleTime.Value := 0.0001; "Filter_PT1_DB_1".Lag := 0.001; //-----Calculation background----- //10V = 27648 Maximum output / Input of Analog Card //10V = SPEED_MAX = 2 * 5030.0 (Selected rpm at FESS inverter Pr0.02) //6000rpm = 10V at Display output //PowerMax = Sqrt(3)*AC_VOLTAGE_MAX*DRIVE_CURRENT_MAX //10V = 62546.27916W = Sqrt(3)*650V * 25A/0.45 //The measured power is filtered with an PT1 Filter</pre>		

Appendix 4 Ringing investigation graph disabled motor inverter



Appendix 5 Spectral analyses

```
close all
figure(1)
%Import data from PLC Datalogger with maximum sampling rate
TsGrid = timeseries(Data1.Grid,Data1.Time);
TsMotor = timeseries(Data1.FESS,Data1.Time);

fs = 9.8809e+03;           % new sampling frequency

% Perform spectral analysis (based on MATLAB help examples)
% Power grid
y = fft(TsGrid.Data);
y0 = fftshift(y);           % shift y values
n = length(TsGrid.Data);   % number of samples

f0 = (-n/2:n/2-1)*(fs/n);   % 0-centered frequency range
power0 = abs(y0).^2/n;      % 0-centered power

plot(f0,power0)
xlabel('Frequency in Hz')
ylabel('Grid power')

% Power motor
hold
y = fft(TsMotor.Data);
y0 = fftshift(y);           % shift y values
n = length(TsMotor.Data);  % number of samples

f0 = (-n/2:n/2-1)*(fs/n);   % 0-centered frequency range
power0 = abs(y0).^2/n;      % 0-centered power
yyaxis right
plot(f0,power0)
xlabel('Frequency in Hz')
ylabel('Motor power')
legend('Grid power','Motor power')
xlim([-25 25])

% Plot signal
figure(2)
plot(TsGrid/1000,'.-')
ylabel('Grid power in kW')
hold
yyaxis right
plot(TsMotor/1000,'.-')
ylabel('Motor power in kW')
xlim([0 1])
xlabel('Time in s')
title('')
legend('Grid power','Motor power')
```

Appendix 6 Implementation approximation

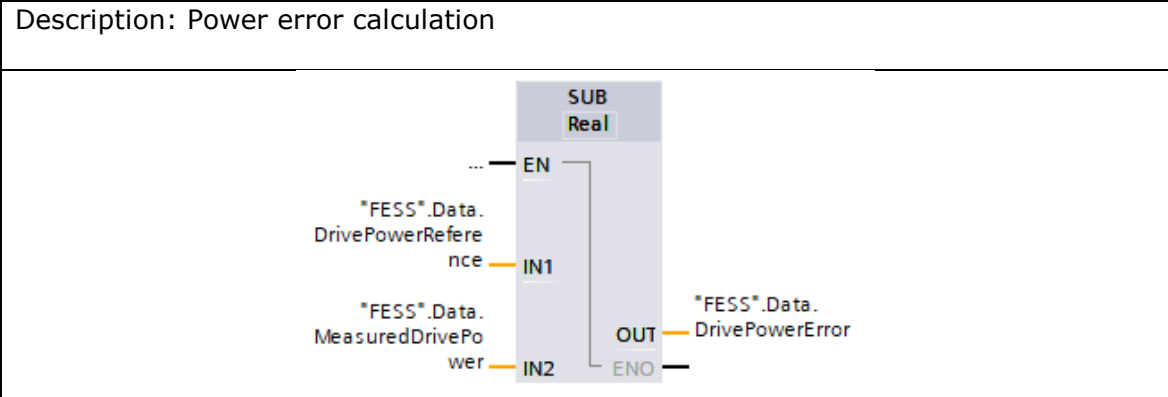
Description: Approximation (FactorAt3000 was introduced during optimization)

<p>The diagram shows a function block named "Approximation" with the following connections: - Input: EN (Enable) - Inputs: rpm (from "MeasuredRotationalspeed"), power (from "#PowerPlout") - Output: TorqueSet (to "SetTorque") - Output: ENO (Enable Out)</p>	<table style="width: 100%; border-collapse: collapse;"> <tr> <td colspan="2">Input</td> </tr> <tr> <td>Rpm</td> <td>real</td> </tr> <tr> <td>Power</td> <td>real</td> </tr> <tr> <td colspan="2">Output</td> </tr> <tr> <td>TorqueSet</td> <td>real</td> </tr> <tr> <td colspan="2">Temp</td> </tr> <tr> <td>TorqueCalc</td> <td>real</td> </tr> <tr> <td colspan="2">Constant</td> </tr> <tr> <td>m</td> <td>real 0.000289609</td> </tr> <tr> <td>maxTorque</td> <td>real 27648.0</td> </tr> <tr> <td>FactorAt3000</td> <td>real 1.150977</td> </tr> </table> <pre> #TorqueCalc := #power / (#m * #rpm); IF #TorqueCalc > #maxTorque THEN #TorqueCalc := #maxTorque; END_IF; IF #rpm > 5100 THEN #TorqueCalc := 0; ELSIF #rpm > 3000 THEN #TorqueCalc := #power * #FactorAt3000; ELSIF #rpm < 200 AND #power < 100 THEN #TorqueCalc := 0; END_IF; #TorqueSet := #TorqueCalc; </pre>	Input		Rpm	real	Power	real	Output		TorqueSet	real	Temp		TorqueCalc	real	Constant		m	real 0.000289609	maxTorque	real 27648.0	FactorAt3000	real 1.150977
Input																							
Rpm	real																						
Power	real																						
Output																							
TorqueSet	real																						
Temp																							
TorqueCalc	real																						
Constant																							
m	real 0.000289609																						
maxTorque	real 27648.0																						
FactorAt3000	real 1.150977																						

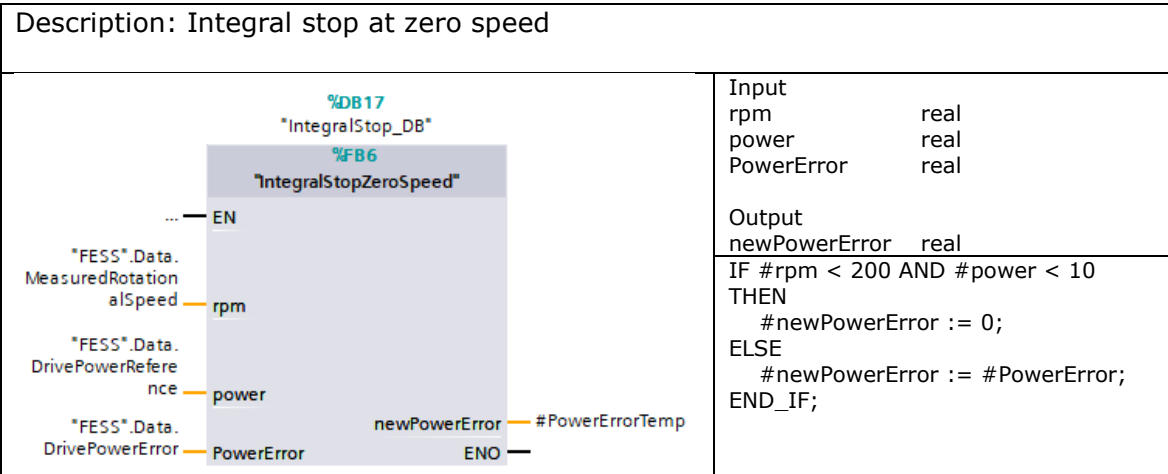
Appendix 7 FESS power controller

The following networks are all part of the FESSpowerControl function. The function is executed in a cyclic OB with one cycle per millisecond.

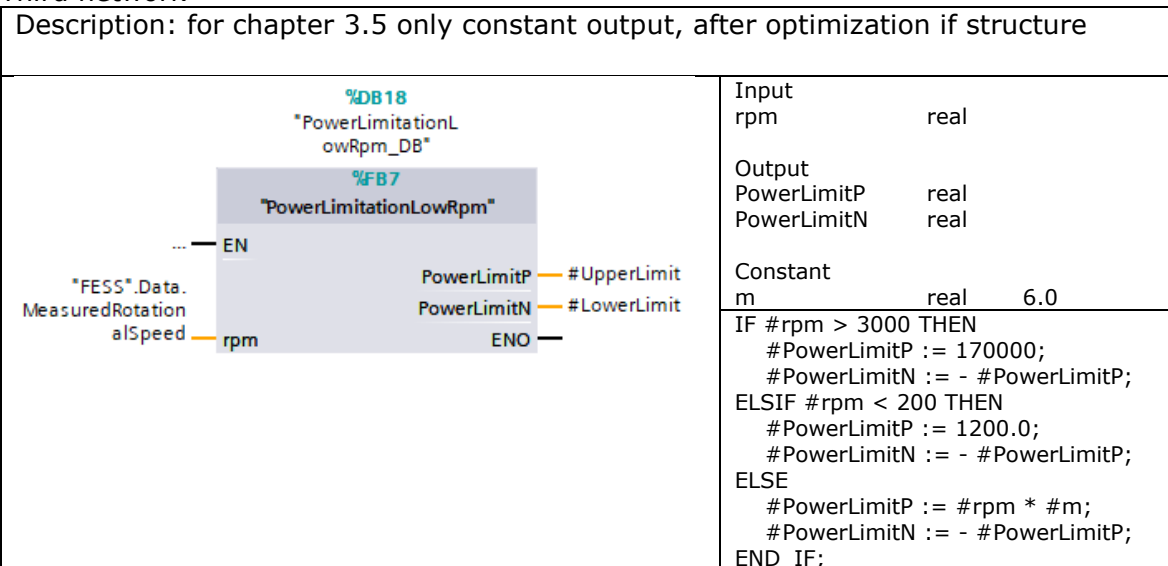
First network



Second network

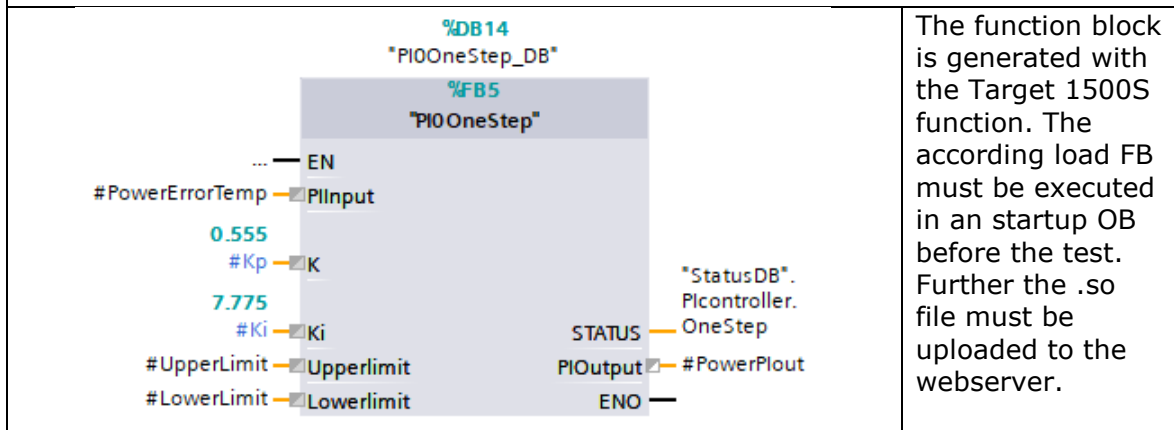


Third network



Forth network (parameters Kp and Ki optimized to Kp = 0.8 and Ki = 13.5)

Description: PI controller from chapter 3.4



The fifth network includes the approximation from appendix 2.

Power controller for flywheel energy storage

Laboratory training

1. Introduction

A flywheel is an energy storage which stores energy in a rotational mass. The benefit of flywheels over other energy storages are its cycling capability without ageing and the high power a flywheel can supply. Battery storages for example loose capacity, the more often they are charged. Further the power a battery storage can supply is lower compared to flywheels.

In Figure 1.1 the cabinet of the flywheel is shown. In the cabinet two inverters, one PLC, a 24V power supply, several relays and terminal blocks and several fuses are located. More information about the devices can be found in the manual of the flywheel [1]. The flywheel itself is shown in Figure 1.2. On top a fan is located which cools the induction motor. The induction motor is located in the center. The induction motors shaft is connected to the rotating mass, which is the bottom part of the assembly.

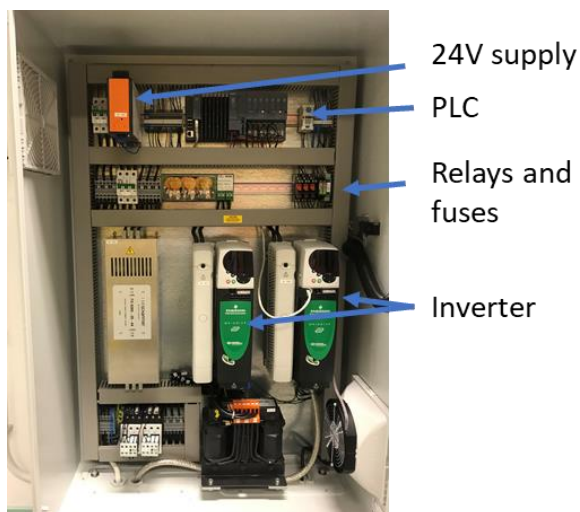


Figure 1.1 Cabinet of flywheel with PLC and inverters

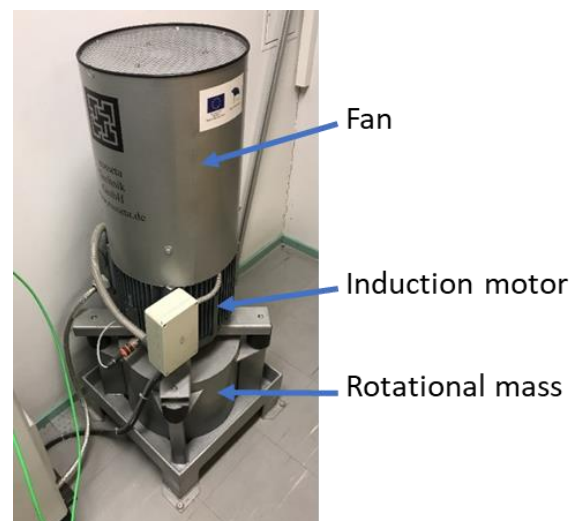


Figure 1.2 Flywheel rosseta Technik T3-15

To charge the flywheel, the rotational mass is accelerated with an electric drive. The motor drive system converts the electrical power into mechanical power. For discharging of the flywheel, the electric drive decelerates the rotating mass and converts the mechanical power back to electrical power. The stored energy E of the flywheel can be calculated with the moment of inertia J and the rotational speed ω , see equation (1):

$$E = \frac{1}{2} \cdot J \cdot \omega^2 \quad (1)$$

The present flywheel is manufactured by the Rosseta Technik GmbH. Its datasheet values are given with:

Maximum power $P_{max} = 15kW$

Maximum stored energy $E_{max} = 300kWs$

Moment of inertia $J = 2.15kgm/s$

At which rotational speed in 1/min is the flywheel fully charged?

There are several different scenarios, in which flywheel energy storages increase the grid resilience and power quality. Due to fast reaction time, flywheels can supply necessary power within milliseconds, while pumped hydropower plants or gas engines need several seconds till they can supply power to the grid. Flywheels enable an uninterrupted power supply. In microgrids with dynamic loads and a lot of volatile power production out of renewable sources, flywheels can smooth the power flow of the grid without ageing itself due to several charging and discharging cycles throughout the day. In combination with batteries, flywheels can extend the life time of the battery. The battery is responsible for the long-term power changes over several minutes two hours, while the flywheel will supply the fast-changing power demand. One last scenario is the use of flywheels as energy buffer for electric vehicle fast charging without big grid impact. Fast charging requires a high power of up to 350kW over several minutes. Not at every location the grid infrastructure is able to provide this power peak during the charging cycle. Flywheels can be charged with a lower power before the electric vehicle is in position. When the vehicle charging cycle starts, the flywheel is discharged with high power and as result enables fast charging of electric vehicles without big investments in the infrastructure.

In all of the mentioned scenarios, the power of the flywheel must be controlled. In the following laboratory, the student will implement a controller for the control of the charging and discharging power of the flywheel.

1.1. Main tasks

The following task must be performed by the student to implement the power controller:

- Understand the test setup
- Understand the control structure
- Determine PI controller parameter
- Implement the output files of the target1500s function
- Tune PI-controller

1.2. Hardware setup

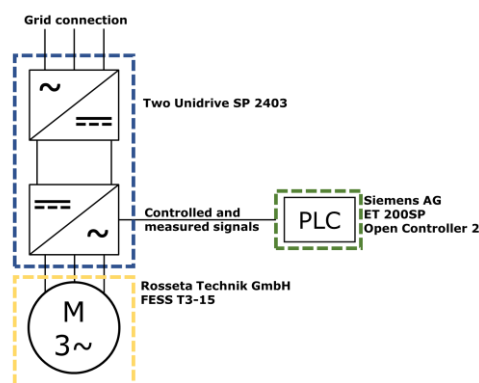


Figure 1.3 Schematic of the hardware setup

Figure 1.3 shows a schematic of the hardware setup. The two Unidrive SP 2403 AC DC inverter work in regen mode and share a DC-link. The inverter, which is connected to the induction motor is controlled by the PLC. All the communication is performed over analog signals.

2. Work performed in preparation at home

The manufacturer of the flywheel reduces the accessible power for rotational speed below 3000rpm. This can be observed while applying different constant values as input signals for the inverter. The first subplot of Figure 2.1 shows the charging power of the flywheel over time, while the second subplot shows the rotational speed over time. At the timestep, when the flywheel reaches 3000rpm, the charging power reaches it maximum and stays constant. Before it was increasing with a constant slope.

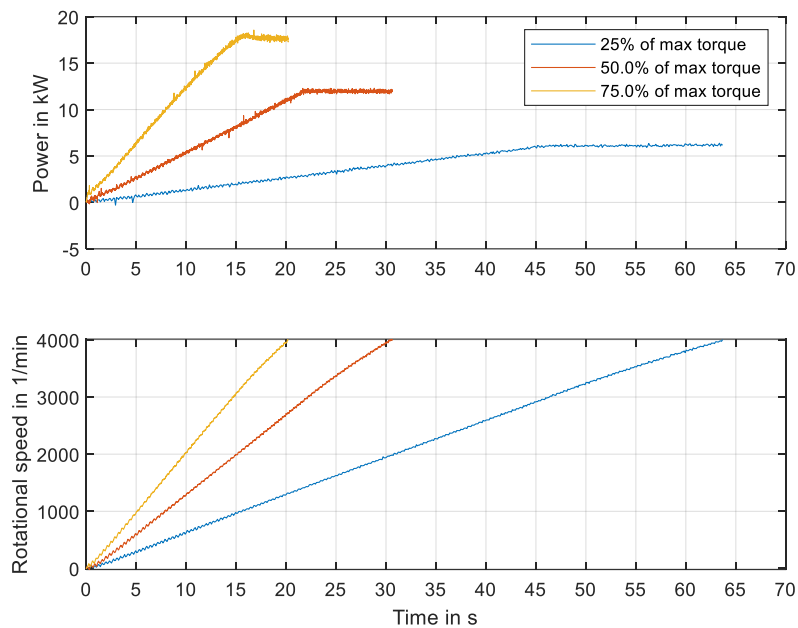


Figure 2.1 Flywheel response to constant inverter input

The figure also shows, that the flywheel could be charged with the final charging power of around 6kW from the measurement with 25% of the maximum torque already around 40s earlier at a rotational speed of 1000rpm, if a higher input values is used. In the appendix, an approximation function is described which is used to calculate the desired torque input value of the inverter, depending on the set power. The result of the approximation is shown in Figure 2.2 from stand still and in Figure 2.3 while already accelerated to 2000rpm. It is visible that the set power and the measured power are close to each other. However, if the power is applied from zero speed, an overshoot occurs before the power starts to level its final charging power. The final power is a bit higher than the desired power.

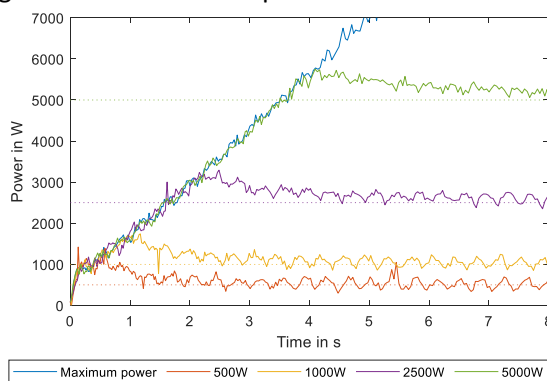


Figure 2.2 Power step from zero rotational speed

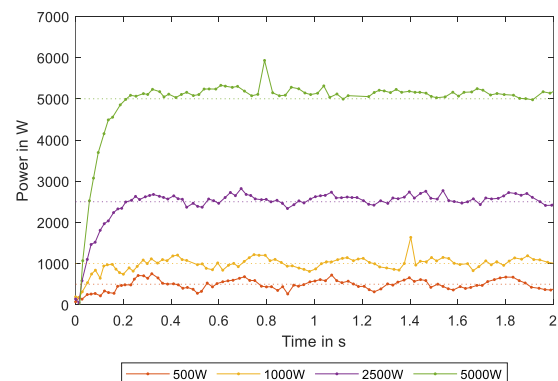


Figure 2.3 Power step while already spinning

The planned control structure of the power controller is shown in Figure 2.4. The approximation between PI controller and flywheel energy storage system (FESS) is the in the appendix described function. Above 3000rpm, the PI-controller output is fed through the approximation block without manipulation.

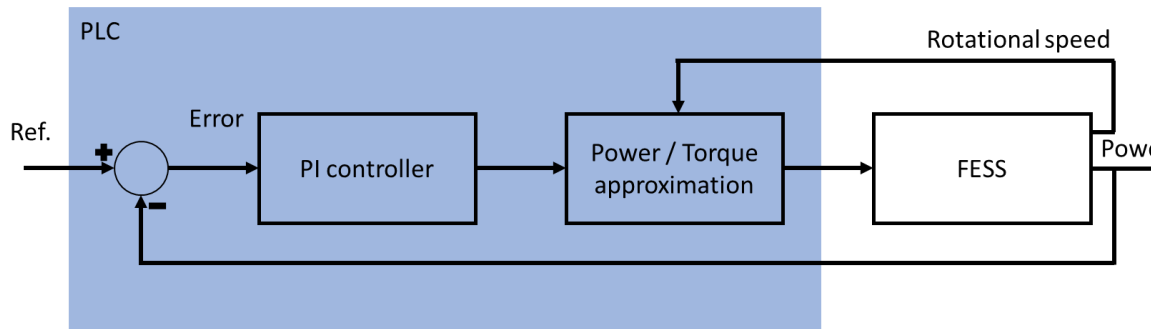


Figure 2.4 Flywheel Control structure

It is the task of the student to eliminate the gain error and increase the robustness of the FESS. Therefore, the student has to define the PI controller parameter. For choosing the controller parameter, the transfer function of the system is necessary.

2.1. Determine flywheel transfer function

The transfer function describes the system response to changes on the input signal. To obtain the transfer function, the flywheel is accelerated to at least 2000rpm. A step is applied to the open loop and the system response is analyzed. In Figure 2.5 the step response of the system is shown. It is estimated, that the flywheel behaves like a first order system. Determine the transfer function of the figure.

$$G_{FESS}(s) = \underline{\hspace{10em}} \quad (2)$$

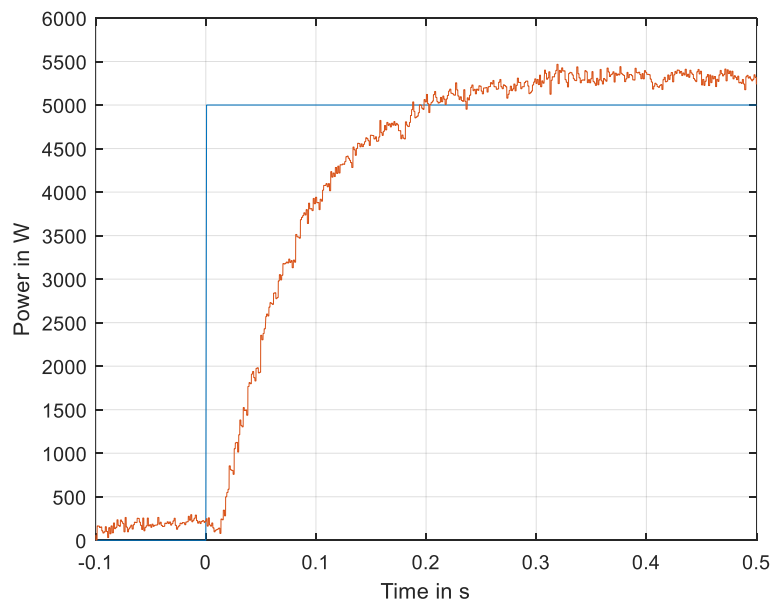


Figure 2.5 Step response flywheel

2.2. Determine PI controller parameters

To determine the PI controller parameter, the pole placement method is used. Here the transfer function of the whole system is compared with a desired system. Perform the pole placement method for the flywheel. Derive the complete system transfer function, including the PI controller. Assume the approximation block feeds the PI controller output directly to the FESS without manipulation. The PI controllers transfer function is given with $G_{PI}(s) = K_p + \frac{K_i}{s}$.

The controller should be stable, but still reach the desired value in less than 500ms. Therefore, a second order transfer function with $D = 1$ and $\omega_0 = 10$ is used for comparison. Compare the parameters of the full system transfer function with the parameters of the given transfer function:

$$\frac{1}{(s^2 + s \cdot 2 \cdot D \cdot \omega_0 + \omega_0^2)}$$

$$K_p = \underline{\hspace{10em}} \quad (3)$$

$$K_i = \underline{\hspace{10em}} \quad (4)$$

The in Figure 2.6 shown PI control structure was developed in MATLAB Simulink. The anti-windup is back clamped with the integral parameter. The saturation limits are variables, so that the user is able to change the limits in TIA portal. With the Siemens Target 1500S function the PIO_ODK.so and the PIO_ODK.scl file were built. In the laboratory, you have to implement the PI controller in a given TIA portal project. The two output files are provided.

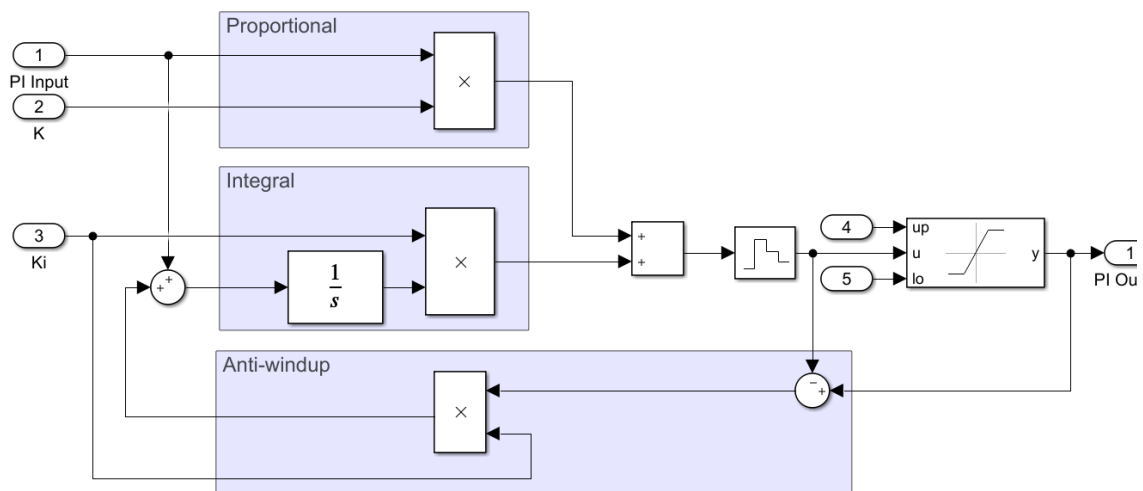


Figure 2.6 PI controller structure

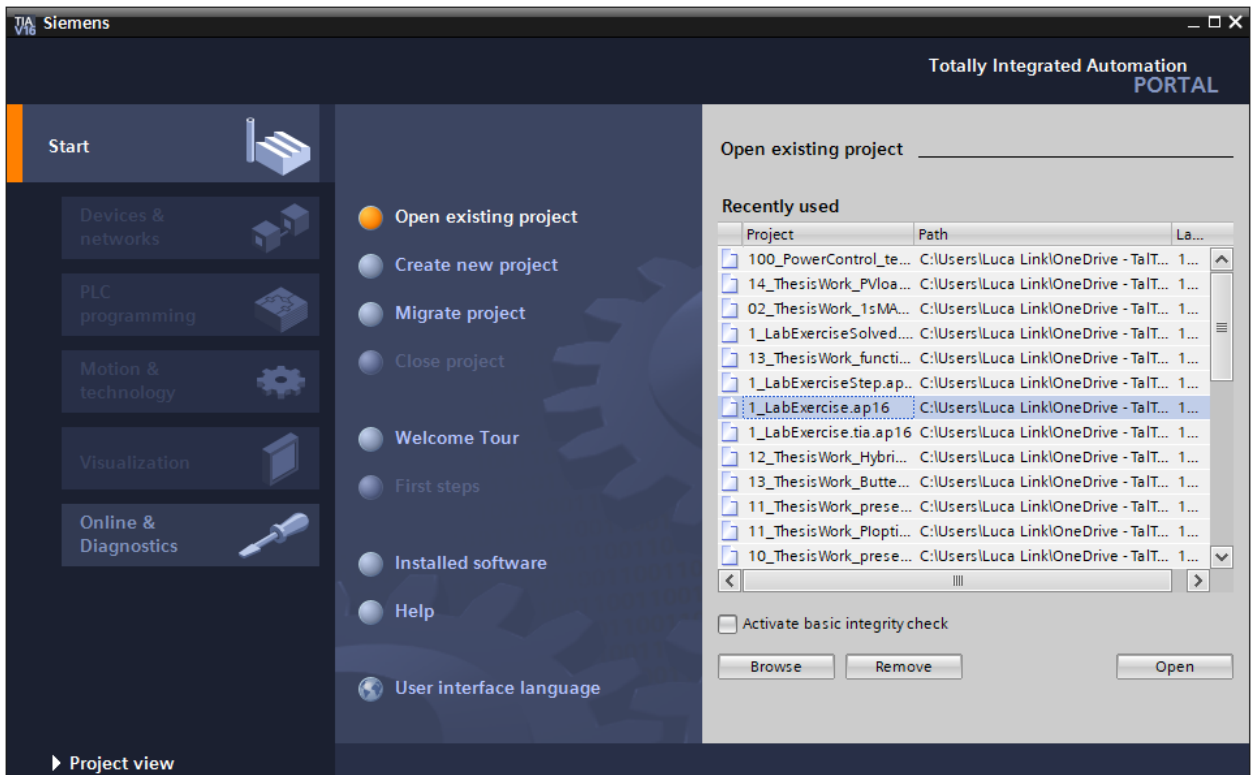
3. Work performed during the laboratory

The following tasks are performed during the laboratory. For the programming of the PLC, the Siemens software Totally Integrated Automation (TIA) Portal and its add-on SIMATIC Target 1500S is used. In the TIA Portal, devices can be configured, the PLC code can be written, the visualization with human machine interfaces can be designed, and much more. For this laboratory, the configuration of the device is already performed. The student will implement some changes in the PLC code and visualize measured signals in the TIA Portal. The Target 1500S function enables the implementation of Simulink models and control architectures into the TIA Portal. The Target 1500S function generates two files out of the Simulink model. The files must be implemented into the PLC program to use the Simulink code. The students will implement an PI controller with anti-windup structure, designed in MATLAB Simulink, on the PLC. This work is similar to workflow in industry, where one engineer designs the control architecture in Simulink and later shares the generated source files with the PLC programming colleges.

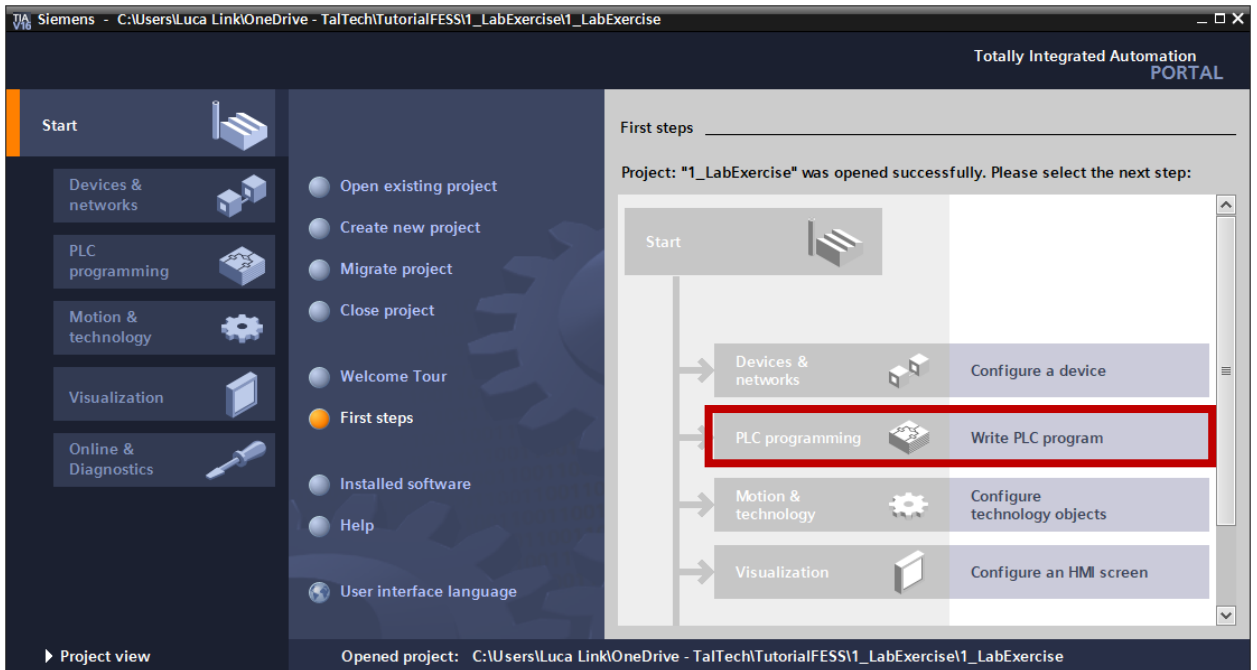
To access a PLC, it is required to connect the PC to the same network. **Therefore, plug the green RJ45 wire into the programming PC and the other side of the wire to the second RJ45 port of the cabinet (right side).** The communication is performed via PROFINET. The analog communication between PLC and inverter is already established and a calculation from integer value to physical values is performed in the allocation function (FC). The allocation function is executed in a cyclic OB.

The following figures show how to open the necessary window of the TIA Portal. Follow the marked spots to get to the PLC coding view.

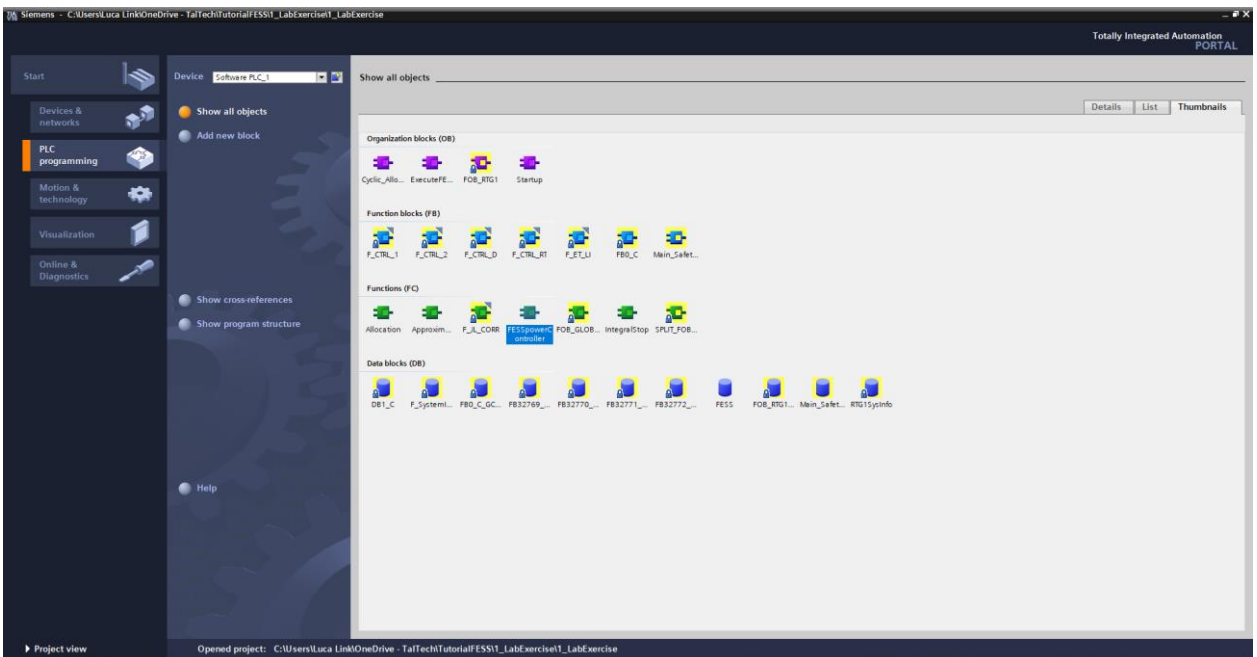
Step 1 – Open prepared project 1_LabExercise.ap16



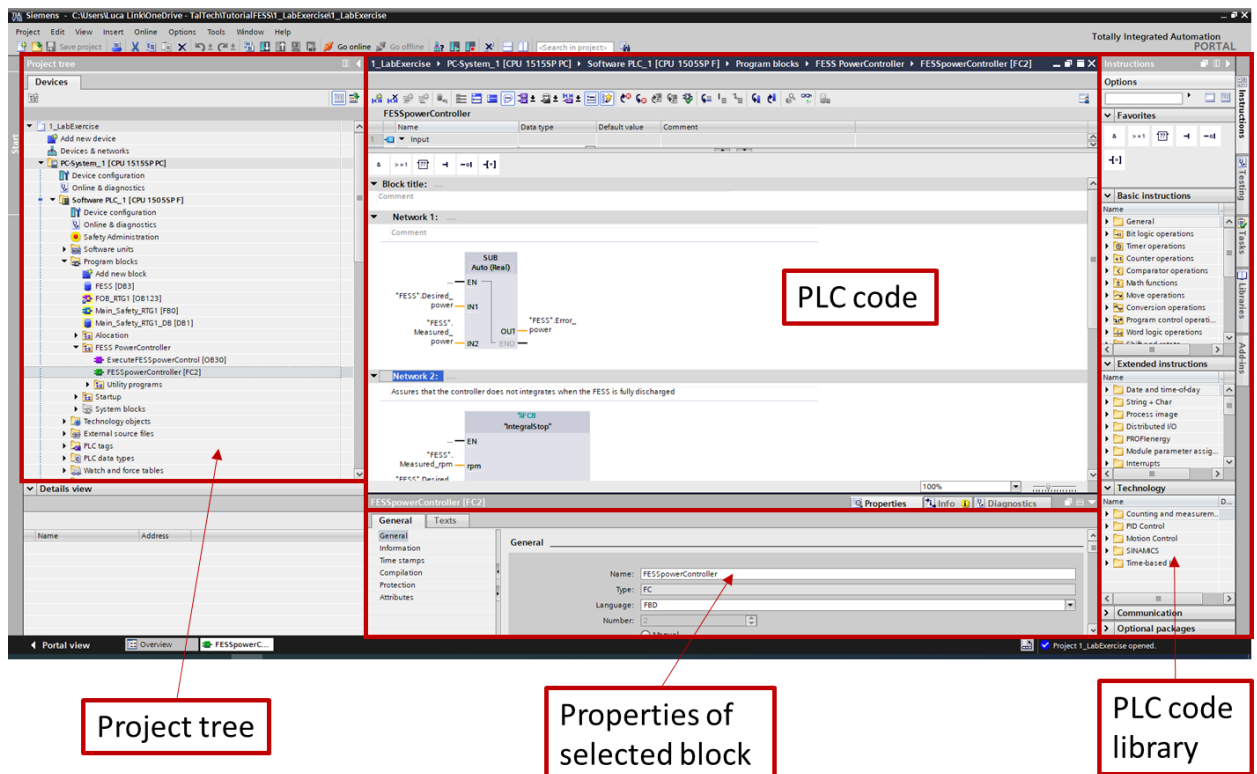
Step 2 – Click on write PLC program



Step 3 – Open the function (FC) FESSpowerController



Step 4 – make yourself familiar with the environment



The Project tree is used to switch between different blocks, and to open different windows at its right side. All open windows can be seen on the bottom below the properties box. In the screenshot only, the overview window and the FESSpowerController FC are open. The project trees is organized with different folders for every device included in the setup.

The PLC code window is used to write the PLC code. The language of the code depends on the settings of the block. It is also possible to mix different languages by adding networks in a different language e.g. SCL to an FBD block.

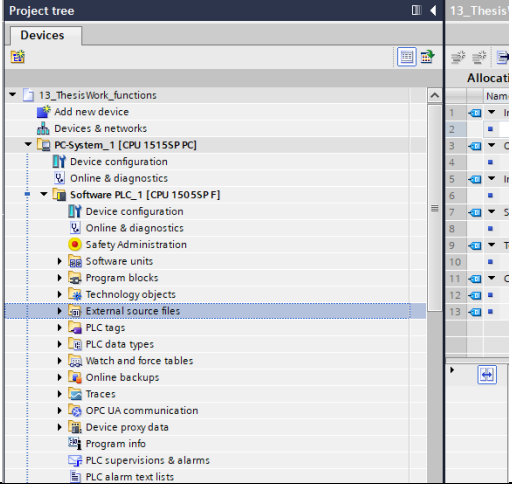
The properties window shows important information of the block. For cyclic interrupt OBs, the cycle time can be changed there. Further in this window the error messages are shown.

The PLC code library includes several standard blocks which can be add to the PLC code window via drag and drop. If the watch table or the trace function was selected in the project tree, the PLC code library is removed with a different window.

The size of the windows can be changed, depending on your working style.

3.1. Implement PI controller in TIA project

Follow the following steps to implement the PI controller

Component	What to do with it
PIO_ODK.so	<p>Load the .so file in the webservice.</p> <ul style="list-style-type: none"> Open the IP address of the PLC (169.254.167.94) in a browser Click on files → odk → and upload the .so file
PIO_ODK.scl	<ul style="list-style-type: none"> Add the .scl file in your project tree as external file. Use a right click on the added file and generate the blocks from source. <p>The FBs are created.</p> 
PIO_Load FB PIO_Unload FB	<p>Add a function to the startup organization block (located under program blocks).</p> <ul style="list-style-type: none"> First add the new function and then execute the function in the startup organization block. In this new function, add the two generated function blocks unload and load. Make sure that first the unload block is executed and afterwards the load block. Set the request signals of the function blocks to true.
PIOOneStep FB	<ul style="list-style-type: none"> To execute the PIOOneStep function block add it in the empty network no. 3 in the function FESSpowerController. In the function FESSpowerController add your two calculated controller parameters Ki and Kp as new real constants variables. Also add the power limits of the flywheel as variables ($\pm 15000W$). Use your defined variables and the pre-defined temporary variable PowerErrorTemp as inputs of the PIOOneStep FB As output, use the predefined variable FESS.PI_output.

After following all the steps, download the project to the PLC (rightclick on SoftwarePLC in project tree → download to device → Software all changes).

3.2. Set values to the PLC

Open the “watch table1” in the project tree.

1. Go online.
2. Monitor the table
3. Modify the desired power in the watch table to 3000
4. Write the modification to the PLC

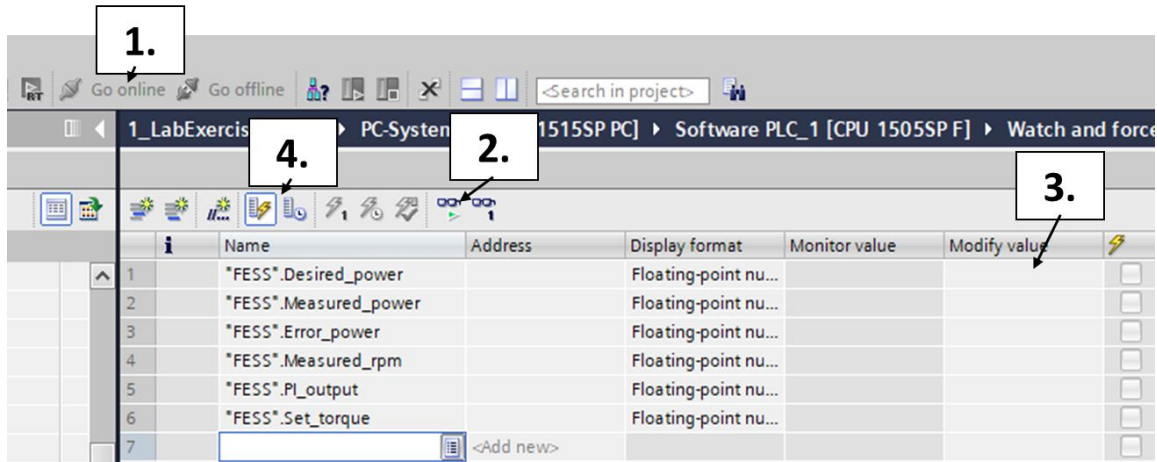


Figure 3.1 Setting desired value to PLC

The flywheel should accelerate and the measured power should settle at 3000W after some seconds. If its not accelerating, check if the disable switch on the right sight of the cabinet is in enable position or if the PLC is running (either on the webserver or at the right sight when observing the watch table).

Stop the flywheel before continuing with the training.

3.3. Trace measured and set signals

Start to prepare a trace function to track the flywheel performance.

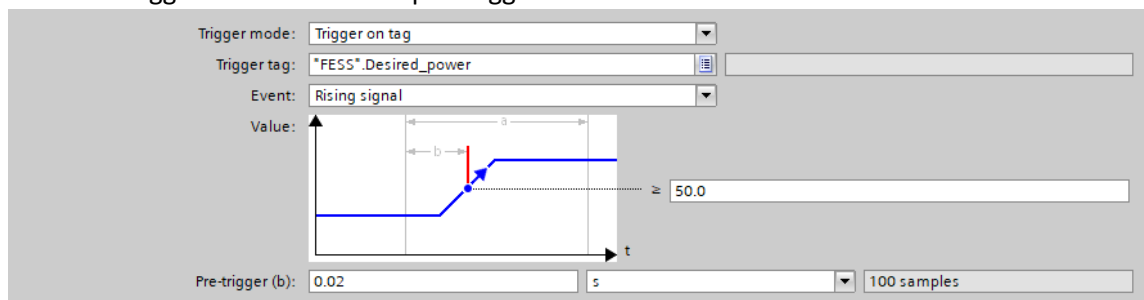
1. Add a new trace to the project tree
2. Observe the FESS.Desired_power, FESS.Measured_power, FESS_Measured_rpm, FESS.PI_output, FESS.Set_torque

Signals				
	Name	Data type	Address	Comment
1	*FESS*.Desired_power	Real		
2	*FESS*.Measured_power	Real		
3	*FESS*.Set_torque	Real		
4	*FESS*.Measured_rpm	Real		
5	*FESS*.Error_power	Real		
6	*FESS*.PI_output	Real		
7			<Add>	

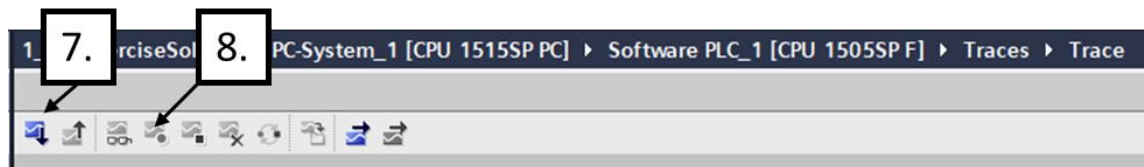
3. Sample the trace with the Cyclic_Allocation OB.
4. Record the signal with every tenth cycle and sample for 15s

Sample with:	*Cyclic_Allocation*	%OB33
Record every:	10	Cycle 0.001 s
Max. recording duration:	16383 samples / 16.383 s	
	<input type="checkbox"/> Use max. recording duration	
Recording duration (a):	15.0	s 15000 samples

5. Use the tag FESS.Desired_power as trigger
6. Set a trigger level of 50.0 and pre-trigger 0.02s



7. Transfer trace function to the PLC
8. Start the trace function



3.4. Validation of PI controller behavior

Apply a step from 10000W from zero speed and use the trace function to plot the curve (set 10000 as modification value in watch table and write modification to PLC). What can you observe in the trace function? Stop the acceleration after the FESS reached the desired 10000W.

How can you reduce the overshoot (hint: take a look on the PI controller output and error when the measured power reaches 10kW for the first time)?

There is a function called PowerLimitationLowRpm. The function calculates flexible saturation limits of the PI controller, depending on the measured speed. Exchange the fixed limits of the PI controller with flexible limits. Download your changed to the PLC and perform the test again. Is the overshoot still occurring?

3.5. Analysis of different controller parameters

Tune your FESS-Power controller by changing your PI controller parameters. To analyze the PI controller, change the sampling time of the trace function to every 2 sample and the sampling time to 2 seconds. Accelerate the flywheel to around 2000rpm and apply steps of 5kW with different Ki and Kp parameters.

What happens if you increase / decrease the parameter Ki?

What happens if you increase/ decrease the parameter K_p ?

4. References

- [1] Rosetta Technik GmbH "*Flywheel T3-15 Manual*", only available as hard copy in the laboratory

5. Appendix laboratory

Power – speed – torque approximation description

In Figure 5.1 the increase in power depending on the rotational speed is shown for constant inverter inputs. A linear approximation is used to determine a function which describes every individual graph. The specific functions are shown in the figure.

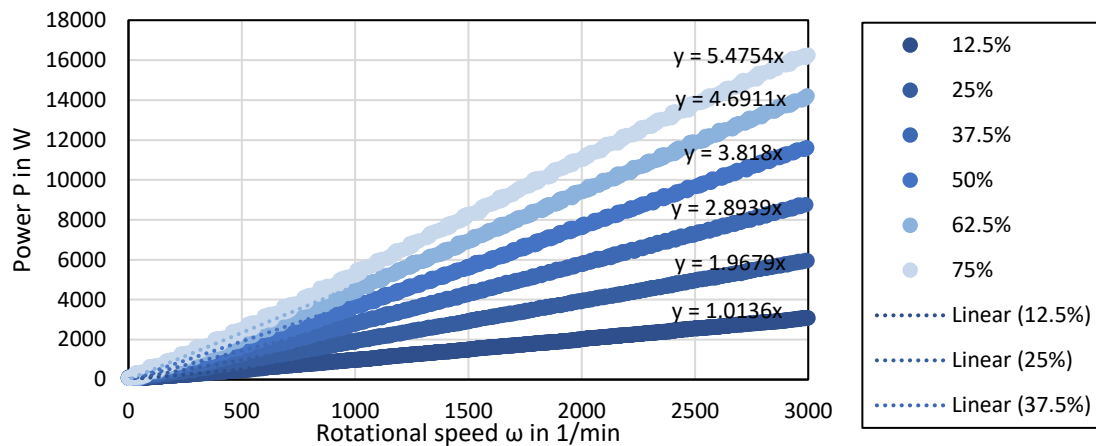


Figure 5.1 Relationship between power and rotational speed below 3000rpm

Since the gradient of the functions are constant on a value depending on the inverter input signal, the gradient is plotted over the input signal in Figure 5.2. To describe the relationship between input signal and gradient, a linear approximation is performed. The approximated function is given in the figure.

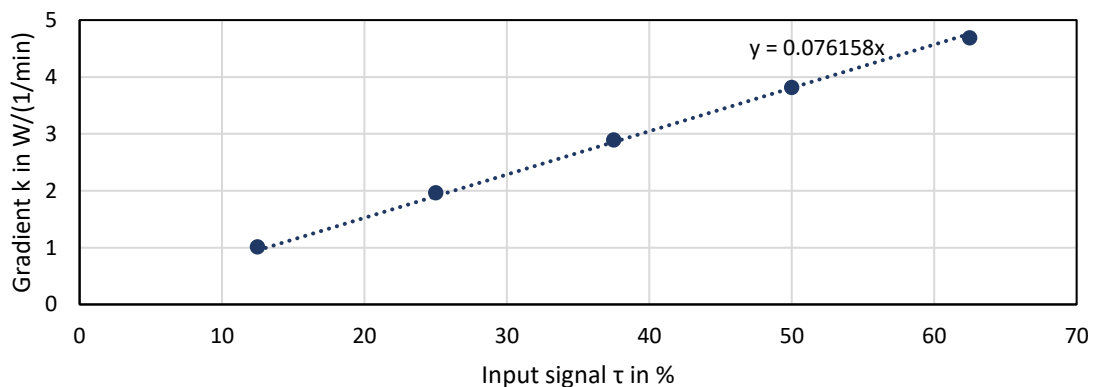


Figure 5.2 Gradient of power-speed relationship over set torque

Due to the two approximations, a relationship between set input signal, rotational speed and power can be build. Out of Figure 5.2, the Power P can be calculated with the gradient k and the rotational speed ω , see equation (5).

$$P(k, \omega) = k \cdot \omega \quad (5)$$

The gradient k can be described with the set input signal. The accelerating torque τ is used as input. In equation (5) the function of the linear approximation is given.

$$k(\tau) = 0.076158 \cdot \tau \quad (6)$$

By inserting equation (5) in equation (6) the flywheel system approximation below 3000rpm can be derived. The result is shown in equation (7).

$$P(\tau, \omega) = 0.076158 \cdot \tau \cdot \omega \quad (7)$$

To verify equation (7), the equations is applied on the previous measured signals of Figure 5.1. In Figure 5.3 the comparison between the calculated and the measured signals is shown. The difference is only marginally.

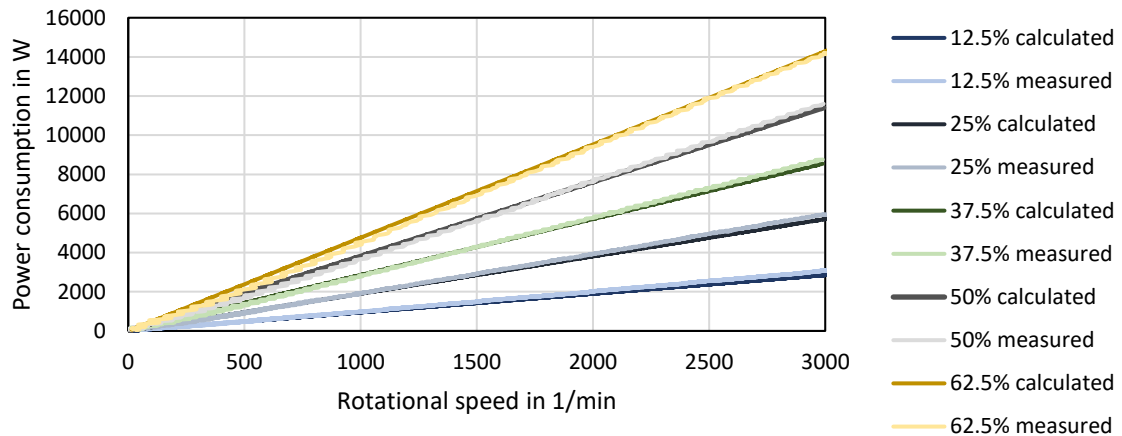


Figure 5.3 Comparison calculation vs. measurement

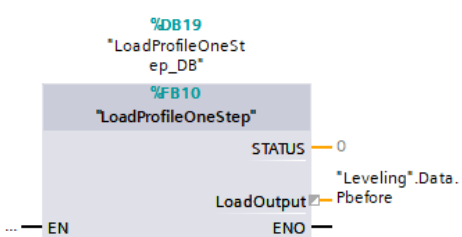
By realign the equation, so that the set torque can be calculated out of the power, and the measured speed it is possible to set a desired power and the PLC is able to calculate the suitable set torque for values below 3000rpm. The structured text of the implemented FC is shown in the table below. The FC also takes care that the flywheel is not accelerating to fast or in negative direction.

Description: Approximation			
		<pre>#TorqueCalc := #power / (#m * #rpm); IF #TorqueCalc > #maxTorque THEN #TorqueCalc := #maxTorque; END_IF; IF #rpm > 5100 THEN #TorqueCalc := 0; ELSIF #rpm > 3000 THEN #TorqueCalc := #power * #FactorAt3000; ELSIF #rpm < 200 AND #power < 100 THEN #TorqueCalc := 0; END_IF; #TorqueSet := #TorqueCalc;</pre>	
Input			
Rpm	real		
Power	real		
Output			
TorqueSet	real		
Temp			
TorqueCalc	real		
Constant			
m	real	0.000289609	
maxTorque	real	27648.0	
FactorAt3000	real	1.150977	
			//m = k/maxTorque*100

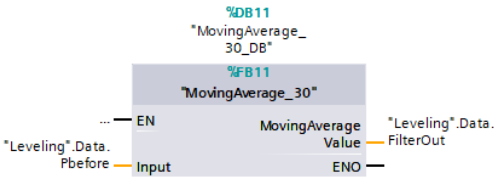
Appendix 9 Implementation of load levelling simulation

The following networks are all part of the load levelling simulation function. By executing the function in a cyclic OB with one cycle per second, the simulation is performed. For the pre-charged scenario, it is necessary to charge the FESS before starting the test. For the application with Butterworth filter, the second network is exchanged with the last network of this appendix.

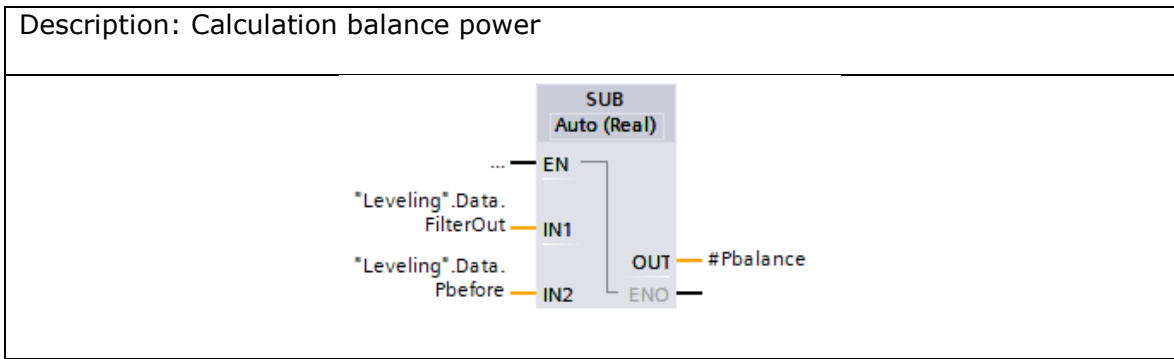
First network

Description: Sampling of load profile	
	<p>The function block is generated with the Target 1500S function. The according load FB must be executed in an startup OB before the test. Further the .so file must be uploaded to the webserver.</p>

Second network

Description: Moving average controller for signal filtering																											
	<table style="width: 100%; border-collapse: collapse;"> <tr> <td style="width: 150px;">Input</td> <td></td> </tr> <tr> <td>Input</td> <td style="text-align: right;">real</td> </tr> <tr> <td colspan="2"> </td> </tr> <tr> <td>Output</td> <td></td> </tr> <tr> <td>MovingAverageValue</td> <td style="text-align: right;">real</td> </tr> <tr> <td colspan="2"> </td> </tr> <tr> <td>Static</td> <td></td> </tr> <tr> <td>History</td> <td style="text-align: right;">Array [0...29] of Real (Array elements filled with initial value)</td> </tr> <tr> <td>sum</td> <td style="text-align: right;">real 0.0</td> </tr> <tr> <td>Pointer</td> <td style="text-align: right;">int 0</td> </tr> <tr> <td colspan="2"> </td> </tr> <tr> <td>Temp</td> <td></td> </tr> <tr> <td>Oldest_value</td> <td style="text-align: right;">real</td> </tr> </table> <pre style="font-family: monospace; padding: 5px;"> // Calculation of moving average value // To decrease calculation time, the sum of the history is stored // Safe the oldest value temporary #Oldest_Value := #History[#Pointer]; // Put the new value to the position of the old value #History[#Pointer] := #Input; // Calculate new sum of stored values #sum := #sum + #Input - #Oldest_Value; // Calculate new average value #MovingAverageValue := LREAL_TO_REAL(#sum / 30.0); // Change position of pointer to now oldest value #Pointer := #Pointer + 1; IF #Pointer > 29 THEN #Pointer := 0; // Beginning of history array END_IF; </pre>	Input		Input	real			Output		MovingAverageValue	real			Static		History	Array [0...29] of Real (Array elements filled with initial value)	sum	real 0.0	Pointer	int 0			Temp		Oldest_value	real
Input																											
Input	real																										
Output																											
MovingAverageValue	real																										
Static																											
History	Array [0...29] of Real (Array elements filled with initial value)																										
sum	real 0.0																										
Pointer	int 0																										
Temp																											
Oldest_value	real																										

Third network



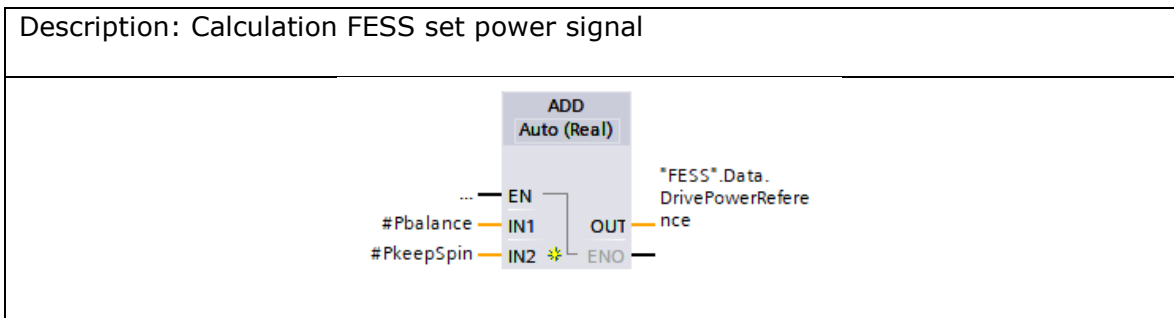
Fourth network

Description: Selection of case

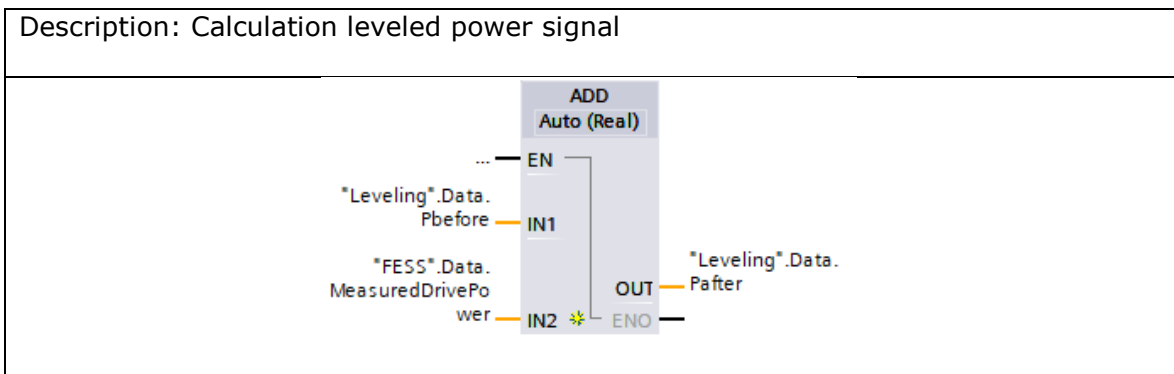
```

IF "KeepCharge" THEN
    #PkeepSpin := 600;
ELSE
    #PkeepSpin := 0;
END_IF;
    
```

Fifth network

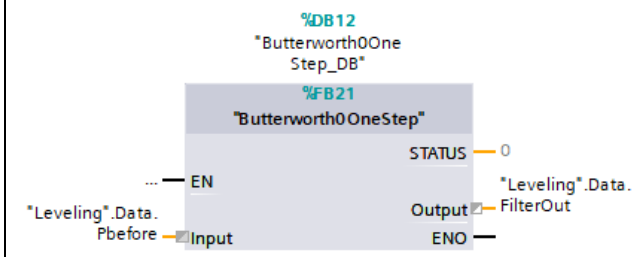


For plotting the load levelling output, the following network is executed in an cyclic OB with 100microseconds.



Network for Butterworth filter, used in exchange to the second network

Description: Butterworth filter for levelling of input signal



The function block is generated with the Target 1500S function. The according load FB must be executed in an startup OB before the test. Further the .so file must be uploaded to the webserver.

Appendix 10 Optimization load levelling filter

```
% -----Optimization of load levelling filter -----  
  
% Loading of Power profile, first 120s set to first sample value  
Power = LoadProfileSimulation.Power;  
t = (-120:1:120);  
  
% Butterworth filter  
n = 2;  
fc = 1/60;  
fs = 1/1;  
[b,a] = butter(n,fc/(fs/2));  
outBu = filter(b,a,Power);  
  
% Moving Average filter  
B = 1/L*ones(L,1);  
outMA = filter(B,1,Power);  
  
% Plot power  
plot(t,Power/1000,'.-',t,outMA/1000, t,outBu/1000, 'MarkerSize',8)  
xlim([0 120])  
ylabel('Power in kW');  
xlabel('Time in s')  
legend({'Load power','Smoothed load MA','Smoothed load Bu'},...  
      'location','southoutside','orientation','horizontal')  
grid  
  
% Plot slope gradient  
figure(2)  
MASlope = diff(outMA);  
Buslope = diff(outBu);  
t = (-119:1:120);  
plot(t,MASlope,t,Buslope)  
xlim([0 120])  
ylabel('Power slope gradient in W/s');  
xlabel('Time in s')  
legend({'Smoothed load MA','Smoothed load Bu'},...  
      'location','southoutside','orientation','horizontal')  
grid
```

Appendix 11 Simulink model for power buffer

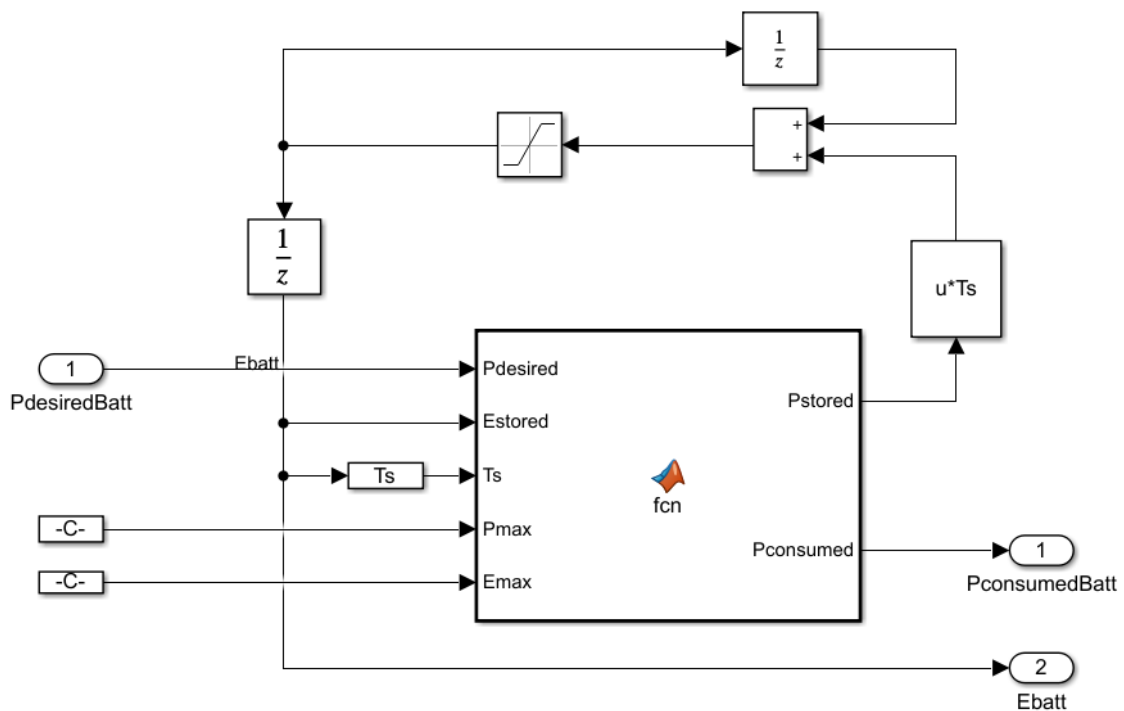
```

%%Initialize Model
EbattMax = 25000*60^2; %Maximum Energy Battery
PbattMax = 4600; %Maximum Power Battery
EbattInit = 500*60^2; %Initial Energy Battery

EfessMax = 36000*60^2; %Maximum Energy FESS
PfessMax = 8000; %Maximum Power FESS
EfessInit = 0; %Initial Power FESS

```

A11.1 Battery model



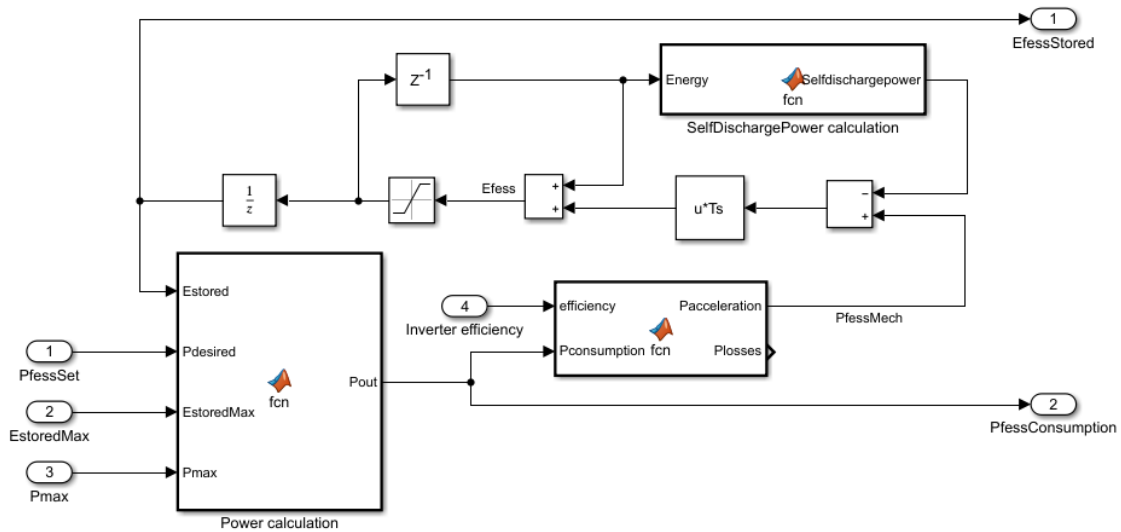
Battery model calculation

```

function [Pstored,Pconsumed] = fcn(Pdesired, Estored,Ts,Pmax,Emax)
% Datasheet values sonnenBatterie 10 10/27.5
eff = 0.95; %Inverter efficiency
if abs(Pdesired) > Pmax %Limitation power
    Pdesired = Pmax*sign(Pdesired);
end
if Pdesired > (Emax-Estored)/Ts %Prevention of over / under loading
    Pdesired = (Emax-Estored)/Ts;
elseif Estored/Ts < Pmax && Pdesired < 0
    Pdesired = Estored / Ts * sign(Pdesired);
end
Pstored = Pdesired * eff;
Pconsumed = Pdesired;

```


A11.2 FESS Model



Power calculation

```
function Pout = fcn(Estored, Pdesired, EstoredMax, Pmax)
if Estored <= 0 && Pdesired < 0      %Discharging limitation
    Pout = 0;
elseif Estored > EstoredMax        %Overcharging limitation
    if Pdesired < 0                %Discharging still possible
        Pout = Pdesired;
    else
        Pout = 0;
    end
else
    Pout = Pdesired;
end
if Pdesired > Pmax || Pout < -Pmax %Power limitation
    Pout = Pmax * sign(Pout);
end
```

Losses calculation

```
function [Pacceleration, Plosses] = fcn(eficiency, Pconsumption)
Plosses = abs(Pconsumption * (1-eficiency));
if Pconsumption > 0
    Pacceleration = Pconsumption - Plosses;
else
    Pacceleration = Pconsumption + Plosses;
end
```

Selfdischarge calculation

```
function Selfdischargepower = fcn(Energy)
%Calculation of rotational speed
rpm=sqrt(abs(Energy)*2/2.15)*30/pi;
%estimation based on Amber Kinetics datasheet
Selfdischargepower = rpm*0.02;
%Selfdischargepower = rpm*0.0083
```

Control for power distribution

```
function [Pbatt,Pfess] = fcn(Phouse,Efess, Ebatt,Ebattmax,Pbattmax)
%Power control of FESS and Battery
if Phouse > Pbattmax      %Power exceeds battery power
    if Ebatt < Ebattmax   %Battery not fully charged
        Pbatt = Pbattmax;
        Pfess = Phouse-Pbatt;
    else                  %Battery fully charged
        Pfess = Phouse;
        Pbatt = 0;
    end
elseif Efess > 0 && Ebatt < Ebattmax   %Energy in FESS and batt. not
full
    Pfess = Phouse - Pbattmax;
    Pbatt = Pbattmax;
elseif Efess > 0 && Ebatt >= Ebattmax  %Energy in FESS and batt. full
    Pfess = Phouse;
    Pbatt = 0;
else                                  %No energy in FESS
    Pbatt = Phouse;
    Pfess = 0;
end
```

Appendix 12 Hybrid storage implementation on PLC

For the hybrid storage simulation, two cyclic OB are used. The first OB is responsible for the simulation data from the grid and the battery. It has a cycling time of one second. The second OB is responsible for the control and is operated with a cycling time of 10ms. First, the simulation function is introduced. It is executed in the one second cycling OB.

A12.1 Hybrid storage simulation function

First network

Description: Power profile from house according to 1.3.3	
	<p>The function block is generated with the Target 1500S function. The according load FB must be executed in an startup OB before the test. Further the .so file must be uploaded to the webserver.</p>

Second network

Description: SonnenBattery Model from Simulink	
	<p>The function block is generated with the Target 1500S function. The according load FB must be executed in an startup OB before the test. Further the .so file must be uploaded to the webserver.</p>

A12.2 Hybrid storage control function

First network

Description: Notification of turn complete discharge of FESS
<pre>IF "HybridStorage".Data.SetPowerBatt < 4600 AND "HybridStorage".Data.FESSEnergy < 500 THEN #FESSempty := TRUE; ELSE #FESSempty := false; END_IF;</pre>

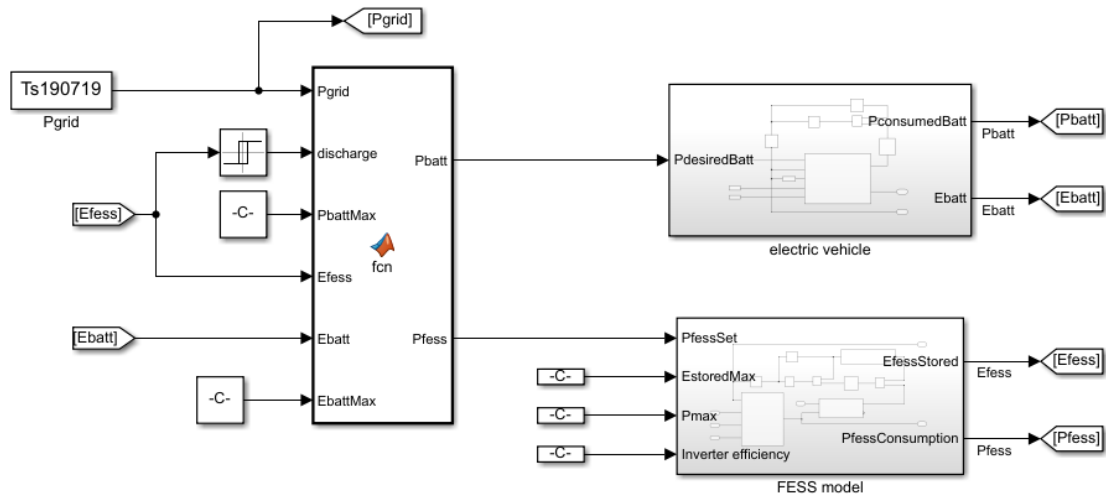
Second network

Description: Timer for optimized turn off behavior
<p>The diagram shows a timer block titled "%DB5" and "IEC_Timer_0_DB". It has two input ports: "IN" (labeled #FESSempty) and "PT" (labeled T#10s). It has two output ports: "ET" (labeled T#0ms) and "Q".</p>

Third network

Description: Hybrid storage controller																																													
<p>The diagram shows a block titled "%FC9" and "HybridStorageController". It has several inputs: "EN" (dashed line), "HousePower" (labeled #Phouse), "MeasuredStoredEnergy" (labeled #Efess), and "BatteryEnergy" (labeled #Ebatt). It has several outputs: "SetPowerBatt" (labeled #Pbatt), "DrivePowerRefere" (labeled #Pfess), and "ENO".</p>	<table> <tr> <td>Input</td> <td></td> <td></td> <td></td> </tr> <tr> <td>Phouse</td> <td>Real</td> <td></td> <td></td> </tr> <tr> <td>Efess</td> <td></td> <td>Real</td> <td></td> </tr> <tr> <td>Ebatt</td> <td></td> <td>Real</td> <td></td> </tr> <tr> <td>Output</td> <td></td> <td></td> <td></td> </tr> <tr> <td>Pbatt</td> <td></td> <td>Real</td> <td></td> </tr> <tr> <td>Pfess</td> <td></td> <td>Real</td> <td></td> </tr> <tr> <td>Constant</td> <td></td> <td></td> <td></td> </tr> <tr> <td>Ebattmax</td> <td>Real</td> <td></td> <td>9.0E7</td> </tr> <tr> <td>Pbattmax</td> <td>Real</td> <td></td> <td>4600.0</td> </tr> <tr> <td>PbfessmaxFactor</td> <td>Real</td> <td></td> <td>4.0</td> </tr> </table>	Input				Phouse	Real			Efess		Real		Ebatt		Real		Output				Pbatt		Real		Pfess		Real		Constant				Ebattmax	Real		9.0E7	Pbattmax	Real		4600.0	PbfessmaxFactor	Real		4.0
Input																																													
Phouse	Real																																												
Efess		Real																																											
Ebatt		Real																																											
Output																																													
Pbatt		Real																																											
Pfess		Real																																											
Constant																																													
Ebattmax	Real		9.0E7																																										
Pbattmax	Real		4600.0																																										
PbfessmaxFactor	Real		4.0																																										
<pre>IF #Phouse > #Pbattmax THEN IF #Ebatt < #Ebattmax THEN #Pbatt := #Pbattmax; #Pfess := #Phouse - #Pbattmax; ELSE #Pfess := #Phouse; #Pbatt := 0; END_IF; ELSIF #Efess > 300 AND #Ebatt < #Ebattmax AND NOT("IEC_Timer_0_DB".Q) THEN IF #Efess > 100000 THEN #Pfess := #Phouse - #Pbattmax; #Pbatt := #Pbattmax; ELSE #Pfessmax := "FESS".Data.MeasuredRotationalSpeed * #PbfessmaxFactor; IF #Pfessmax > #Pbattmax - #Phouse THEN #Pbatt := #Pbattmax; #Pfess := #Phouse - #Pbattmax; ELSE #Pfess := - #Pfessmax; #Pbatt := -"FESS".Data.MeasuredDrivePower + #Phouse; END_IF; END_IF; ELSIF #Efess > 300 AND #Ebatt >= #Ebattmax AND NOT("IEC_Timer_0_DB".Q) THEN #Pfess := #Phouse; #Pbatt := 0; ELSE #Pbatt := #Phouse; #Pfess := 0; END_IF;</pre>																																													

Appendix 13 EV fast charging simulation



```

function [Pbatt,Pfess] = fcn(Pgrid,discharge, PbattMax, Efess, Ebatt,
EbattMax)
%Power control of FESS and Battery
if discharge
    if Efess > 0
        %EV plugged in
        %Energy stored in FESS
        Pfess = Pgrid-PbattMax;
        Pbatt = PbattMax;
    elseif Ebatt < EbattMax
        %FESS completely discharged
        Pbatt = Pgrid;
        Pfess = 0;
    else
        %EV completely charged
        Pbatt = 0;
        Pfess = 0;
    end
else
    %Charging FESS, no EV
    Pfess = Pgrid;
    Pbatt = 0;
end
end

```

The submodel electric vehicle is identical to the battery submodel and the submodel of the FESS is identical to the submodel of the FESS in Appendix 11Appendix 11.

Appendix 14 EV fast charging implementation PLC

The following networks are all part of the EVcharging simulation function. By executing the function in a cyclic OB with one cycle per second, the simulation is performed.

First network

Description: FESS precharging before starting EV charging

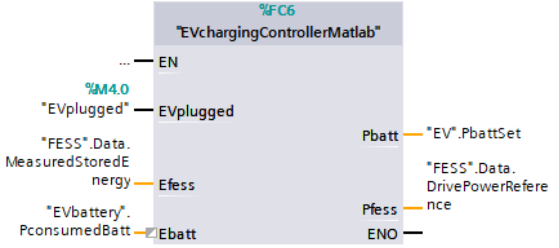
```

1 IF "FESS".Data.MeasuredRotationalSpeed > #SpeedMax AND "EVplugged" = FALSE THEN
2     "EVplugged" := TRUE;
3
4 END_IF;

```

Second network

Description: Controller for FESS as power buffer for EV charging

	<table style="width: 100%; border-collapse: collapse;"> <tr> <td style="width: 150px;">Input</td> <td></td> <td></td> </tr> <tr> <td>EVplugged</td> <td>Bool</td> <td></td> </tr> <tr> <td>Ebatt</td> <td>Real</td> <td></td> </tr> <tr> <td>Efess</td> <td>Real</td> <td></td> </tr> <tr> <td>Output</td> <td></td> <td></td> </tr> <tr> <td>Pbatt</td> <td>Real</td> <td></td> </tr> <tr> <td>Pfess</td> <td>Real</td> <td></td> </tr> <tr> <td>Constant</td> <td></td> <td></td> </tr> <tr> <td>Pgrid</td> <td>Real</td> <td>5000.0</td> </tr> <tr> <td>PbattMax</td> <td>Real</td> <td>200000.0</td> </tr> <tr> <td>EbattMax</td> <td>Real</td> <td>1.62E8</td> </tr> </table> <pre style="margin-top: 10px;"> IF #EVplugged THEN IF #Efess > 5000 THEN #Pfess := #Pgrid - #PbattMax; #Pbatt := #PbattMax; ELSIF #Ebatt < #EbattMax THEN #Pbatt := #Pgrid; #Pfess := 0; ELSE #Pbatt := 0; #Pfess := 0; END_IF; ELSE #Pfess := #Pgrid; #Pbatt := 0; END_IF; </pre>	Input			EVplugged	Bool		Ebatt	Real		Efess	Real		Output			Pbatt	Real		Pfess	Real		Constant			Pgrid	Real	5000.0	PbattMax	Real	200000.0	EbattMax	Real	1.62E8
Input																																		
EVplugged	Bool																																	
Ebatt	Real																																	
Efess	Real																																	
Output																																		
Pbatt	Real																																	
Pfess	Real																																	
Constant																																		
Pgrid	Real	5000.0																																
PbattMax	Real	200000.0																																
EbattMax	Real	1.62E8																																